School of Faculty of Engineering and Science

Wettability Alteration and Adsorption of Methyl Ester Sulphonate / Polystyrene Nanofluid to Enhance Oil Recovery from Sandstone Reservoir

Stanley Sim Sze Lim

0000-0002-7463-6824

This thesis is presented for the Degree of
Master of Philosophy
of
Curtin University

December 2022

Thesis Committee
Chair: A/P Dr. Jobrun Nandong
Supervisor: Henry Elochukwu Okafor
Co-Supervisor: Dr. Ziad Bennour

To the best of my knowledge and belief, this report contains no material previously published by any other person except where due acknowledgement has been made. This report contains no material which has been accepted for the award of any other degree or diploma in any university.

Signature : _____
Name : **Stanley Sim Sze Lim**
Date : 05/08/23

Acknowledgement

First and foremost, I would like to give my warmest thanks to all my family members, especially my parents. They gave me strength and fully supported me all of the time during my study. Without their understanding, I could not have the strength to complete my research study.

Besides, I would like to acknowledge to Fundamental Research Grant Scheme for giving me the chance to join the research project. With the grant, I could do the research study efficiently.

Next, I would like to acknowledge and give my utmost respect to my supervisor, Mr. Henry Elochukwu, for his detailed guidance and support. His professional guidance was not only on the experimental work but also on the thesis writing. His guidance and advice led me to the end of the study and made the work possible.

In addition, I also thankfully acknowledge my thesis committee, Dr Jobrun Nandong and Dr Ziad Bennour. Their support, professional suggestions and comments allowed me to improve my work significantly, which also made my work go smoothly.

I would like to express my deepest gratitude to graduate school Curtin Malaysia for making my research study smoothly and giving me support in many ways.

I also would like to express my deepest appreciation to the assessors, Dr Henry Foo and Dr Wee Siaw Khur for the professional suggestions and comments which allowed me to mitigate my research study and thesis writing. They also allow me to have enjoyable moments during my milestone presentations.

Lastly, I would like to give my special thanks to my fellow friends, who directly and indirectly gave me support all the time. Their mental support gives me the strength to complete the research study with a positive mentality.

Executive Summary

The primary recovery method of production from oil reservoirs is usually dominated by natural drive mechanism while secondary recovery method maintains reservoir pressure long enough to sustain production. However, both primary and secondary recovery methods leave behind more than 50% of OOIP (original oil in place) in the reservoir. Hence, Tertiary recovery method is required to recover the residual oil in the reservoir. Chemical enhanced oil recovery (c-EOR) method is a tertiary recovery technique to recover residual oil from oil reservoirs by injecting chemical materials such as salinity water, nanofluid, surfactant, polymer, or combination of chemical materials. Major drawback of c-EOR surfactant flooding is excessive adsorption of surfactant to the sandstone reservoir and the residual oil preferentially wet the sandstone rock. These drawbacks lead to poor oil displacement and sweep efficiency resulting to low overall oil recovery. This research project set out to investigate low salinity water/Methyl Ester Sulphonate (MES) surfactant/nanoparticles synergy to enhance oil recovery from sandstone reservoir. Series of experimental tests were conducted to ascertain the effect of the synergy solution on wettability alteration and surfactant adsorption reduction. The IFT (Interfacial Tension) between Tapis crude oil and the synergy solution under alkaline condition was 0.0315mN/m which is considered low and acceptable. The lowest contact angle measured was 12.2^o with the synergy solution of 750 ppm MES and 250 ppm $CaCl_2$ at high pH (9.5-10) condition compared to 91.7^o formation water used as reference. Maximum adsorption capacity was used as criteria to measure surfactant adsorption loss reduction. It was observed that surfactant adsorption capacity reduced from 6.1 mg/g to 0.43 mg/g when 25 ppm nano-polystyrene was added to the synergy solution at 70^oC temperature. In the oil recovery study, the highest additional oil recovered from sandstone rock sample at reservoir condition was 19.61% with the synergy solution of (750ppm MES surfactant/250ppm $CaCl_2$/25ppm nano-polystyrene) under alkaline condition. This study shows that the synergy solution was able to restore wettability to preferable water-wet condition to support oil recovery and reduce excessive loss of surfactant to the sandstone reservoir rock. The wettability alteration to water-wet state and alkaline condition supports the detachment of oil from the sandstone rock. In addition, this study also identifies the governing driving mechanism for c-EOR with the synergy of Low Salinity Water

Flooding (LSWF)/Surfactant and nanoparticles. This synergy solution can find application in the oilfield as the surfactant adsorption reduction supports the economic feasibility of the c-EOR project in terms of efficient cost savings on quantity of surfactant usage for the project and greatly improve additional oil recovery.

Table of Contents

LIST OF FIGURES

LIST OF TABLES

LIST OF ABBREVIATIONS

DSA	Drop Shape Analyzer
MES	Methyl Ester Sulfonate
CMC	Critical Micelle Concentration
UV-Vis	Ultraviolet – Visible light
EOR	Enhanced Oil recovery
IFT	Interfacial Tension
SDS	Sodium Dodecyl Sulfate
c-EOR	Chemical Enhanced Oil recovery
LSWF	Low Salinity Water Flooding
LSWI	Low Salinity Water Injection
PV	Pore Volume
NPs	Nanoparticles
NaCl	Sodium Chloride
$CaCl_2$	Calcium Chloride
$MgCl_2$	Magnesium Chloride
NaOH	Sodium Hydroxide
SiO_2	Nano-Silica

List of Symbol

q	Amount of surfactant adsorbed (mg/g)
C_i	Initial surfactant concentration (mg/L)
C_{Ae}	Equilibrium concentration
V	Total solution volume (ml)
$M_{sandstone}$	Total sandstone mass (g)
q_e	Equilibrium amount of adsorbed surfactant (mg/g)
K_L	Langmuir equilibrium constant (L/mg)
q_{max}	Maximum amount of adsorption of surfactant (mg/g)
C_e	Concentration of equilibrium surfactant (mg/L)
K_F	Freundlich equilibrium constant related to capacity of adsorption (mg/g)

CHAPTER ONE
INTRODUCTION

1.1 Background

The global energy demand continues to increase as world energy consumption increases. Figure 1.1 shows the total energy consumption in Malaysia which demonstrates increasing trend with time. Therefore, maximizing energy supply from oil and gas resources is important to meet the demand for energy. The oil recovery process can be classified into three phases: primary oil recovery, secondary oil recovery and tertiary oil recovery. Primary oil recovery is the extraction of crude oil with the natural energy from the reservoir. Secondary oil recovery process is the injection of gas or water into the reservoir to maintain reservoir pressure in the reservoir. Tertiary oil recovery is the technique applied to enhance the oil recovery and extend the life span of the reservoir. Tertiary oil recovery is also called enhanced oil recovery (EOR) which is applied after primary and secondary oil recovery process. There are several EOR techniques such as gas injection, thermal injection, water-alternating-gas injection, and chemical injection.
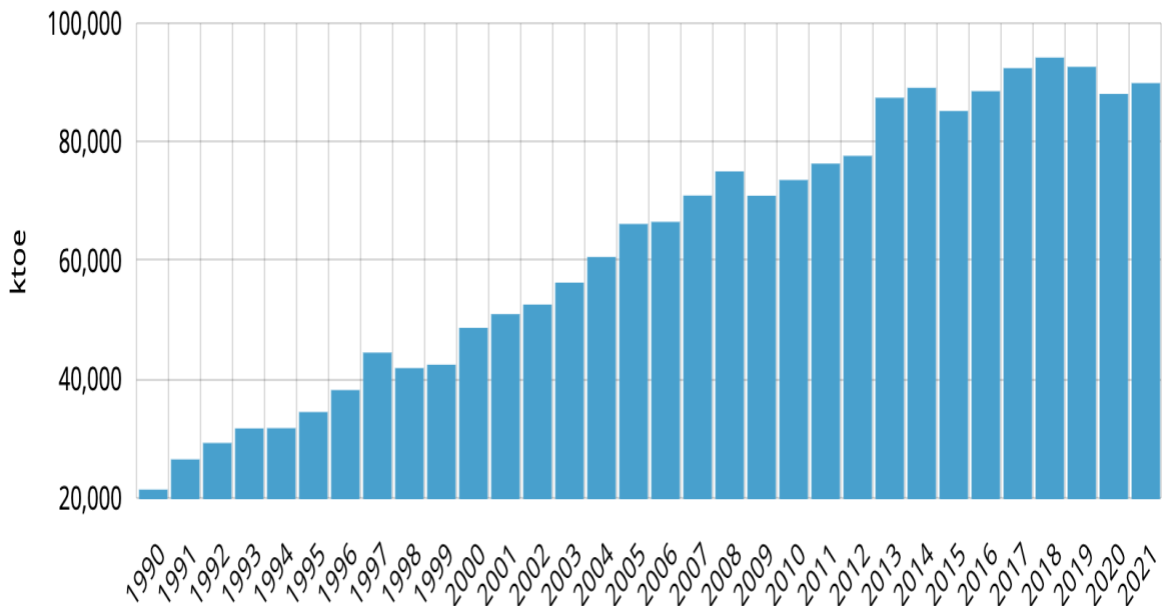
Figure 1.1: Total Energy Consumption in Malaysia (Enerdata 2022)

Chemical injection is the injection of surfactant, polymer, alkaline, NPs, and other chemical materials into the reservoir. Chemical injection also called chemical-EOR (c-EOR) method. Chemical-EOR method is one of the promising method due to the economic and technical feasibility, considerable capital cost and high efficiency. Chemical-EOR method is becoming popular due to the advancement of technology which allows us to understand the mechanism behind it. The mechanisms behind it could be wettability alteration, multi-ion exchange, electric double layer expansion, mineral dissolution, pH value (Purswani et al., 2017; Al-Saedi et al., 2019; Khishvand et al., 2019; Yue et al., 2020). The additional oil recovery from the reservoir depends on the effectiveness of the injected fluid. It is crucial to investigate the interaction between the injected fluid and the mineral rock in the reservoir.

The conventional chemical-EOR method support enhance oil recovery by improving specific mechanism. Surfactant flooding is usually applied to reduce the interfacial tension (IFT) between the fluid and oil. This could enhance the oil recovery by improving the oil mobility and wettability in the reservoir. Polymer flooding increase the viscosity of the fluid which improving the sweep efficiency and enhance the oil recovery. However, surfactant flooding would experience serious adsorption onto the rock surface which causes surfactant loss and economical loss (Madani et al., 2019). The viscosity of the polymer would be reduced due to the high temperature condition present in the deep reservoir. Chemical EOR methods can be the combination of several chemical materials to overcome the issues that occurred in single chemical fluid injection and further enhance oil recovery. Several combinations such as polymer/surfactant, alkaline/surfactant, alkaline/polymer, alkaline/surfactant/polymer are studied. Numerous studies indicated the efficiency and feasibility of the combination of chemical materials to reduce interfacial tension, improve wettability alteration and sweep efficiency (Sangwook et al., 2016; Saha et al., 2017; Almahfood et al., 2018; Olayiwola et al., 2020; Liu et al., 2021). Advancement of nanotechnology has also gained interest in the oil and gas industry (Bera et al., 2016). Previous studies mentioned that nanoparticles can support wettability alteration and increase the macro sweep efficiency due to its smaller size (Alnarabiji et al., 2018; Gbadamosi et al., 2019; Olayiwola et al., 2019; Shirazi et al., 2019). Besides, it is

capable to work under harsh conditions such as high temperature and high salinity environment. There are studies that also highlighted the benefits of nanoparticles with other chemical materials to further enhance the oil recovery and mitigate the excessive surfactant loss issue (Ma et al., 2013; Zargartalebi et al., 2014; Wu et al., 2017; Liu et al., 2020a; Venancio et al., 2020).

1.2 Problem Statement

This research project investigates the synergy the methyl ester sulphonate (MES) anionic surfactant with low salinity water and nanoparticles. However, the main issue of the injected MES surfactant is the excessive adsorption of surfactant onto the rock surface. The loss of surfactant would cause the recovery process to become economically unfeasible and reduce the effectiveness of the synthesized solution. There are also several factors that could cause MES surfactant to adsorb on the rock surface, and these includes: pH value, ion composition, salinity, and temperature (Ahmadi et al., 2015). Increasing of pH value and temperatures could reduce the excessive surfactant adsorbs onto the rock surface while increasing salinity has very minor effect on the reduction of excessive surfactant losses. The nanoparticles (NPs) is utilized to mitigate the excessive surfactant loss onto the rock surface (Afzali et al., 2018; Kazemzadeh et al., 2019). The NPs could be playing the role as sacrificial agent. Meanwhile, the NPs will compete with the surfactant molecules to adsorb on the rock surface leading to a less quantity of surfactant losses. Therefore, it is crucial to have a deep understanding about the efficiency and feasibility of NPs to mitigate excessive surfactant adsorption loss. NPs also has the potential to achieve favorable wettability alteration. In recent studies, the combinations of different types of nanoparticles with varying surfactants also showed positive results on wettability alteration, surfactant adsorption reduction and higher oil recovery (He et al., 2022; Zhao et al., 2022; Hassan et al., 2023). However, limited studies discuss how specific nanoparticles combined with MES anionic surfactant could achieve several mechanisms simultaneously and satisfactorily. Hence, it is essential to study the wettability and adsorption of the combination of Polystyrene NPs/MES anionic surfactant/low salinity water. Determination of oil recovery performance could provide a clear understanding about the synergistic solution.

1.3   Objectives

The main objectives of this research project are as follows:

1. To investigate the wettability alteration of Methyl Ester Sulphonate (MES)/polystyrene nanofluid on sandstone reservoir rock.
2. To determine the static adsorption capacity of MES/polystyrene nanofluid on sandstone reservoir rock.
3. To determine the oil recovery efficiency from sandstone reservoir rock by core-flooding test.

1.4   Scope of Study

This research focuses on studying the wettability alteration and adsorption capacity of synthesized solution (MES anionic surfactant/low salinity water/nanoparticles) under alkaline conditions for sandstone reservoir. Contact angle measurement of MES surfactant is used to compare different synthesized solution scenarios. It is used for comparing the results obtained from various concentration of MES surfactant and MES surfactant/low salinity water under alkaline condition to analyze the pH and salinity effect on wettability alteration. The impact of NPs on wettability also evaluated through the contact angle measurement of MES surfactant/low salinity water/NPs. Adsorption capacity of the synthesized solutions is determined to evaluate the efficiency of the NPs to reduce excessive surfactant loss. Factors such as concentration of surfactant, temperature, pH value and salinity are used as parameters to evaluate the performance of the synthesized solutions. The best performing synthesized solution is employed for core-flooding test to obtain additional oil recovery. The core-flooding test will be simulating the reservoir conditions where reservoir temperature (70℃) and pressure (1500 psi) will be applied.

1.5 Organization of thesis

Chapter 1 of this thesis includes the introduction part, thesis overview and problem statement. The main objectives and scope of study are presented in this chapter.

Chapter 2 provides an extensive literature review about the present study. The mechanism behind the wettability alteration, surfactant adsorption and additional oil recovery were thoroughly reviewed.

Chapter 3 demonstrates the details of the methodology applied for this study and the procedure of each of the phases of the experimental work. The experimental work is divided into several phases where the first phase is the material preparation, and the second phase is contact angle measurement. The third phase of the experiment is the adsorption study with UV-Vis spectrophotometer. The last phase is about core-flooding test procedure.

Chapter 4 analysis and discussion of experimental results obtained from every phase of the study. The mechanism behind wettability and adsorption study are thoroughly discussed.

Chapter 5 conclusion and highlights of every crucial part of the study. The feasibility of the low salinity water/MES/nano-polystyrene to be applied for chemical-EOR process.

CHAPTER TWO
LITERATURE REVIEW

2.1   Overview

The combination of low salinity water/anionic surfactant/nanoparticles purposely induces the wettability alteration and reduces the excessive surfactant adsorbs onto the rock surface. The wettability of the rock shift toward a strong water-wet state could indicate that the synergy of the chemical materials has a high potential to mobilize the residual oil in the reservoir rock and enhance the additional oil recovery. In this chapter, the driving mechanisms of wettability alteration and surfactant adsorption is discussed comprehensively. This chapter also cover the application of nanoparticles to enhance additional oil recovery. The recent experimental works regarding to low salinity water flooding, surfactant flooding, nanofluid flooding, and synergy of chemical materials flooding is discussed thoroughly in this chapter.

2.2   Low Salinity Water Flooding

Low salinity water is a specially adjusted brine solution with salt concentration less than 2000 mg/L (Katende et al., 2019). Meanwhile, the low salinity water flooding can be beneficial to the oil and gas industry due to its advantages including low cost, environmentally friendly and simple application (Chen et al., 2021). Researchers mentioned that the wettability of oil-wet rocks could be shifted towards water-wet state via low salinity water flooding (Al-Saedi et al., 2018; Wang et al., 2020). There are several driving mechanisms behind the low salinity water flooding (LSWF). Besides, the interactions between the oil/brine and rock has to be explained to further understand the mechanisms behind it.

2.3   Mechanism of Low Salinity Water Flooding

Recently, the application of low salinity water flooding has been extensively investigated. The researchers suggested several driving mechanisms behind low salinity water flooding, such as Multi-ion Exchange (MIE), Electric Double Layer Expansion (EDLE) and pH effect (Duffy et al., 2019; Katende et al., 2019; Mehraban et al., 2022).

2.3.1 Multi-Ion Exchange

Lager et al., (2008) proposed the Multi-ion Exchange (MIE) which is one of the mechanisms behind LSWF. MIE is included with the cation exchange, anion exchange, ligand exchange, cation bridging, water bridging, hydrogen bonding, protonation, and Van Der Waals interactions. The positively charged organic compound is attracted to the negatively charged rock surface via direct bonding which can be referred to as cation exchange. Meanwhile, the divalent cations present on the clay surface would attract the negatively charged organic materials and this resulted to the formation of organometallic complexes (Collins et al., 2018). Desorption of positively and negatively charged organic molecules occurs during LSWF which is attributed to the MIE mechanism. The organic polar materials and organometallic complexes are substituted by the cations (Na^+ and H^+) which exist in the low salinity water and therefore removed from the rock surfaces. The divalent ions are detached from the rock surface together with the organic materials and therefore the rock surface shifted towards water-wet state and lead to higher crude oil production.

Proton exchange causes large amount of OH^- released in the aqueous phase and result in higher surrounding pH value (Yue et al., 2020). Therefore, this generates higher repulsive force at the area near to the rock surface, which shift the wettability toward water-wet state. The van der Waals attractive force become crucial when the surrounding ionic strength is high. The bonding between divalent cations and the carboxylate groups can be referred to as ligand bonding. Meanwhile, ligand bonding is more capable to cause the organometallic complexes desorbed from the rock surface while compared to cation exchange and cation bridging (Katende et al., 2019). In addition, cation bridging occurs when the functional groups of the organic materials attracted to the negatively charged rock surface where divalent cations will play the role as a bridge (Khishvand et al., 2019). It is a weak adsorption mechanism and therefore, the organic materials can be released easily during LSWF and the wettability can be shifted towards water-wet state.

2.3.2 Electric Double Layer Expansion

Electric double layer (EDL) phenomenon refers to the structure that is present on parts of the mineral rock when it is in contact with the fluid. Several researchers mentioned that EDL expansion is one of the key mechanisms to cause wettability alteration shift towards water-wet state (Ahmadi et al., 2019a; Duffy et al., 2019). The electric double layer expansion can be classified into several phases. The first phase is the ions attraction between the rock surface and the organic materials with opposite ion charge. The second phase is the adsorption of the ions to the rock surface which become loose after low salinity water is injected. At the same time, the presence of the co-ions in the aqueous phase tend to repel from the rock surface. Meanwhile, the thickness of EDL expansion depends on the electrical surface charge as well as the concentration and types of the ions in the salinity water (Xie et al., 2019). In a high salinity condition, the EDL will become very compact due to the presence of high concentration of ions. On the other hand, low salinity water flooding would lead to higher zeta potential value which results to EDL expansion. Meanwhile, the monovalent ions such as Sodium (Na^+) and Hydrogen (H^+) tend to penetrate through the electric double layer and replace the previous adsorbed divalent cations. Consequently, the electrostatic repulsive forces are increased, and causes the detachment of the oil molecules. This occurs when the electrostatic repulsive force is greater than the divalent cations bridging (Bhicajee and Romero-Zeron, 2021). In conjunction with pH value increment, the wettability alteration is shifted towards strong water-wet state and further enhance the oil recovery. Overwhelming studies have provided the evidence where significant positive impact of wettability alteration achieved by low salinity water flooding while compared to high salinity water flooding (Pooryousefy et al., 2018; Kim et al., 2020; Rahimi et al., 2020; Farhadi et al., 2021; Mehraban et al., 2021).

2.3.3 pH Effect

The main cause for the increment of pH value during LSWF are mineral dissolution and cation exchange (Alhuraishawy et al., 2018; Mehraban et al., 2022). The clay particles in the mineral rock act as the cation exchanger. Primarily, polar components from the crude oil will adsorb together with divalent cations present in the formation water to the clay surface where the condition remains in chemical equilibrium. During LSWF, the

chemical equilibrium is disturbed, resulting in detachment of divalent ions (Mg^{2+} and Ca^{2+}). Substitution of H^+ occurs to compensate for the released divalent cations and therefore Hydrogen ions would attach to the clay surface. Consequently, the surrounding pH value is increased leading to acid-base proton transfer reaction. Meanwhile, desorption of polar components could cause the wettability shift towards water-wet state. Furthermore, excessive OH^- is released when dissolution of clay particles occurs, and this will lead to a higher pH value. Nonetheless, the amount of clay content in the mineral rock can still affect the process. But, this process would be relatively slow when it occurs on silicates surface (Aminian et al., 2019). Several studies showed that the increment of local pH value can enhance oil recovery (Torrijos et al., 2018; Al-Saedi et al., 2019; Abbasi et al., 2021).

2.4   Surfactant Flooding

Surfactant is a surface-active agent which acts as a wetting agent to reduce the interfacial tension between two different phases in the system. Molecules of surfactant are usually organic compounds comprised of hydrophobic tail part and hydrophilic head part. Surfactants can be classified into several categories such as anionic surfactant, cationic surfactant, zwitterionic surfactant and non-ionic surfactant (Khayati et al., 2020). Anionic and cationic surfactants are usually used for the c-EOR method to reduce the interfacial tension between oil and water in the sandstone and carbonate reservoir rocks (Shirazi et al., 2019; Koparal et al., 2021). Cationic surfactants are usually used for carbonate reservoirs instead of sandstone reservoirs because the adsorption on sandstone rock is relatively high. Due to the constraint of cost, zwitterionic surfactant usually get less attention when applied for c-EOR method (Atta et al., 2020). The non-ionic surfactant is commonly applied together with cationic or anionic surfactants to improve its performance (Esfandyari et al., 2020).

2.4.1 Effect Of Concentration Of Surfactant

Critical micelles concentration (CMC) is the lowest point where aggregation of surfactant monomer occurs and results in the formation of micelles. It is usually measured by plotting graph of interfacial tension versus different concentrations of surfactant (Manshad et al., 2017). The surfactant molecule is present as a single monomer in the solution when the concentration of surfactant is below the CMC. Meanwhile, it is essential for monomer concentration to remain below CMC point in order to achieve wettability alteration and interfacial reduction. Interaction between surfactant monomer and adsorbed components on the rock surface can cause wettability alteration towards water-wet state (Yao et al., 2021). The interfacial tension remains constant as the surfactant monomer concentration reaches the maximum when it is above the CMC. Hirasaki et al. (2011) mentioned that higher surfactant concentration could cause more water and oil to solubilize and form type III Winsor solution, leading to additional oil recovery. A Winsor Type III system occurs when a micro-emulsion is formed between the aqueous and oil phases, indicating high efficiency in reducing interfacial tension in the system which leads to higher oil recovery (Riswati et al., 2019). Besides, a low concentration of surfactant is not capable of achieving favourable wettability and low IFT. Experimental work from Apaydin et al., (2001) indicated that relatively high surfactant concentration might establish pressure gradient with end effect, resulting in the opposite flow direction. The pressure gradient built up from the outlet will cause the surfactant to flow toward the core sample in the direction of the inlet. However, laboratory work from Sun et al., (2021) revealed that IFT reduction and oil recovery increased gradually with increasing concentration of surfactant below the CMC point. Once the concentration of surfactant is beyond the CMC point, the oil recovery decreased as concentration of surfactant increased. Meanwhile, part of the surfactant might be lost due to adsorption onto the mineral surface. This will affect the efficiency of surfactant to achieve wettability alteration and IFT reduction and also economic losses (Saxena et al., 2019; Bashir et al., 2021; Kalam et al., 2021).

2.4.2 Effect Of Divalent Ions

Experimental work by Negin et al., (2017) showed that the concentration of divalent cations such as Mg^{2+} and Ca^{2+} should be under low concentration condition. Presence of divalent cations promote the bridging effect between negatively charged rock surface and the surfactant which causes higher surfactant adsorption.
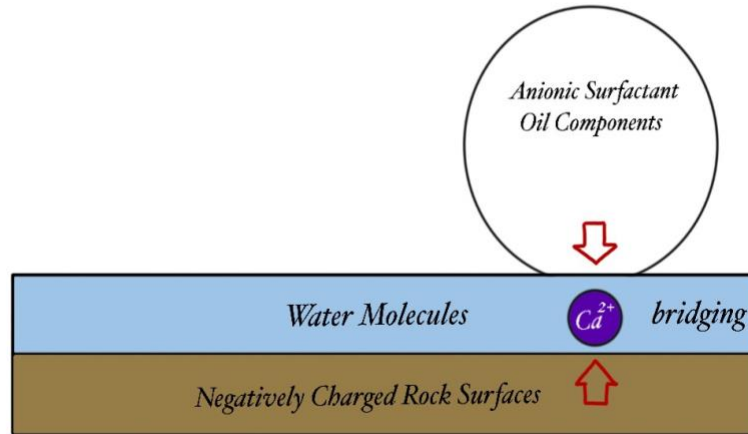
Figure 2. 1: Bridging effect with negatively charged rock surfaces

The presence of lower or optimum divalent cations is needed to decrease the surfactant adsorption and at the same time promote the bridging between oil molecules and clay particles (Hanamertani et al., 2018; Aminian et al., 2019; Paternina et al., 2020). Meanwhile, the bridging effect could be further elucidated through the Figure 2.1. According to (Nelson, 1981), divalent ions are more sensitive compared to monovalent ions during anionic surfactant flooding, especially under the condition of low surfactant concentration. However, the presence of divalent ions is inevitable, and therefore, researchers suggested applying surfactant with higher resistance such as surfactants with the units of carboxylate, sulfonate or ethoxy in the structure (Negin et al., 2017; Massarweh et al., 2020).

2.4.3   Effect Of Sulfonate

Atta et al. (2020) revealed that sulfonate type surfactants are the most widely used surfactants. Sulfonate surfactant can originate from fatty acids in natural oils. The main reactions to produce bio-based sulfonate surfactants are transesterification or esterification and sulfonation (Hutchinson et al., 2006). The bio-based sulfonate surfactant contains a hydrophilic part with sulfonate group and ethyl or methyl ester. Hirasaki et al. (2011) highlighted that the presence of units of sulfonate in the surfactant improved and prolonged the stability under high temperature reservoir condition. Researchers mentioned that sulfonate type surfactant could lead to higher oil recovery with low adsorption in harsh formation condition and at the same time achieve lower CMC (Tai et al., 2018; Li et al., 2020, Lin et al., 2020).

2.4.4   Effect Of pH Value

The level of pH in the reservoir and the injected solution can relatively affect the efficiency of the surfactant especially on the adsorption process. According to Saxena et al. (2019), the researchers indicated that increasing alkalinity of surfactant solution could reduce the excessive adsorption of surfactant to the rock surface due to higher electrostatic repulsion formed. Southwick et al. (2016) also mentioned that increasing pH level to a particular range could efficiently reduce the anionic surfactant adsorption on the sandstone rock surface. However, experimental work conducted by Liu et al., (2020c) revealed that reduction of pH level of the injected surfactant solution led to lower density charge on the silica surface, which resulted in lower adsorption to the rock surface. Even though the majority of researchers proposed that higher pH level of injected solution can reduce excessive surfactant adsorption (Massarweh et al., 2020; Kalam et al., 2021; Abbas et al., 2022).

2.4.5   Adsorption Isotherm Models

Adsorption isotherms helps to estimate surfactant reduction due to adsorption onto the mineral surface. There are two adsorption models commonly used to describe the amount of adsorbed surfactant with respect to the equilibrium concentration of surfactant under certain temperatures: Langmuir isotherm and Freundlich isotherm (Doan et al., 2021; Qiao et al., 2021). Table 2.1, as shown below briefly describes both isotherm models.

Table 2.1: Langmuir and Freundlich isotherm models

Isotherm models	Equation and Parameters	Description
Langmuir	$$q_e = \dfrac{q_{max} K_L C_e}{1 + K_L C_e}$$ q_e = Equilibrium amount of adsorbed surfactant (mg/g) K_L = Langmuir equilibrium constant (L/mg) q_{max} = Maximum amount of adsorption of surfactant (mg/g) C_e = Concentration of equilibrium surfactant (mg/L)	A single layer is formed with the adsorbate molecules on the surface of the adsorbent. The monolayer adsorption occurs where the limited amount of localized sites is adsorbed on the adsorbent surface and there is no interaction within the adsorbate molecules. Therefore, it is assumed that adsorption will not occur in the areas occupied with adsorbate.
Freundlich	$$q_e = K_F C_e^{1/n}$$ q_e = Equilibrium amount of adsorbed surfactant (mg/g) K_F = Freundlich equilibrium constant related to capacity of adsorption (mg/g) C_e = Concentration of equilibrium surfactant (mg/L) $1/n$ = heterogeneity factor	Freundlich isotherm demonstrates the process of reversible and non-ideal adsorption where multilayer adsorptions occur with heterogeneous surfaces. Meanwhile, Estimation of infinite surface coverage can be achieved mathematically which is applicable for multilayer adsorptions (Qiao et al., 2021).

2.5   Nanoparticles (NPs)

Nanotechnology has been extensively applied in different sectors (Olayiwola et al., 2019). With the advancement of technology, nanoparticles (NPs) can be produced easily and cost effectively (Yu et al., 2010; Chen et al., 2021). The NPs size is within the range of 10 to 100 nm, and due to the advancement in its size, it can demonstrate distinctive chemical and physical properties. This can improve the application in many industrial sectors and be conducive to existing technology. NPs are usually dispersed and suspended in a colloidal solution (nanofluid), with water or surfactant solution as base solution. Currently, c-EOR method can be presented in many ways of combination such as injection of low salinity water with surfactant, low salinity water with NPs, surfactant with polymer and other types of chemical materials combination (Almahfood et al., 2018; Hashemi et al., 2020; Yekeen et al., 2020). This could further improve the efficiency of c-EOR method as compared to a single chemical EOR injection. However, the effectiveness of combining various chemical materials with NPs will be affected by the concentration of chemical materials in the solution. The selection of appropriate chemical materials and NPs is vital to achieve several key mechanisms to maximize oil recovery. The key mechanisms are included wettability alteration, interfacial tension reduction, mobility control (Ali et al., 2020). Meanwhile, Olayiwola et al., (2020) proved that the use of nanoparticles in the reservoir together with low salinity water could control the issue of fines migration and further improve the capability of altering the wettability of rock surface towards desirable water-wet state. Studies also revealed that NPs can increase the macroscopic sweep efficiency and mitigate the viscous fingering issue which can be further illustrated with Figure 2.2 (Alnarabiji et al., 2020). The enhancement in sweep efficiency allow more oil to be replaced by the fluid and extract to the surfaces.
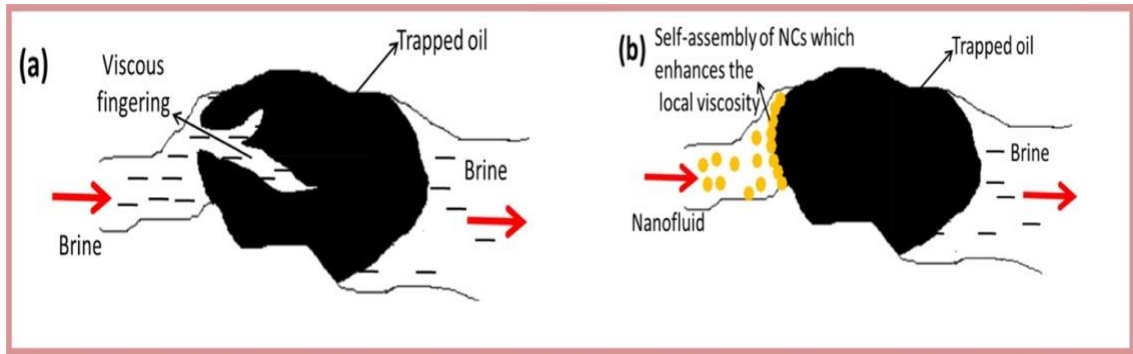
Figure 2. 2: (a) Brine injection induced viscous fingering issues (b) NPs mitigate the viscous fingering issues by self-assembly (Alnarabiji et al., 2020)

2.5.1 Size Of Nanoparticles

The different sizes of NPs can affect the performance of wettability alteration and IFT reduction especially when the applied nanofluid is under low concentration (Minakov et al., 2021). Several researchers revealed that the smaller the NPs size, the lower the IFT could be achieved (Kim et al., 2016; Adil et al., 2020; Udoh, 2021). Panchal et al. (2021) mentioned that smaller NPs could provide better performance on wettability alteration because of their larger charge density resulting in larger electrostatic repulsive force and hence increasing the strength of disjoining pressure. Besides, smaller NPs can easily penetrate through the small pore throat and prevent trapping (Kazemzadeh et al., 2019). This could be demonstrated with Figure 2.3.
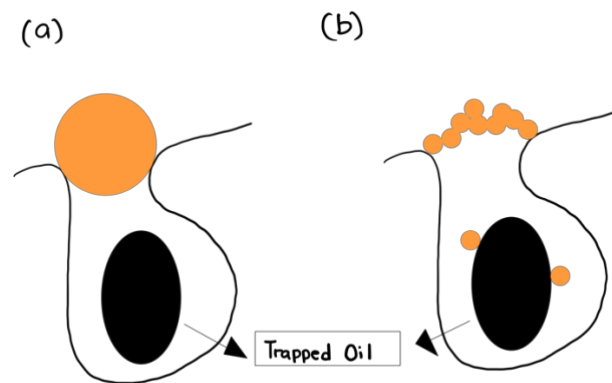
Figure 2. 3: (a) chemical materials with larger size (b) size of NPs (Alnarabiji et al., 2020)

Nevertheless, the size of NPs should be considered within an ideal range so that it can perform well without causing log-jamming (Sofla et al., 2018; Youssif et al., 2018; Panchal et al., 2021). Log-jamming is the phenomenon of NPs accumulating at the entrance of the pore throats thereby blocking potential flow paths. This occurs due to constant differential pressure and smaller pore throat size (Youssif et al., 2018). This issue might further cause pore blockage, reduction of oil recover and formation damage (Foroozesh et al., 2020; Nasr et al., 2021a; Yakasai et al., 2022).

2.5.2 Concentration Of Nanoparticles

Varying concentration of NPs maybe detrimental to overall recovery as too high concentration might cause pore blockage while too low concentration may have little or no effect on oil recovery. Panchal et al. (2021) mentioned that increasing the concentration of NPs can lead to higher Brownian motion and disjoining pressure which could aid wettability alteration and increase oil recovery. Afekare et al., (2021) highlighted that concentration of NPs higher than 5000ppm might cause rise in adhesive force and even reverse wetting effect. An experiment conducted by Sagala et al. (2020a) demonstrated that among different concentrations of Hydroxyl-functionalized silicate-based NPs (25ppm, 50ppm, 75ppm, 100ppm), nanofluid with 25ppm can achieve the lowest contact angle measurement with sandstone reservoir. Meanwhile, researchers also highlighted that higher concentration of NPs has higher tendency to cause aggregation of NPs and pore blockage which further reduce fluid mobility (Wu et al., 2017; Nasr et al., 2021b; Yakasai et al., 2022). Besides, increasing NPs concentration beyond the optimum concentration, would not lead to much reduction in IFT, but it will lead to economic loss (Sagala et al., 2020a). Meanwhile, increasing the concentration of NPs will only lead to additional oil recovery when it is within the optimum concentration. On the other hand, it might cause NPs to aggregate and block the pore throat, reducing the oil recovery. Therefore, optimum concentration target should be considered to achieve favourable wettability alteration, oil recovery factor and economic viability.

2.5.3 Salinity

The salinity in the reservoir is significantly high and therefore, the interaction between NPs/oil/rock and the influence of different concentrations of salinity is needed to verify whether NPs can withstand the high salinity condition. According to literature studies, increasing salinity will reduce the stability of NPs and affect the efficiency of NPs injection to enhance oil recovery (Panchal et al., 2021; Yakasai et al., 2022). The electrostatic repulsion force between the NPs/oil/rock is the main mechanism that affect the stability of dispersed NPs in aqueous solution (Rezvani et al., 2018; Udoh, 2021). In the high salinity environment, the ionic strength will be high, and this will cause the compression and reduction of the size of electrostatic double layer and lead to lower zeta potential. Consequently, the electrostatic repulsion force between the NPs will be drastically reduced. Surface neutralization with the NPs might occur due to the presence of large number of ions in the solution. Meanwhile, Van der Waal attractive force becomes significant in high salinity condition, where the attraction force occur between the regions of molecules with high electron regions and low electron regions (Alnarabiji et al., 2020).

Few studies mentioned that injection of NPs into high salinity reservoirs could cause the NPs to aggregate and retain in the porous media (Kim et al., 2015.; Aziz et al., 2019; Foroozesh et al., 2020). In conjunction with that, experimental work by (Kumar et al., 2020a) indicated that the oil recovery reduced by approximately 10% when the salinity level was increased from 0 to 3wt% of NaCl. However, experimental work from (Liu et al., 2021) showed that the introduction of high salinity water with Janus-silica NPs did not lead to any significant effect, especially, the effect on the IFT reduction was noticeably unchanged.

2.5.4 pH Effect

The pH level in the reservoir varies for different reservoir and usually not in the neutral pH level (Alnarabiji et al., 2020). Accordingly, the stability of NPs dispersed in the solution is strongly affected by the environment with different pH level (Kumar et al., 2016). Besides, the surface charge of NPs also depends on the pH environment (Yakasai

et al., 2022). Meanwhile, the surface charge magnitude between the NPs and the medium becomes higher as the pH value deviate from the isoelectric point (IEP). On the other hand, aggregation of NPs might occur when the pH values approach IEP or become zero, leading to a favorable Van der Waals attractive force. Afekare et al. (2021) revealed that the IEP of quartz and mica are within the range of 2 to 3 and therefore the surface charge of these minerals becomes positively charged when immersed in solution with the pH value smaller than 3. Meanwhile, when the pH value of the solution is higher than 3, the surface charge of the minerals will turn negatively charged.

An experiment conducted by (Rezvani et al., 2018) indicated that dispersion of NPs in the alkaline fluid could achieve higher stability of NPs and higher wettability alteration compared to the dispersion of NPs in the acidic fluid due to the higher electrostatic repulsion force that occurred between the interactions of oil/brine/NPs and rock surface. Besides, experimental work from (Sagala et al., 2020a) revealed that increasing the pH value of the nanofluid can reduce the distribution of the hydrodynamic size of hydroxylated nanopyroxene NPs (HPNP) from 300mm to 10mm. Besides, the researchers also agreed that increasing the pH value of the HPNP can achieve wettability alteration towards water-wet state and even increased the oil recovery by an additional 4.37%. Therefore, it is essential to obtain the optimum pH value where the dispersion of NPs in the solution could be stable and function efficiently to achieve wettability alteration towards water-wet state and increase additional oil recovery.

2.5.5 Effect Of Temperature

Generally, the temperature in the reservoir is relatively higher than the surface condition. Thus, investigation on sustainability and reliability of specific NPs for EOR is needed to confirm that NPs are highly resistant to thermal degradation under high temperature condition. Researchers found out that by reducing the acidity of nanofluid, thermal degradation of silica NPs can be reduced (Taborda et al., 2021). Experimental works by (Bila et al., 2020) proved that different types of silica NPs have different sensitivity to the surrounding temperature.

Therefore, investigation on the tolerance of different types of NPs at higher temperature is required to validate the feasibility of appropriate types of NPs to be applied for c-EOR process. Nasr et al. (2021a) and Sharma et al. (2014) mentioned that increasing temperature would affect the stability of NPs, which could directly reduce the efficiency of NPs as c-EOR chemical material. Meanwhile, Nasr et al., (2021b) also mentioned that the Brownian motion of NPs will increase as temperature increases, which could reduce the stability and efficiency of NPs. On the other hand, Panchal et al., (2021) proposed that increasing the temperature will lead to higher displacement efficiency, which could directly increase the oil recovery. The mechanism of temperature with the NPs is complicated and under dispute, hence, further investigation is needed to understand the mechanism comprehensively.

2.5.6   Wettability Of Nanoparticles (NPs)

The majority of existing NPs are synthesized and they could be classified into several groups according to their wettability, including neutral-wet polysilicon, hydrophobic and lipophilic polysilicon and lipophobic and hydrophilic polysilicon (LHP) (Udoh, 2021). Hydrophilic NPs tend to attract towards the water phase while hydrophobic NPs attract to oil phase (Panchal et al., 2021). The wettability of NPs defines their position in the water and oil interface. The adsorption of NPs onto the rock surface prompts the wettability alteration towards water-wet state where the oil molecules on the rock surface is removed. Thus, this could lead to higher oil recovery from the reservoir. Some studies have reported positive effects of using hydrophilic NPs to enhance oil recovery (Afekare et al., 2020; Hendraningrat et al., 2013; Negi et al., 2021; Youssif et al., 2018). Yakasai et al. (2020) suggested that hydrophilic NPs are more appropriate for viscosity enhancement and wettability alteration. Meanwhile, they recommended that partially hydrophilic and hydrophobic nanoparticles are more suitable for IFT reduction. However, the researchers mentioned that iron oxide NPs (IONPs) would cause retention and deposition due to the hydrophilic nature of IONPs when applied in the salinity environment that lacks functional groups (Yakasai et al., 2022).

On the other hand, Ahmadi et al., (2019b) and Singh et al., (2020) mentioned that hydrophilic NPs also played an important role in selective pore channel plugging to increase pressure drop and enhance the oil recovery. Nevertheless, the occurrence of pore plugging might lead to a reduction of additional oil recovery (Omidi et al., 2020). Previous studies indicated that hydrophilic NPs could improve the stability of the foam and do not cause deterioration to the foamability when applied for EOR process (Bashir et al., 2019; Rasid et al., 2021; Yang et al., 2021).

2.5.7   Mineralogy Of Reservoir Rock

Several researchers inferred that the pore structure and mineralogy of the rock might affect the efficiency of nanofluid flooding (Afekare et al., 2021; Wang et al., 2021). Besides, Panchal et al., (2021) noted that the grain size of the rock could affect the retention of NPs in the porous media. The surface area per unit bulk volume decreased when the grain size of the mineral rock is larger than the surface area. Meanwhile, retention of NPs on the mineral rock surface increases as the reduction of surface area per unit bulk volume increases. Caldelas et al. (2010) mentioned that clay content in the rocks could lead to retention of NPs on the rock surface. The free spaces between the mineral rock grains are occupied by clay particles and hence reduce the porosity of the reservoir. In addition, the retention of NPs on the clay surface increases when the surface area per unit bulk volume of clay particles increases. Furthermore, the surface charge of the reservoir rock is different due to the various mineral composition such as micas (illite and mucsovite), carbonate rocks (dolomite and calcite), clay (chlorite and kaolinite) and feldspars (Foroozesh et al., 2020). Two conditions could mitigate the fines migration issue: adsorption of NPs onto the rock surfaces and reduction of surface potential between the fines and the rock surfaces (Yuan et al., 2018). The adsorption of nanoparticles could reduce the surface potential between the fines and rock surfaces and thus resulting in lower repulsive forces (Moghadasi et al., 2019; Diez et al., 2020). Consequently, the fines migration could be mitigated.

2.6   Summary Of Literature Review

Most experimental works only focused on applying a single type of chemical EOR agent. Although, low salinity water could provide favorable additional oil recovery, the amount of the additional oil recovery is still limited compared to the injection of the combination of chemical materials. Experimental work from Da Costa et al. (2020) obtained an approximately 5% additional oil recovery with low salinity water flooding. Meanwhile, replacing conventional single-type chemical injection with the synergy of other chemical materials to enhance additional oil recovery could be of considerable interest.

Besides, surfactant flooding would experience excessive surfactant loss due to the adsorption of surfactant onto the rock surface. Thus, nanoparticles play a vital role in reducing excessive surfactant loss. However, the recent studies investigating the feasibility of nanoparticles to reduce excessive surfactant loss are very limited. Hence, it would be of great interest to investigate the potential of nanoparticles to minimize the excessive surfactant losses on rock surfaces. Furthermore, recent studies demonstrated the trending tendency of nanoparticles to achieve wettability alteration towards a desirable water-wet state and further enhance the oil recovery from the reservoirs (Amrouche et al., 2023; Xu et al., 2023). Therefore, introducing nanoparticles not only for reducing the excessive surfactant losses, the investigation on the potential of nanoparticles to shift the wettability towards favorable water-wet state and further enhance the additional oil recovery is noteworthy.

This project addresses the potential of nanoparticles to reduce excessive surfactant loss and achieve additional oil recovery. This research project integrates the different chemical materials to achieve several crucial mechanisms such as wettability alteration towards desired water-wet state, reduction of excessive surfactant loss and enhance additional oil recovery.

Table 2.2, 2.3 and 2.4 presents summary of previous experimental works on low salinity water injection, surfactant flooding, nanoparticles flooding and the combinations of chemical materials flooding.

Table 2.2: Summary of literatures on low salinity water flooding experimental works

References	Rock types	Experiment condition	Salinity water (ppm)	Proposed mechanisms	Findings
Chen et al., 2020	Berea sandstone	1500psi and 200psi, ambient temperature and pressure	142,431ppm (high salinity water), 142.31ppm (low salinity water)	Wettability alteration, Multi ion exchange, mineral dissolution, electric double layer, surface complexation	Mineral dissolution due to the interaction between clays, brine, and oil. Detachment of oil from the mineral surface occurred. Meanwhile, rock/brine and oil/brine systems became more negatively charged resulting in larger EDL expansion and higher repulsive force. An additional 5% oil recovery from low salinity water injection compared to high salinity water injection was obtained.
Da Costa et al., 2020	Sandstone	20°C-60°C, atmospheric pressure	1,000ppm to 200,000ppm (low to high salinity water)	Multi-ion exchange, EDL expansion, wettability alteration, IFT reduction, fines migration, pH values	Reduction of monovalent in the effluent indicated that replacement of monovalent with divalent ions in the system led to wettability alteration. Increment of pH value and higher density of negatively charged ions on rock surface which was induced by LSWF could aid the detachment of oil

					molecules from the rock surface. However, LSWF led to significant positive impact on wettability alteration and higher oil recovery factor (8% additional oil) instead of HSWF which can reduce certain amount of IFT and result in a lower oil recovery factor.
Kim et al., 2020	Sandstone	25℃, 1000psi	1,400ppm to 5,000ppm (low salinity water), 30,000ppm (high salinity water)	Wettability alteration, multi-ion exchange, EDL expansion, increment of local pH value, types of clay content	LSWF is more suitable to apply in sandstone rock which contains kaolinite compared to other kinds of clay content especially illite since kaolinite will lead to higher positive impact on EDL expansion and MIE which aid wettability alteration. The oil recovery factor obtained from the core flooding test was 16% for sandstone with kaolinite.

| Da Costa et al., 2021 | Sandstone rock | 60°C, 2184kPa | 1,700ppm to 28,000ppm (low salinity water in different concentration), 200,000ppm (high salinity water) | Multi-ion exchange, pH value, EDL expansion | Monovalent cation replacement happened and caused the Ca^{2+} to be released from rock surfaces together with oil molecules. Low salinity water induced higher pH value in the oil/brine/rock system which led to larger EDL expansion and resulted in wettability alteration towards water-wet state. Additional oil recovered was up to 6%-8% with low salinity water injection. |

Table 2.3: Summary of literatures on surfactant flooding experimental works

References	Types of surfactant	Rock Types	CMC	Retention mechanism	Findings/Remarks
Liu et al., 2020c	Anionic surfactant (Alcohol Alkoxy Sulfate) (AAS)	Sandstone	0.005wt% (0.07mM)	Adsorption	pH value and concentration of calcium ions increased the adsorption of AAS. The local charged rock sites became more negatively charged as pH value increased. Polystyrene sulfonate was added into the system and 85% of surfactant adsorption reduction was achieved and oil recovery factor increased simultaneously.
Koparal et al., 2021	Anionic surfactant	Sandstone	-	Adsorption	Adding 1wt% of sodium polyacrylate into the system can reduce the anionic surfactant adsorption from initial 0.2mg/g to 0.11mg/g.

Zhong et al., 2021	Anionic surfactant (hybrid fluorinated surfactant, sodium 2-[2-(perfluorooctyl)] acetoxy ethanesulphonate (HFS8), sodium dodecylbenzene sulfonate (SDBS)	Sandstone	0.4g/L	Adsorption	The negatively charged surfactant minimized the potential to be adsorbed onto the rock surface while HFS8 achieved higher oil recovery factor compared to SDBS.
Hanamertani et al., 2018	Anionic surfactant (internal olefin sulfonate (IOS), in house-surfactant (MFOMAX))	sandstone	IOS-100ppm, MFOMAX-250ppm	Adsorption	Adsorption of these surfactants reduced the efficiency of surfactant flooding in the porous media where the amount of adsorption process influenced by the various concentration and types of surfactants. Introduction of ionic liquid significantly reduced the excessive surfactant loss. Electrostatic interaction is the main mechanism to cause adsorption of surfactant to the rock surface, and therefore, anionic surfactant is suitable to be applied for sandstone reservoirs to create electrostatic repulsive force.

Table 2.4: Summary of nanoparticles (NPs) and synergy fluid experimental works

References	Rock types	Type of injection fluid	Pressure/ Temperature	Mechanisms	Findings and Remarks
Kumar et al., 2020b	Sandstone	Hydrophilic SiO_2 NPs, salinity water, polymer PAM, SDS	Ambient temperature, ambient pressure	Electrostatic forces, surfactant adsorption reduction	The concentration of salinity water increased which led to higher ionic strength thereby reducing the electrostatic repulsive force of NPs and caused the aggregation of NPs. Reduction of surfactant adsorption onto the rock surface can be achieved in low and moderate saline condition with the presence of NPs. Combination of surfactant/silica NPs/optimum salinity water can achieve additional oil recovery up to 13%.
Agi et al., 2020	Sandstone	Rice husk silica NPs	120℃, 3000psi	Electrostatic attraction and repulsive forces	The application of rick husk silica NPs is low cost and environmentally friendly. NPs can function in high temperature condition. Additional oil recovery was achieved in the range 10% to 24%.
Shakiba et al., 2020	Unconsolidated sandstone	Seawater, formation water, SiO_2 NPs	65℃, 650psi	Wettability alteration, IFT reduction, disjoining pressure, fines migration	Calcium ions possess a better effect on the total precipitation compared to Magnesium and Sulphate ions. This is because Mg^{2+} ions are less chemically reactive compared to Ca^{2+} ions. Breakthrough time (BT) was reduced

| | | | | | with the presence of NPs which indicated that NPs has the potential to control fines migration problem. NPs can significantly reverse the wettability towards water-wet state. An additional 10% oil was recovered with the presence of NPs in the optimum diluted seawater. |
| Mansouri et al., 2019 | Sandstone | SiO_2 NPs, Al_2O_3 NPs, MgO NPs, salinity water | Ambient temperature, 700 psi | Fines migration control, surface charges, wettability alteration | Among the different types of nanoparticles, SiO_2 nanoparticle has the highest capability to control the fines migration problem and led to higher oil recovery factor. Al_2O_3 NPs and MgO nanoparticles will agglomerate and form considerable particle size due to higher sensitivity in the ionic concentration. Surface charges between nanoparticle and mineral surfaces are the main mechanism that control the fines migration issue. They mentioned that contribution of fines migration on EOR is considered as insignificant. An additional 10% oil recovery was achieved with the presence of SiO_2 nanoparticle in the low salinity water flooding. |

Fan et al., 2021	Sandstone	Silica NPs, salinity water (monovalent ions), Partially hydrolyzed polyacrylamide (HPAM)	60℃, 12MPa	IFT reduction, wettability alteration	Presence of low concentration of silica NPs and polymer in the system increased the surface hydrophilicity and resulted in significant contact angle reduction. Increasing the concentration of NPs which further reduced the IFT due to the continuous reduction of Gibbs energy. An additional of 15% of the oil recovery was obtained from the polymer-Nanosilica flooding which is higher than polymer flooding and water flooding.
Gbadamosi et al., 2019	Sandstone	Aluminium oxide NPs, Silicon dioxide NPs, Partially hydrolyzed polyacrylamide (HPAM)	90℃, 2500psi	Wettability alteration, IFT reduction, viscosity, electrostatic interactions, disjoining pressure	Al_2O_3 polymeric nanofluid performed better on wettability alteration, IFT and viscosity reduction and the enhancement on sweep efficiency compared to SiO_2. Larger structural disjoining pressure created by Al_2O_3 NPs and stronger electrostatic attraction occurred between the NPs and sandstone rock surface leading to larger contact angle reduction. Approximately 5% of additional oil recovery was achieved by Al_2O_3 polymeric nanofluid compared to SiO_2 polymeric nanofluid.

| Youssif et al., 2018 | Sandstone | Silica NPs | Not specified | IFT reduction, wettability alteration, electrostatic interactions, disjoining pressure, concentration of NPs, | Increasing the concentration of NPs up to optimum concentration can increase the oil recovery. Concentration beyond the optimum point will cause permeability impairment due to pore blockage and hence affect the oil recovery. Electrostatic repulsive force was the main mechanism on wettability alteration. An additional of 13.28% of oil recovery was obtained during tertiary flooding with 0.1wt% NPs. |

CHAPTER THREE
METHODOLOGY

3.1   Overview

In this research study, the process of experiment can be classified into several main phases which includes materials, preparation, and formulation of nanofluid, contact angle measurement (wettability study), static adsorption study and core flooding.

3.2   Experimental Materials

Monovalent salt, (NaCl, $\geq$ 99% mass fraction) (Merck), Divalent salts, (CaCl$_2$, $\geq$ 98% mass fraction) (Merck) and (MgCl$_2$, $\geq$ 98% mass fraction) (Acros), Anionic surfactant, Methyl Ester Sulphonate (MES, $\geq$ 99% mass fraction) (Chemithon), Sodium Hydroxide, (NaOH, $\geq$ 98% mass fraction), (Merck) Nano-polystyrene (Phosphorex, Inc), Nano-silica (SiO$_2$ $\geq$ 99% mass fraction) (US Research Nanomaterials), Tapis crude oil (Petronas Carigali), Buff and Grey Berea Sandstone rock samples (Kocurek).

Table 3.1: Properties of Tapis Oil

Crude oil	API Gravity (degree API)	Specific Gravity	Pour Point, ^{o}F
Tapis crude oil	42.7	0.812	60.8

Table 3.1 shows the properties of Tapis crude oil. Tapis crude oil is originally from Tapis oilfield Malaysia. The high API gravity indicated that the Tapis crude oil is a very light crude oil.

Table 3.2: Mineralogy and physical properties of Buff and Grey Berea

Types of Sandstone	Grey Berea	Buff Berea
Quartz	91%	90%
Kaolinite	8%	9%
Montmorillonite	1%	-
Smectite	-	1%
Porosity	20% to 21%	20% to 21%
Permeability	60mD to 100mD	250mD to 500mD
Grain Size	$250\mu m$ to $500\mu m$	$125\mu m$ to $250\mu m$

Table 3.2 shows the clay content of Grey and Buff Berea sandstone. Both types of rocks have clay content less than 10%. The sandstone rock contains different composition of clay minerals such as Kaolinite, Montmorillonite and Smectite listed in the Table 3.2. The porosity, permeability and grain size of the rocks are also stated in Table 3.2.

3.3   Methods

3.3.1   Low Salinity Water/MES Surfactant/NPs Preparation

The MES surfactant is prepared with different concentrations (100ppm, 250ppm, 500ppm,750ppm, 1000ppm, 1250ppm, 1500ppm, 1750ppm, 2000ppm, 3000ppm, 4000ppm and 5000ppm). By adding several drops of 0.2M of NaOH to adjust the pH value. Measurement of pH value is necessary to make sure the pH values for all the solutions are constant which is within (9.5 to 10). The values set within the ranges because the alteration of pH condition with NaOH could be difficult to obtain at a fixed value for all different synthesized solutions. Adding specific concentration of divalent cations into different concentration of alkaline MES surfactant. Then, the NPs are added into the synthesized solutions and ultra-sonicator was used to disperse the NPs in the solution. All the prepared synthesized solutions are tabulated in Table 3.3, 3.4 and 3.5.

Table 3.3: Synthesized solutions of MES surfactant with divalent cations

Concentration of MES surfactant (ppm)	Concentration of $CaCl_2$ (ppm)	Concentration of $MgCl_2$ (ppm)
100	100/250/500/1000	100/250/500/1000
250	100/250/500/1000	100/250/500/1000
500	100/250/500/1000	100/250/500/1000
750	100/250/500/1000	100/250/500/1000
1000	100/250/500/1000	100/250/500/1000
1250	100/250/500/1000	100/250/500/1000
1500	100/250/500/1000	100/250/500/1000
1750	100/250/500/1000	100/250/500/1000

2000	100/250/500/1000	100/250/500/1000	
3000	100/250/500/1000	100/250/500/1000	
4000	100/250/500/1000	100/250/500/1000	
5000	100/250/500/1000	100/250/500/1000	

Table 3.4: Synthesized solutions of MES surfactant with divalent cations

Concentration of MES surfactant (ppm)	Concentration of Nano-Silica (ppm)	Concentration of $CaCl_2$ (ppm)	Concentration of $MgCl_2$ (ppm)
250	25	250	-
500	25	250	-
750	25	250	-
1000	25	250	-
1250	25	250	-
250	25	-	250
500	25	-	250
750	25	-	250
1000	25	-	250
1250	25	-	250

Table 3.5: Synthesized solutions of MES surfactant with divalent cations and Nano-polystyrene

Concentration of MES surfactant (ppm)	Concentration of Nano-Polystyrene (ppm)	Concentration of $CaCl_2$ (ppm)	Concentration of $MgCl_2$ (ppm)
250	25	250	-
500	25	250	-
750	25	250	-
1000	25	250	-
1250	25	250	-

250	25	-	250
500	25	-	250
750	25	-	250
1000	25	-	250
1250	25	-	250

The table 3.6 showed the density for the optimum synthesized solutions which would be focus in oil recovery study.

Table 3.6: Density of the Synthesized Solutions

Synthesized Solutions	**Density (g/mL)**
750ppm MES + Alkaline Condition	1.0029
750ppm MES + Alkaline Condition + 250ppm CaCl$_2$	1.0061
750ppm MES + Alkaline Condition + 250ppm CaCl$_2$ + 25ppm Nano-polystyrene	1.0065

3.3.2 Nanofluid Characterization (Zeta Sizer/Zeta Potential/PDI)

Measurement of particle size, polydispersity index (PDI) and zeta potential were conducted to analyze the stability of the synthesized solutions with the presence of NPs. Zeta sizer Nano Series ZS (Malvern) which could work in high temperature conditions was used to measure the particles size, PDI and zeta potential of the synthesized solutions. The larger the zeta potential, the more stable the synthesized solution. The synthesized solution was injected into the disposable polystyrene cuvette (DTS0012) by using a syringe. The cuvette must be filled within the range 10mm to 15mm. It is important to make sure the cuvette is well fitted in the specific compartment to attain accurate and consistent results. The measurements are conducted under two conditions which are room temperature (25°C) and reservoir temperature (70°C). All the synthesized solutions with the presence of NPs are tested under these two conditions.

| Formulation of synthesized solutions with the presence of NPs | → | Fill the cuvette with the synthesized solutions within the required range | → | Conduct the zeta sizer, PDI and zeta potential measurement at room temperature condition (25℃) | → | Repeat the measurement at reservoir temperature (70℃) |

Collect and analyze the results data
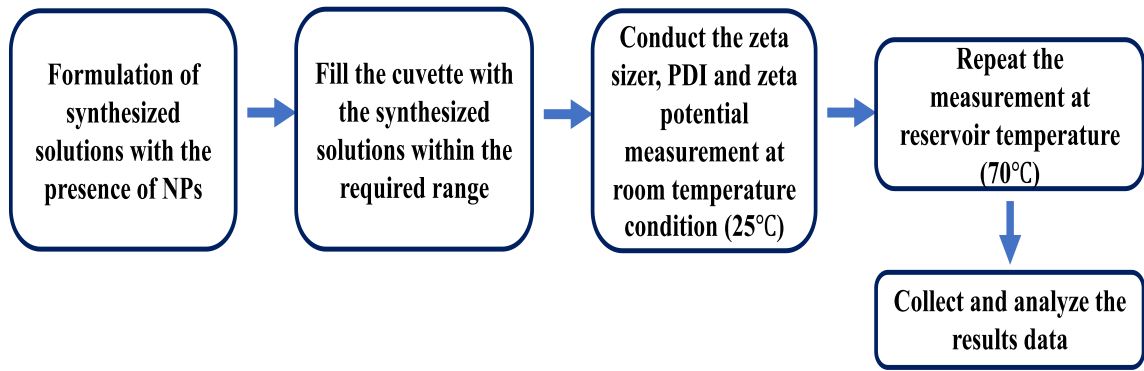
Figure 3.1: Experiment flow of characterization of nanofluid

3.3.3 Process Of Wettability Study

The contact angle measurement is conducted with Drop shape analyzer DSA 100B (KRÜSS). The contact angle formed between the oil-wet rock surface and a drop of synthesized solution is measured and analyzed. Firstly, the sandstone rock samples are prepared by cutting the sandstone rock samples into quarter. Appendix E.1 show the figure of slices sandstone rock samples. The rock samples are then rinsed with deionized water to remove the impurities and dried overnight with vacuum oven to make sure they are totally dry. Then, immerse the sliced rock samples in the formation water (19000ppm NaCl) under 90℃ for 2 days. Next, immerse them with Tapis crude oil for 3 days at 90℃ to make sure they are fully saturated with Tapis crude oil. Confining pressure of 1500 psi is applied to simulate the reservoir conditions. In this study, the number of readings is set at 30 sets since the transformation of the contact angle gets smaller after 30 sets of data. Meanwhile, the interval of each set of data is 1 second where the 30 sets of data will be recorded in 30 seconds. The contact angle measurement was conducted with varying concentrations of synthesized solution and each measurement was repeated for three times to confirm the results are consistent and accurate. Appendix E.2 shows the figure of contact angle measurement via the Drop Shape Analyzer. Figure 3.2 shows the flow of sample preparation and wettability measurements.

```
┌──────────────┐   ┌──────────────┐   ┌──────────────┐   ┌──────────────┐
│ Preparation of│  │ Saturation and│  │ Designation and│ │ Altering pH of│
│ Grey and Buff │→ │ Aging of quarter│→│ formulation of │→│ synthesized  │
│ Berea sandstone│ │ rock samples  │  │ MES/Low salinity│ │ solution into│
│ rock samples (cut│ │with Formation│  │ water/NPs in   │ │ Alkaline    │
│ into quarter  │  │ water (48hrs) │  │ different      │  │ condition   │
│ pieces) and grind│ │and then with │  │ concentrations │ └──────────────┘
│ with 45 μm    │  │ Tapis crude oil│ └──────────────┘         │
└──────────────┘   │ (72hrs)       │                           ↓
                   └──────────────┘                    ┌──────────────┐
                                                       │ Contact angle │
                                                       │ measurement   │
                                                       │ between oil-wet│
                                                       │ rock and      │
                                                       │ synthesized   │
                                                       │ solution with │
                                                       │ Drop Shape    │
                                                       │ Analyzer      │
                                                       └──────────────┘
```

Figure 3.2: Experiment flow of wettability study

3.3.4   Adsorption On Rock Surface Study

The aim of the adsorption study is to investigate the reduction of surfactant adsorbed onto the rock samples via adsorption capacity. The ranges of the concentration of MES surfactant applied in this phase are within the range 250ppm to 1500ppm. This is because the contact angle measured within this range provide significant contact angle reduction.

Firstly, the sandstone rocks are crushed and sieved into $125\mu m$ size. Then, fine grain samples are washed with deionized water to remove impurities. Next, the fine grains are dried overnight to ensure they are fully dried. 50ml of the different concentration of MES anionic surfactant are poured into the conical flask separately and 2g of the cleaned fines rock sample was added into each of the conical flask. Afterwards, they are placed into the shaking incubator at 150 rpm for 24 hours at ambient condition which could be referred to Appendix E.3. The same procedure was then repeated for 70℃. Next, centrifuge the supernatant solution for 30 minutes for 4000 rpm at room temperature. Lastly, the supernatant is collected from the centrifuge tube for UV-Vis spectrophotometer test to obtain the absorbance value. Throughout the processes, equilibrium concentration, C_{Ae}

can be obtained from calibration curve through Beer's Law. The amount of the adsorbed surfactant can be calculated from Eq. (3.1). The workflow for adsorption study is illustrated in Figure 3.3.

$$q = \frac{V \times (C_i - C_{Ae})}{m_{sandstone}} \times 10^{-3}$$

(3.1)

q = Amount of surfactant adsorbed (mg/1000 mg)

Ci = Initial surfactant concentration (mg/1000 ml)

CAe = Equilibrium concentration

V = Total solution volume (ml)

M$_{sandstone}$ = Total sandstone mass (mg)
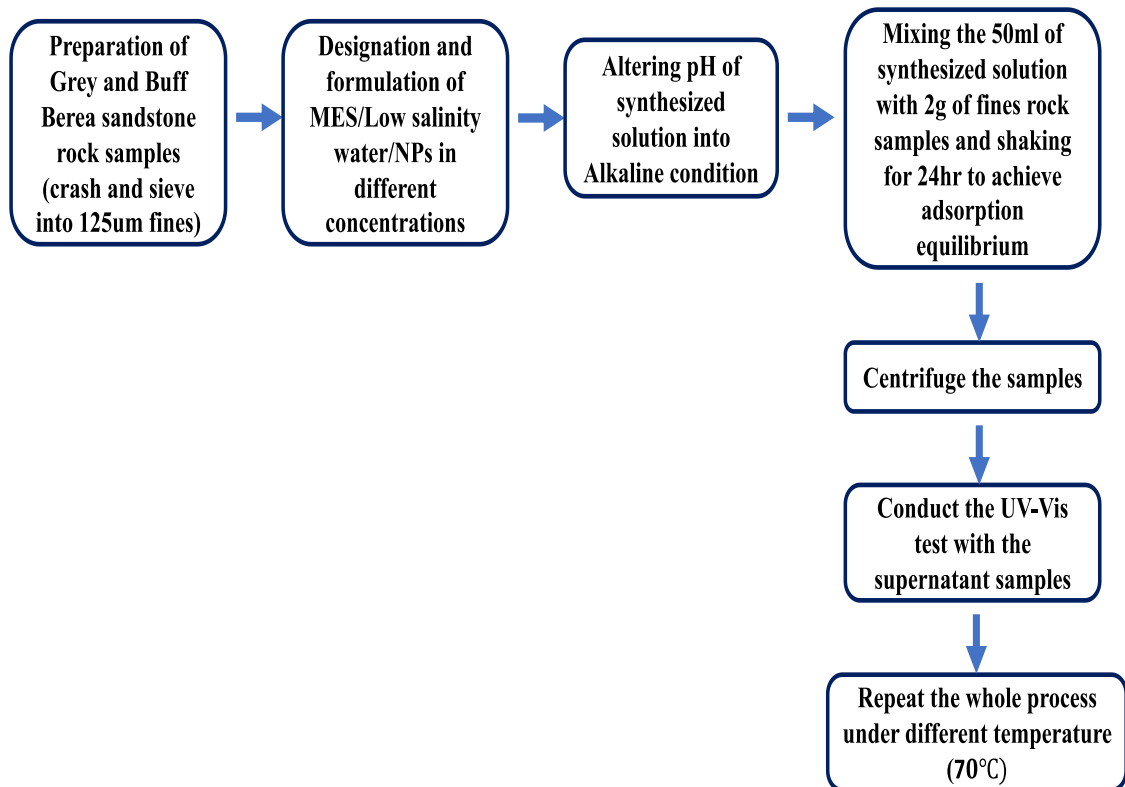
Figure 3.3: Experiment flow for adsorption study

3.3.5 Process Of Oil Recovery Study

The core-flooding test was conducted to obtain additional oil recovery from the sandstone rock with several optimum synthesized solutions. The selected optimum synthesized solutions are capable to achieve strong water-wet state and reduce surfactant losses significantly. Figure 3.4 and 3.5 shows the core-flooding equipment which was used for the oil-recovery study. Firstly, the transfer of core rock sample, formation water, Tapis crude oil, selected synthesized solution into the core-flooding accumulator. Then, the system was set at 1500psi and 70°C to simulate the reservoir condition. Removal of air bubbles from the system is crucial to prevent two-phase flow. Appendix E.4 shows the control valves which will be used during the injection of formation water, Tapis crude oil and synthesized solution. The procedure is to saturate the sandstone core sample with formation water (3.5 hours) and Tapis crude oil (5 hours). 1 pore volume (PV) of the formation water is injected at the flow rates of (0.2ml/min) through the sandstone rock core sample to obtain the oil recovery. The core sample is then injected with selected synthesized solution at 2.5 PV and follow by a post flush of 1 PV of the formation water. The whole core-flooding process is done in semi-batches processes which divided into two sections: saturation and injection sections. Monitoring the crude oil production along the injection process is needed to record the accumulated oil recovery and calculate the additional oil recovery. The workflow for core-flooding test illustrated in Figure 3.6.

Figure 3.4: Basic Core-flooding equipment

Figure 3.5: Basic core-flooding equipment
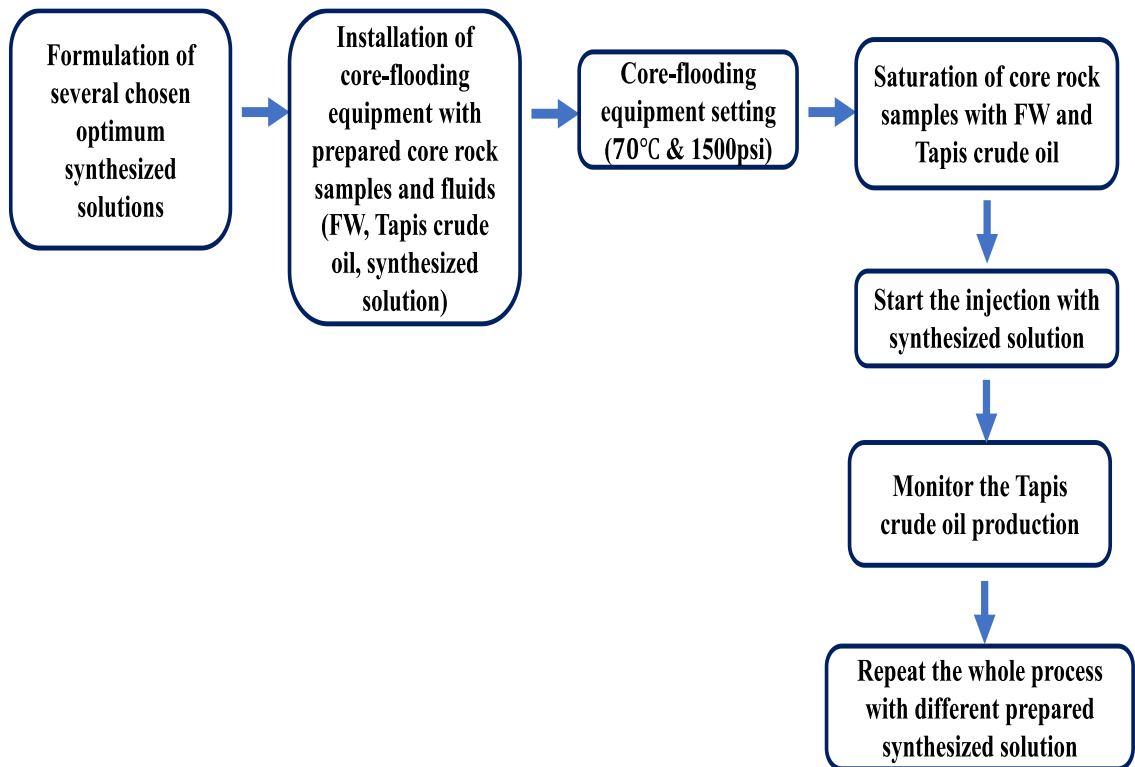
Figure 3.6: Experiment flow of oil recovery study

3.3.6   Process Of Winsor Phase Test And IFT Study

Winsor phase test is also known as phase behavior test which is used to verify the compatibility between surfactants, formation water and crude oil. The selected synthesized solutions are mixed with the formation water and Tapis crude oil in a centrifuge tube then transferred to a pipette. Then, the pipette was transferred to an oven with temperature maintained at $70\,°C$ for 1 day (24hr). The type of Winsor phase is evaluated according to the observation from the pipette. The Winsor types can be categorized into 4 types: Winsor Type I, Winsor Type II, Winsor Type III and Winsor Type IV. Winsor type III is the ideal Winsor type which indicates a low interfacial tension between the oil and the synthesized solution. Winsor type III is confirmed when a micro-emulsion phase is formed between the interface of Tapis crude oil and the synthesized solution. Estimation of interfacial tension (IFT) is determined from Chun Huh equation listed in Eq. (3.2). (3.3) and (3.4) below (Winanda et al., 2021). The workflow for phase behavior identification and IFT measurement is presented in Figure 3.6.

$$\sigma_o = \frac{V_o}{V_s} \, ; \quad \sigma_w = \frac{V_w}{V_s} \tag{3.2}$$

σ_o = oil solubility ratio

σ_w = water solubility ratio

v_o = volume of oil presence in microemulsion (ml)

v_w = volume of water presence in microemulsion (ml)

v_s = volume of added surfactant (ml)

$$\frac{1}{\sigma_o} + \frac{1}{\sigma_w} = \frac{2}{\sigma^*} \tag{3.3}$$

$$\gamma = \frac{C}{(\sigma^*)^2} \tag{3.4}$$

Where,

$\gamma = IFT$ (mN/m)

C = empirical constant value (0.3 mN/m)

σ^* = solubility ratio

| Formulation of several chosen optimum synthesized solutions | → | Mixed the specific amount of synthesized solution with formation water and Tapis crude oil | → | Observation and analyzation on the Winsor Types | → | Record the required data an estimate the IFT with Chun Huh equation |
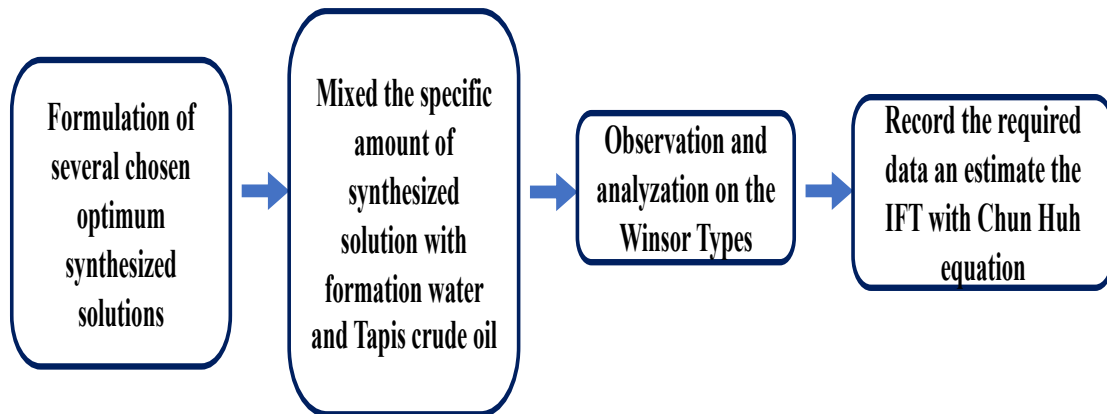
Figure 3.7: Phase behavior and IFT measurement

CHAPTER FOUR
RESULT AND DISCUSSION

4.1   Overview

In this chapter, the effectiveness and feasibility of the synthesized solutions to enhance additional oil recovery from the sandstone reservoir is analyzed and discussed. Each of the chemical materials, including low salinity water, surfactant and nanofluid, has the potential to increase the additional oil recovery individually. Besides, the nano-polystyrene plays an essential role in the synthesized solution. It not only shifts the oil-wet rock toward a stronger water-wet state, but it also functions to reduce the surfactant adsorption onto the rock surface, which could improve the synthesized solution effectiveness and economic performance. The experimental work covers the nanofluid characterization to identify the nanofluid stability. Contact angle measurement is used to evaluate the potential of a wide range of synthesized solutions to achieve a strong water-wet state. Some specific results of contact angle measurement are presented in Appendix A. The set of the synthesized solutions is then narrowed down for an adsorption study after the evaluation of the results from the wettability study. Lastly, the core-flooding test was implemented and result of additional oil recovery presented and discussed.

4.2   Characterization (Nanoparticles Size, PDI, Zeta Potential)

Zeta potential is the electrical potential exhibited by the slipping plane of any particle in the suspension. Meanwhile, it is the electrical potential difference between the static layer of the dispersion fluid attracted with the dispersed particles and the mobile dispersion fluid. The nanofluid is considered unstable when the zeta potential values range between +30mV to -30mV (Elochukwu et al., 2017). This is because flocculation and aggregation of nanoparticles tend to happen within the ranges of +30mV to -30mV. Therefore, it is essential to attain a larger magnitude of zeta potential to maintain the stability of the nanofluid and prevent aggregation of nanoparticles. A larger magnitude of zeta potential could incur larger repulsion forces between the particles in the synthesized solution. Aggregation of nanoparticles would cause log-jamming and formation damage which could negatively impact the oil recovery process (Ab Rasid et al., 2021).

4.2.1 Effect Of pH On Zeta Potential Of Synthesized Solutions

The effects of pH value on the stability of the synthesized solutions with nanoparticles was investigated. Table 4.1 shows the zeta potential results in acidic and alkaline conditions at ambient temperature. The synthesized solutions in acidic condition ranged between -4mV to -8mV, which is in the unstable region. Therefore, in the unstable region, a high tendency for nanoparticle aggregation occurs in the synthesized solution due to the lower repulsive force. The acidic condition would shift the zeta potential toward a positive zeta potential value due to the protonation where a substantial number of positive ions is released (Choi et al., 2014). The adsorption of H^+ ions and the negatively charged nanoparticles has reduced the electrostatic repulsive forces. Despite the synthesized solution being in the acidic condition, the zeta potential obtained were still in the negatively charged condition. It is because the pH value of the synthesized solution did not reach the isoelectric point, where there is no repulsive force occurring at the isoelectric point (Cacua et al., 2019). Therefore, the results indicated that the acidic condition would negatively impact the stability of the synthesized solution.

Table 4.1: Zeta potential of synthesized solutions at ambient temperature conditions

Synthesized solutions	Average Zeta Potential (mV)
750ppm MES + 250ppm $CaCl_2$ + 25ppm Nano-polystyrene + Alkaline Condition	-64.10
750ppm MES + 250ppm $CaCl_2$ + 25ppm Nano-polystyrene + Acidic Condition	-6.28
750ppm MES + 250ppm $MgCl_2$ + 25ppm Nano-polystyrene + Alkaline Condition	-58.00
750ppm MES + 250ppm $MgCl_2$ + 25ppm Nano-polystyrene + Acidic Condition	-4.42
750ppm MES + 250ppm $CaCl_2$ + 25ppm Nano-silica + Alkaline Condition	-70.87

750ppm MES + 250ppm CaCl$_2$ + 25ppm Nano-silica + Acidic Condition	-7.36
750ppm MES + 250ppm MgCl$_2$ + 25ppm Nano-silica + Alkaline Condition	-64.3
750ppm MES + 250ppm MgCl$_2$ + 25ppm Nano-silica + Acidic Condition	-6.30

On the other hand, Figure 4.1 indicated that the synthesized solutions in the alkaline conditions achieved a stable region at ambient temperature. The values of the zeta potential of the synthesized solutions ranged from -58mV to -70.86mV. Apparently, the zeta potential values were apart from the unstable region. The alkaline condition played an essential role in achieving the high stability of the synthesized solutions. The nanofluid will acquire more negative charge when turning into an alkaline condition which is attributed to the deprotonation. Meanwhile, in the alkaline condition, a more significant repulsion force occurred between the nanoparticles, anionic surfactant, and salinity water. Thus, the nanoparticles suspended in the salinity water will repel each other and agglomeration of the nanoparticles can be prevented. Several studies revealed that the pH value of the suspension is the most critical parameter in affecting the value of the zeta potential (Radnia et al., 2018; Chakraborty et al., 2020; Jafarbeigi et al., 2022). Study from Liu et al. (2020a) mentioned that the stability of the nanoparticles would affect the EOR process where unstable will cause agglomeration, which encourages pore throat blockage that reduces oil recovery. Therefore, applying the c-EOR method with the high-stability nanofluid is essential to achieve improvement in oil recovery. Meanwhile, turning the nanofluid into a high alkaline condition (more than 9.5 units) could maintain the stability of the nanofluid where a larger magnitude of zeta potential values can be achieved. Furthermore, the high pH condition can be favorable for the sandstone reservoir as it could result in larger repulsive forces and then detach the oil molecules from the rock surface.
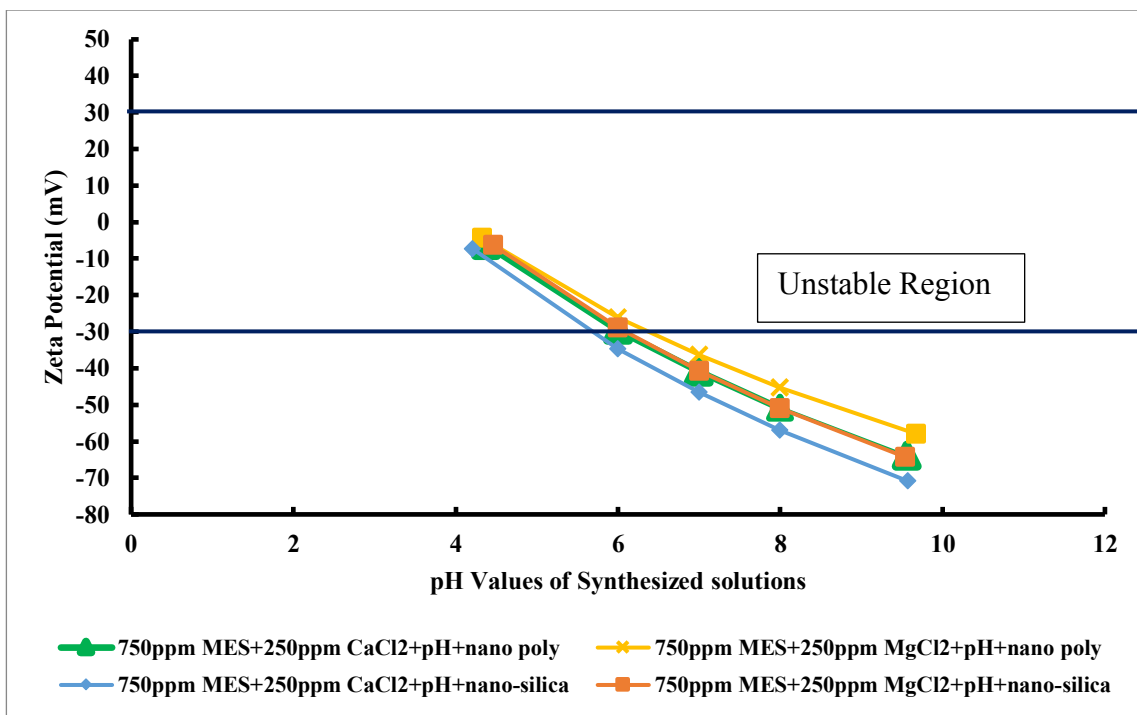
Figure 4.1: Zeta potential of synthesized solutions at ambient temperature conditions (25°C)

4.2.2 Effect Of Divalent Cations On Zeta Potential Of Synthesized Solutions

The present study investigated the effect of two different types of divalent cations ($CaCl_2$ and $MgCl_2$) which are synthesized under alkaline condition at 750ppm MES and 25ppm nanoparticles. According to Figure 4.1, the results revealed that the synthesized solution (250ppm $CaCl_2$ + 750ppm MES + 25ppm nanoparticles + alkaline conditions) showed a larger magnitude of the zeta potential compared to the synthesized solutions with $MgCl_2$. This can be attributed to the Mg^{2+} possessing a smaller atomic radius and higher affinity to water when compared to the Ca^{2+} (Liu et al., 2020b). Besides, the Mg^{2+} demonstrated stronger cation bridging and ion attraction due to the smaller atomic radius and higher electric charge (Liu et al., 2018). Therefore, it created a lower repulsive force, reducing the zeta potential magnitude. Consequently, the zeta potential of synthesized solutions with $MgCl_2$ are less negatively charged compared to the synthesized solutions with $CaCl_2$. Hence, the results indicated that synthesized solutions with the divalent cations ($CaCl_2$) showed a better combination than $MgCl_2$. Therefore, the synthesized

solution with the divalent cations ($CaCl_2$) should be prioritize for wettability, adsorption, and oil recovery studies.

4.2.3 Effect Of Types Of Nanoparticles On Zeta Potential Of Synthesized Solutions

This study investigated the effects of two different types of nanoparticles (nano-silica/nano-polystyrene) on the zeta potential of the synthesized solutions. The results indicated that synthesized solutions with nano-silica achieved a higher magnitude of zeta potential when compared to nano-polystyrene. This could be explained by the charge of the nanoparticles. The nano-silica is more negatively charged when compared to nano-polystyrene. Therefore, nano-silica could create a higher repulsive force when suspended in the synthesized solutions. In contrast, the less negatively charged nano-polystyrene has led to lower repulsive force in the synthesized solutions. The alkaline conditions and anionic surfactant MES promote the repulsive force in the synthesized solutions. Therefore, the synthesized solutions are in stable regions which beyond the ranges from +30mV to -30mV. Although the combinations of synthesized solutions with nano-silica are slightly higher than nano-polystyrene, the results in Figure 4.1 indicated that all the selected synthesized solutions are still capable of achieving high stability. Notably, the key function of the nanoparticles is to reduce surfactant losses during the c-EOR process. Therefore, nano-polystyrene with less negatively charged could be a better choice. The nano-polystyrene can be more attracted to the negatively charged rock surfaces and replace the excessive surfactant adsorption to the rock surfaces. Meanwhile, it is notably that combinations of (750ppm MES + 250ppm $CaCl_2$ + 25ppm nano-silica + alkaline conditions) achieved the highest stability among the selected synthesized solutions at ambient temperature. Nevertheless, both types of nanoparticles can achieve high stability, as shown in Figure 4.1. Therefore, both types of nanoparticles should be considered for further study. The polystyrene nanofluid could be considered in all rock types since it is stable and there is no study regarding polystyrene nanofluid flooding in different rock types.

4.2.4 Effect Of Temperatures On Zeta Potential Of Synthesized Solutions

Only limited studies investigated the effects of temperature on the zeta potential of the synthesized solution. Therefore, the present study investigated the effects of temperatures on zeta potential for the selected synthesized solutions. The zeta potential measurement was conducted in two different temperature conditions, which are ambient temperature (25℃) and reservoir temperature (70℃). The zeta potential measurement is conducted at reservoir temperature to verify the potential of the selected optimum synthesized solutions to maintain high stability at higher temperature.

The overall results are shown in Figure 4.2, only the synthesized solutions in alkaline conditions are in the stable region where the magnitude of zeta potential values are larger than -30mV. However, the synthesized solutions in acidic conditions range from -14mV to -18mV, which are in the unstable region. The overall results indicated that higher temperatures would affect the zeta potential of the synthesized solutions. The zeta potential of the synthesized solutions became less negatively charged due to the high sensitivity of the divalent cations in the synthesized solutions. The divalent cations aggressively attract the counter ions at a higher temperature. Thus, the repulsive force between the ions is reduced, and a smaller value of zeta potential is obtained which is less negatively charged. Moreover, study from Rezvani et al. (2018) indicated that elevated temperature negatively impacts the stability of the nanofluid. Nevertheless, the synthesized solutions under alkaline conditions are still within the stable region. In fact, alkaline condition can be assumed as a key parameter to maintain the synthesized solutions at a stable region which indicated that the repulsive force under alkaline conditions is still capable to prevent the aggregation of nanoparticles at reservoir temperature.

The results in Table 4.2 also indicated that the synthesized solutions with divalent cation (Ca^{2+}) could lead to a larger magnitude of zeta potential at reservoir temperature. Meanwhile, the synthesized solutions with Ca^{2+} ions are more stable compared to Mg^{2+} ions at reservoir temperature. It can be explained by the smaller radius and higher electric charged of Mg^{2+} ions compared to Ca^{2+} ions. Therefore, the Mg^{2+} ions led to stronger

attraction to the counter-ions such as the anionic surfactant and negatively charged NPs in the synthesized solution. Consequently, the stability of nanofluid is reduced. Meanwhile, this happened at the reservoir temperature (70℃), which has been verified with the results in Figure 4.2. Meanwhile, experimental work from Vinogradov et al., (2018) also revealed that the divalent cation (Mg^{2+}) is more sensitive to temperature compared to Ca^{2+} ions, which results in a smaller magnitude of zeta potential when the temperature increases. Study from Jaafar et al., (2009) mentioned that the zeta potential is independent when the ionic strength in the fluid is larger than 0.45 M. Reducing the concentration of salinity water could increase the repulsive forces and hence increase the magnitude of zeta potential (Sadatshojaei et al., 2019). However, 250ppm of divalent cations could perform better results in wettability alteration. Thus, it is considered the optimum concentration of salinity water to combine with the MES surfactant and nanoparticles. Meanwhile, it is notable that synthesized solutions with 250ppm of divalent cations under alkaline conditions were still within the stable region.

The zeta potential measurement conducted with the synthesized solutions combined with different types of nanoparticles (nano-silica/nano-polystyrene) at reservoir temperature. Based on the results in Table 4.2, the synthesized solution of (750ppm MES + 250ppm $CaCl_2$ + 25ppm Nano-silica + Alkaline Condition) showed the largest magnitude of zeta potential which is -40.13mV. The difference between the synthesized solution of (750ppm MES + 250ppm $CaCl_2$ + 25ppm Nano-polystyrene + Alkaline Condition) is only 2.4mV which can be considered as insignificant. The results indicated that synthesized solutions with nano-silica are slightly higher either in alkaline or acidic conditions. Besides, the magnitude of zeta potential also demonstrated a slightly higher value for the nano-silica combined with two types of divalent cations compared to nano-polystyrene. This can be attributed to the lesser negative charge of polystyrene. Thus, synthesized solutions with nano-silica created larger repulsive forces and a higher magnitude of zeta potential. Hence, nano-polystyrene could demonstrate stronger adsorption to the sandstone rock surfaces compared to nano-silica. Meanwhile, the nano-polystyrene can occupy more space on the rock surface and prevent the surfactant to adsorb onto the rock surface.

Table 4.2: Zeta potential of synthesized solutions at reservoir temperature conditions

Synthesized solutions	Average Zeta Potential (mV)
750ppm MES + 250ppm $CaCl_2$ + 25ppm Nano-polystyrene + Alkaline Condition	-37.73
750ppm MES + 250ppm $CaCl_2$ + 25ppm Nano-polystyrene + Acidic Condition	-15.63
750ppm MES + 250ppm $MgCl_2$ + 25ppm Nano-polystyrene + Alkaline Condition	-35.67
750ppm MES + 250ppm $MgCl_2$ + 25ppm Nano-polystyrene + Acidic Condition	-14.43
750ppm MES + 250ppm $CaCl_2$ + 25ppm Nano-silica + Alkaline Condition	-40.13
750ppm MES + 250ppm $CaCl_2$ + 25ppm Nano-silica + Acidic Condition	-18.47
750ppm MES + 250ppm $MgCl_2$ + 25ppm Nano-silica + Alkaline Condition	-38.13
750ppm MES + 250ppm $MgCl_2$ + 25ppm Nano-silica + Acidic Condition	-16.37
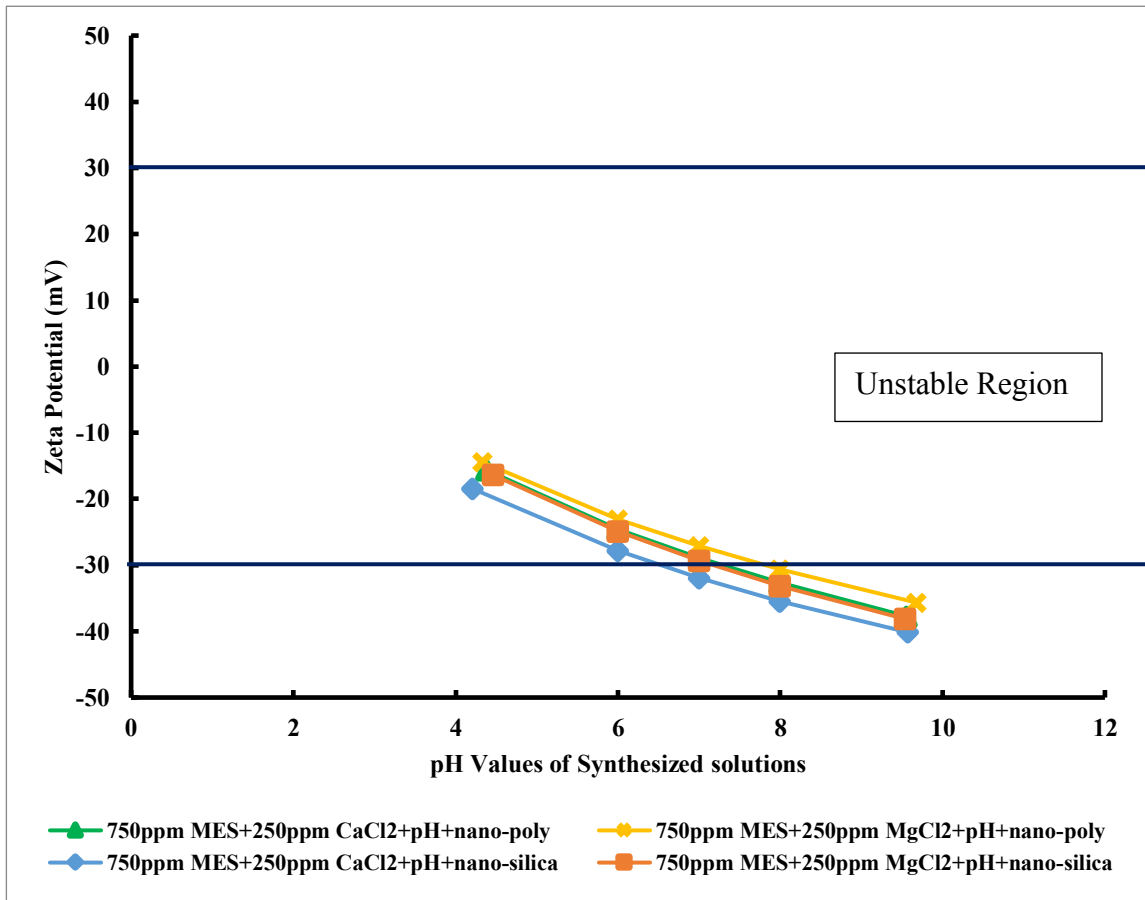
Figure 4.2: Zeta potential of synthesized solutions at reservoir temperature conditions (70°C)

4.2.5 Characterization Of Nanoparticles Size Of The Synthesized Solutions

Z-average size is measured with the zeta sizer via Dynamic Light Scattering (DLS). This technique measures the brownian motion and provides the relation to the suspended nanoparticles size. The Z-average measurement is achieved with the illumination of particles via the laser beam where the intensity of scattered light fluctuations is then recorded through the digital correlator. Meanwhile, the homogeneity between two signals is measured and calculated. The Z-average size of nanoparticles is measured, and the mean values are calculated because of its high reliability, accuracy, and stability. However, it is notable that the measurement of nanoparticles size only valid for the dispersion of nanoparticles in the liquid form because the measurement of Z-average is in

hydrodynamic parameter. Any minor modifications of the nanofluid would affect the reading of the results especially when there is small proportion of clump in the nanofluid. Therefore, measurement of zeta sizer Z-average should be taken immediately after the sonication to avoid agglomeration of nanoparticles in the suspension.

The effects of pH on the Z-average of the synthesized solutions at ambient temperature is shown in Figure 4.3. The Z-average of the selected synthesized solutions ranged from 260 d.nm to 382 d.nm either in alkaline or acidic conditions. Therefore, the nanoparticles suspended in the synthesized solutions are within the acceptable range, indicating that the NPs could maintain acceptable size in different pH conditions. Experimental work from Liu et al., (2020b) mentioned that different pH conditions only lead to an insignificant effect on the size of nanoparticles but substantially affect the zeta potential. Behera et al., (2022) obtained an average size of nano-silica with 432nm while synthesizing with the surfactant, low salinity water and polymer. Besides, their experimental work proved that it is sufficient to achieve an oil recovery factor of up to 12.7%. Sofla et al., (2018) mentioned that typical conventional sandstone reservoirs have pore throats size larger than 2000nm and carbonate reservoirs range from 3000nm to 7000nm. Therefore, the size of the nanoparticles obtained from the present study is far apart to cross the typical pore throat size of the reservoirs.

Meanwhile, the effectiveness of the synthesized solutions with nanoparticles could be maximized, and the log-jamming at the pore throats could be avoided. According to Figure 4.3, the Z-average of the nanoparticles under acidic conditions are slightly larger than the size in alkaline conditions. This is due to the lower repulsive forces created under the acidic conditions. In contrast, the size of nanoparticles in alkaline conditions is smaller due to the higher repulsive forces where the nanoparticles possess a higher potential to repel each other and avoid flocculation in the synthesized solutions. Nevertheless, the present study indicated that both alkaline and acidic conditions only lead to insignificant changes in nanoparticle size. Furthermore, the sizes of the nanoparticles presented in Table 4.3 indicated that it is within the acceptable ranges and suitable for further study.

The effects of two different divalent cations on the Z-average of nanoparticles at ambient temperature is shown in Figure 4.3. In comparison, the Z-average obtained from the synthesized solution (750ppm MES + 250ppm $CaCl_2$ + 25ppm Nano-polystyrene + Alkaline Condition) is 260.7d.nm, while from the synthesized solution (750ppm MES + 250ppm $MgCl_2$ + 25ppm Nano-polystyrene + Alkaline Condition) is 269.53d.nm. The difference in the Z-average between these two synthesized solutions can be trivial, where only less than 10 d.nm is obtained. Meanwhile, the nanoparticles size of the synthesized solutions with different types of divalent cations obtained in acidic conditions also presented a minor difference. However, the overall results proved that the synthesized solutions with $CaCl_2$ are slightly lower than $MgCl_2$. This is due to the smaller ionic radius of Mg^{2+}, which has a higher electric charge. Therefore, Mg^{2+} has stronger reaction strength compared to Ca^{2+}. The hydration forces promote the penetration of smaller cations through the water layer of nanoparticles and thus resulting in smaller repulsive forces. As a result, the combinations of synthesized solutions with Mg^{2+} would lead to larger nanoparticles size compared to Ca^{2+}. Study from Liu et al., (2020b) also revealed that Ca^{2+} has a higher critical aggregation concentration (CAC) compared to Mg^{2+}. Meanwhile, synthesized solutions of nanofluid with Ca^{2+} would lead to higher zeta potential and smaller nanoparticles. Although Mg^{2+} provided slightly higher size of nanoparticles, the nanoparticles ranges are still acceptable. Nevertheless, the present study proved that Ca^{2+} is more suitable for the synthesized solution with the MES anionic surfactant and nanoparticles with negative charge.

From the overall results in Table 4.3, it is clearly observed that the Z-average of the synthesized solutions with nano-polystyrene are smaller than nano-silica. This is observed at different pH value conditions and divalent cations conditions. The synthesized solution of (750ppm MES + 250ppm $CaCl_2$ + 25ppm Nano-polystyrene + Alkaline Condition) recorded the nanoparticles size of 260.7 d.nm while the synthesized solution of (750ppm MES + 250ppm $CaCl_2$ + 25ppm Nano-silica + Alkaline Condition) obtained with 324.23d.nm. The difference in Z-average between the two types of synthesized solution with similar pH conditions and the same divalent cation is 63.53d.nm. Meanwhile, the difference between the two types of nanoparticles in the synthesized solutions with

acidic conditions are similar in the alkaline condition. Thus, this indicates that nano-silica exhibited larger nanoparticles size compared to nano-polystyrene while suspended in the synthesized solutions. This can be attributed to the original size of the NPs in powder-solid form. The size of nano-silica is within the ranges of 30nm to 70nm, while the size of nano-polystyrene has an average of 30nm. Thus, the nano-silica suspended in the synthesized solutions are larger than the size of polystyrene. Nevertheless, the difference in the size of the nanoparticles in different synthesized solutions can still be considered insignificant. The less negatively charged nano-polystyrene increased the size of nano-polystyrene in the synthesized solutions due to the lesser repulsive forces between the particles. Based on Figure 4.3, the overall results are acceptable, where nano-polystyrene demonstrated a smaller size in all the selected synthesized solutions. By analyzing the overall results in Table 4.3, the effects of pH values and the types of NPs are more significant compared to the effect of divalent cations. However, both types of NPs sizes are small enough to penetrate through the typical pore throat of sandstone reservoirs.

Table 4.3: Z-average of nanoparticles in synthesized solutions at ambient temperature conditions

Synthesized solutions	Average Size (d.nm)
750ppm MES + 250ppm $CaCl_2$ + 25ppm Nano-polystyrene + Alkaline Condition	260.70
750ppm MES + 250ppm $CaCl_2$ + 25ppm Nano-polystyrene + Acidic Condition	297.90
750ppm MES + 250ppm $MgCl_2$ + 25ppm Nano-polystyrene + Alkaline Condition	269.53
750ppm MES + 250ppm $MgCl_2$ + 25ppm Nano-polystyrene + Acidic Condition	314.30
750ppm MES + 250ppm $CaCl_2$ + 25ppm Nano-silica + Alkaline Condition	324.23
750ppm MES + 250ppm $CaCl_2$ + 25ppm Nano-silica + Acidic Condition	368.43

750ppm MES + 250ppm MgCl$_2$ + 25ppm Nano-silica + Alkaline Condition	339.73
750ppm MES + 250ppm MgCl$_2$ + 25ppm Nano-silica + Acidic Condition	381.07
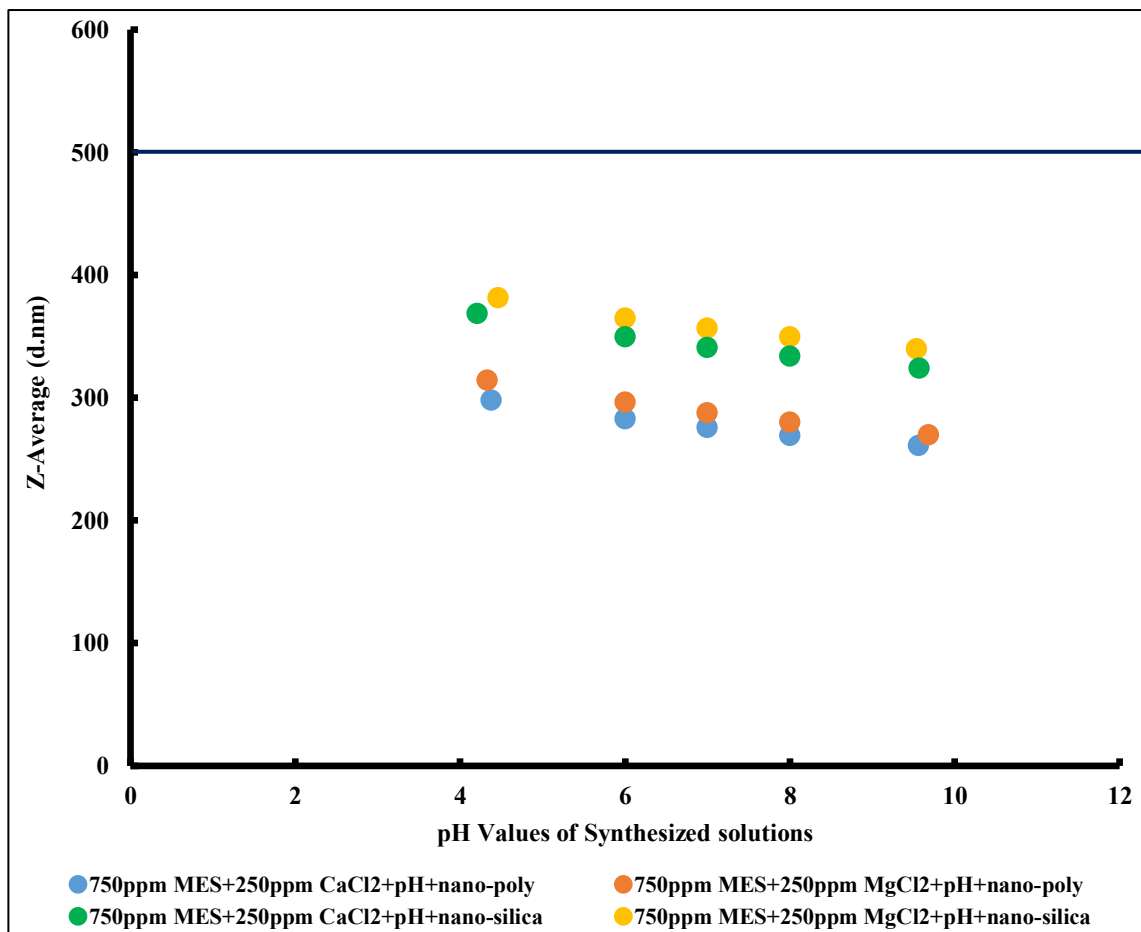
Figure 4.3: Z-average of nanoparticles in synthesized solutions at ambient temperature conditions (25°C)

4.2.6 Characterization Of Nanoparticles Size Of The Synthesized Solutions At Reservoir Temperature Conditions

In comparison, the Z-average shown in Figure 4.3 are slightly higher than in Figure 4.2. Thus, this indicated that increasing temperatures up to reservoir temperature minor effect on the size of the nanoparticles. However, the effects of pH value on the Z-average size of synthesized solutions are verified, where they have demonstrated a similar trend in

ambient and reservoir temperature conditions. The synthesized solutions with the alkaline condition could achieve smaller nanoparticles size distribution at reservoir temperature compared to acidic condition.

The relationship between the two different types of divalent cations and the size of nanoparticles at reservoir temperature has also been confirmed. The trend is similar to the ambient temperature condition. The size of the nanoparticles at reservoir temperature is slightly larger than the NPs in ambient temperature. This could be attributed to the presence of divalent cations. The negatively charged nanoparticles tend to attract to the divalent cations in the synthesized solution. The increasing temperature would increase the activities of divalent cations where stronger attraction forces between the divalent cations and the negatively charged NPs are promoted. Meanwhile, the presence of MES anionic surfactant will attract the divalent cations, which causes the instability of NPs. In conjunction with the zeta potential results in Figures 4.1 and 4.2, the stability of NPs reduced as the temperature increased. Thus, the NPs size slightly increased can be attributed to the attraction between the divalent cations and the NPs. A study by Mahmoudi et al., (2019) revealed that the temperature increase will reduce the stability of nanoparticles with the presence of salinity water (divalent cations) and consequently reduce the oil recovery factor. However, the present experimental work indicated that size of the NPs would not be significantly affected by the increase in temperature.

The difference in the Z-average between nano-silica and nano-polystyrene are mainly due to the original size of the nanoparticles and the strength of the negative charge of nanoparticles. The average original size of nano-silica in the powder form are larger than the nano-polystyrene. Thus, the Z-average of the nano-silica are larger than nano-polystyrene when suspended in the synthesized solution. In comparison with the results in ambient temperature condition, the difference in the Z-average between nano-polystyrene and nano-silica at reservoir temperature are similar to the size at ambient temperature. Thus, this indicates that temperature would not significantly affect the size of the nanoparticles suspended in the synthesized solution. The key parameter that affect the size of nanoparticles are the pH value, divalent cations, and the original size of the

nanoparticles. Udoh, (2021) mentioned that the reduction of nanoparticle size would increase the particle density and generate higher structural disjoining pressure. Hence, the larger disjoining pressure could easily detach the oil molecules from the rock surface. Nevertheless, the overall size of the different types of synthesized solutions showed an acceptable and good Z-average of nanoparticles size either with nano-silica or nano-polystyrene. Besides, it is noteworthy that alkaline condition could significantly reduce the size of the nanoparticles, whether it is ambient or reservoir temperature.

Although the size of the nanoparticles for the synthesized solutions, either with nano-polystyrene or nano-silica, overall fall between the ranges of 300d.nm to 500d.nm, they can still find application in condition as the sizes of the nanoparticles are significantly smaller than the typical pore throat sizes. The present study has proven that the size of the nanoparticles could be reduced to the range of 1 to 100nm. However, this only happens when the nanofluid is sonicated at high amplitude and extended sonification time. In this present study an attempt was made to achieve particle distribution below 100 d.nm by applying sonification amplitude of 60 for 20 minutes and particle size for synthesized solution 750ppm MES + 250ppm $CaCl_2$ + 25ppm Nano-polystyrene + Alkaline Condition measured 94 d.nm and 750ppm MES + 250ppm $CaCl_2$ + 25ppm Nano-silica + Alkaline Condition measured 96 d.nm. This implies that nanofluid status can be achieved for the synthesized solutions but at higher sonification criteria. Besides, the size of the nanoparticles larger than 100d.nm could be attributed to the delay time of measurement.

Table 4.4: Z-average of nanoparticles in synthesized solutions at reservoir temperature conditions

Synthesized solutions	Average Size (d.nm)
750ppm MES + 250ppm $CaCl_2$ + 25ppm Nano-polystyrene + Alkaline Condition	288.03
750ppm MES + 250ppm $CaCl_2$ + 25ppm Nano-polystyrene + Acidic Condition	306.00

|	
750ppm MES + 250ppm MgCl$_2$ + 25ppm Nano-polystyrene + Alkaline Condition	297.63
750ppm MES + 250ppm MgCl$_2$ + 25ppm Nano-polystyrene + Acidic Condition	321.37
750ppm MES + 250ppm CaCl$_2$ + 25ppm Nano-silica + Alkaline Condition	356.40
750ppm MES + 250ppm CaCl$_2$ + 25ppm Nano-silica + Acidic Condition	493.60
750ppm MES + 250ppm MgCl$_2$ + 25ppm Nano-silica + Alkaline Condition	398.70
750ppm MES + 250ppm MgCl$_2$ + 25ppm Nano-silica + Acidic Condition	520.97
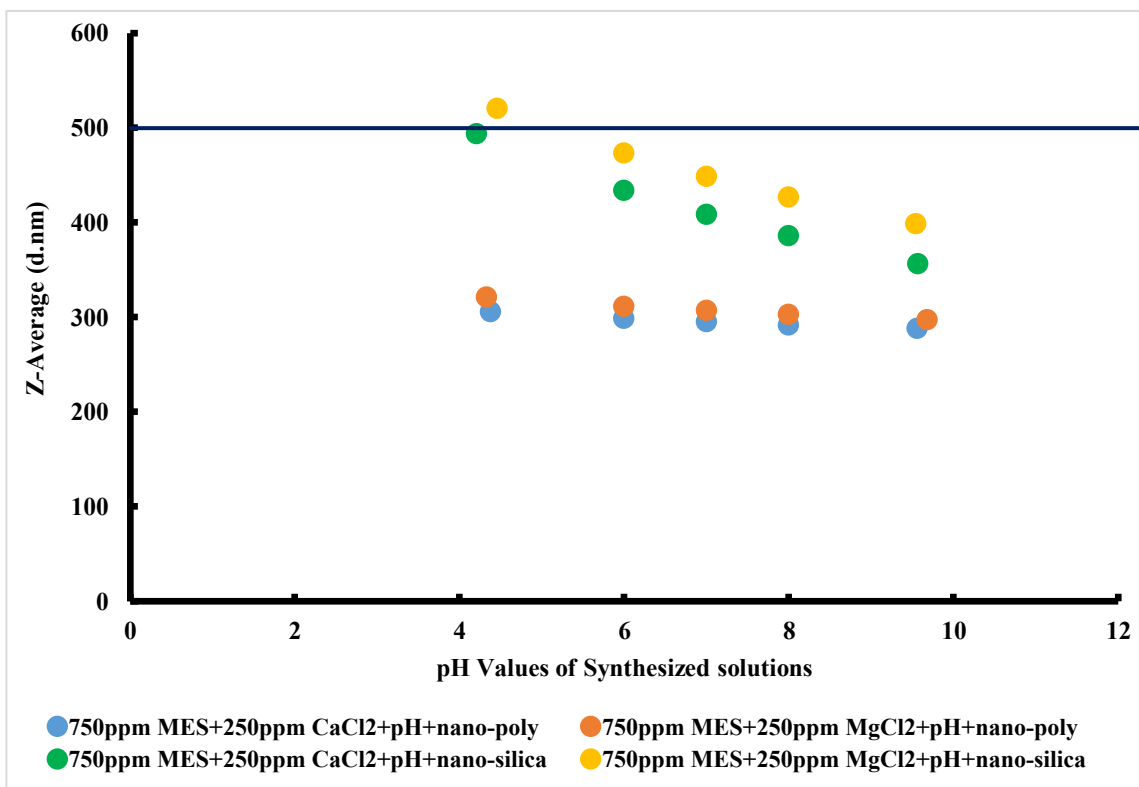
Figure 4.4: Z-average of nanoparticles in synthesized solutions at reservoir temperature conditions (70°C)

4.2.7 Characterization Of PDI Values Of The Synthesized Solutions At Ambient Temperature Condition

The polydispersity index (PDI) is used to determine the wideness of the particle size distribution, which exhibited the tendency of the nanoparticles to aggregate in the solution. Thus, sonication of the nanofluid is crucial to prevent the agglomeration of nanoparticles in the synthesized solution. PDI is a dimensionless number, which can be used to identify the homogeneity of the nanoparticles dispersed in the synthesized solution. Generally, a PDI value greater than 0.7 is considered extremely polydisperse, where the distribution of nanoparticles is very broad. On the other hand, a PDI value smaller than 0.5 is typically referred to the monodisperse solution.

Figure 4.5 shows the PDI values of the synthesized solutions in all the selected conditions at ambient temperature below 0.6. The synthesized solutions under acidic condition ranged from 0.4 to 0.6. However, the PDI values of the synthesized solutions under alkaline condition are within the range of 0.2 to 0.32, which are lower than the PDI values in acidic condition. Therefore, turning the synthesized solutions into alkaline condition could relatively reduce the PDI values to the desired values. Besides, the PDI values for all the synthesized solutions under alkaline condition can be considered homogeneous solution as the PDI values are very low. According to Agi et al., (2020), the nanofluid can be considered as relatively homogeneous solution when the PDI value is lower than 0.5. The results in Table 4.5 below indicated that the PDI values of the synthesized solution ($750ppm\ MES + 250ppm\ CaCl_2 + 25ppm\ Nano$-$polystyrene + Acidic$ Condition) is more than 0.5, which cannot be considered as homogeneous solution. The effects of different types of divalent cations on the PDI values of the synthesized solutions can be considered insignificant. This is because the difference in the PDI values between the synthesized solutions with $CaCl_2$ and $MgCl_2$ are small.

Besides, the overall results shown in Table 4.5 indicated that nano-silica demonstrated lower PDI values compared to nano-polystyrene. This could be attributed to the higher negative charge of the nano-silica compared to nano-polystyrene. Thus, higher repulsion force between the particles were created, which achieved lesser clustering

and ensures homogenous particles size distribution (Lin et al., 2019). The overall results indicated that most of the synthesized solutions are homogeneous solutions. This can be attributed to the pH conditions and type of nanoparticles. Besides, the presence of co-ions in the synthesized solutions with divalent cation might reduce the stability of the synthesized solutions, resulting in larger nanoparticle size and higher PDI values (Keykhosravi et al., 2019). Meanwhile, the presence of MES anionic surfactant and cations divalent simultaneously might negatively impact the stability, size and PDI values of the nanofluid. The present study clearly revealed that pH values, types of nanoparticles and the presence of different types of divalent cations would affect the PDI values. Nevertheless, all the selected synthesized solutions in Figure 4.5 fall in the acceptable ranges, which are considered relatively homogeneous solution except the synthesized solution (750ppm MES + 250ppm $CaCl_2$ + 25ppm Nano-polystyrene + Acidic Condition).

Table 4.5: PDI values of synthesized solutions presence with NPs at ambient temperature conditions

Synthesized solutions	Polydispersity Index (PDI)
750ppm MES + 250ppm $CaCl_2$ + 25ppm Nano-polystyrene + Alkaline Condition	0.312
750ppm MES + 250ppm $CaCl_2$ + 25ppm Nano-polystyrene + Acidic Condition	0.579
750ppm MES + 250ppm $MgCl_2$ + 25ppm Nano-polystyrene + Alkaline Condition	0.243
750ppm MES + 250ppm $MgCl_2$ + 25ppm Nano-polystyrene + Acidic Condition	0.457
750ppm MES + 250ppm $CaCl_2$ + 25ppm Nano-silica + Alkaline Condition	0.244
750ppm MES + 250ppm $CaCl_2$ + 25ppm Nano-silica + Acidic Condition	0.422
750ppm MES + 250ppm $MgCl_2$ + 25ppm Nano-silica + Alkaline Condition	0.318

750ppm MES + 250ppm MgCl$_2$ + 25ppm Nano-silica + Acidic Condition	0.410

Figure 4.5: PDI values of synthesized solutions presence with NPs at ambient temperature conditions (25°C)

4.2.8 Characterization Of PDI Values Of The Synthesized Solutions At Reservoir Temperature Conditions

Figure 4.6 shows the results of PDI values with the selected synthesized solutions at reservoir temperature condition. The overall PDI values obtained were still within the acceptable ranges where the selected synthesized solutions are considered homogeneous solutions. Based on Table 4.6, there is only one synthesized solution that exceeded the acceptable PDI value (less than 0.5), which is (750ppm MES + 250ppm CaCl$_2$ + 25ppm Nano-silica + Acidic Condition). Evidently, the synthesized solution under alkaline condition at reservoir temperature still led to lower PDI values compared to acidic condition. Therefore, it is essential to apply the alkaline condition to the synthesized

solution to achieve high nanofluid stability. The effects of different types of divalent cations only led to minor changes at reservoir temperature. Hence, this study indicated that different types of divalent cations would not drastically affect the size and PDI value of nanofluid. The nano-silica presented larger PDI values compared to nano-polystyrene, which is in line with the results of the size of the nanoparticles. It is noticeable that nano-polystyrene demonstrated smaller particle size and lower PDI values either at ambient temperature or reservoir temperature conditions. This is because of the smaller average size of nano-polystyrene before being suspended in the synthesized solutions. Even though the nano-silica has led to higher PDI values, it is still below 0.5 which is still considered as homogeneous solution. Therefore, the synthesized solutions with nano-polystyrene and nano-silica are suitable for further study. For instance, nano-polystyrene could be combined with other types of chemical materials to investigate the efficiency of wettability alteration and oil recovery enhancement. The application of NPs could also be applied in different sectors of the oil and gas industry since they demonstrated an acceptable and low PDI value while dispersed in the fluid.

Table 4.6: PDI values of synthesized solutions presence with NPs at reservoir temperature conditions

Synthesized solutions	Polydispersity Index (PDI)
750ppm MES + 250ppm $CaCl_2$ + 25ppm Nano-polystyrene + Alkaline Condition	0.187
750ppm MES + 250ppm $CaCl_2$ + 25ppm Nano-polystyrene + Acidic Condition	0.316
750ppm MES + 250ppm $MgCl_2$ + 25ppm Nano-polystyrene + Alkaline Condition	0.173
750ppm MES + 250ppm $MgCl_2$ + 25ppm Nano-polystyrene + Acidic Condition	0.387
750ppm MES + 250ppm $CaCl_2$ + 25ppm Nano-silica + Alkaline Condition	0.251

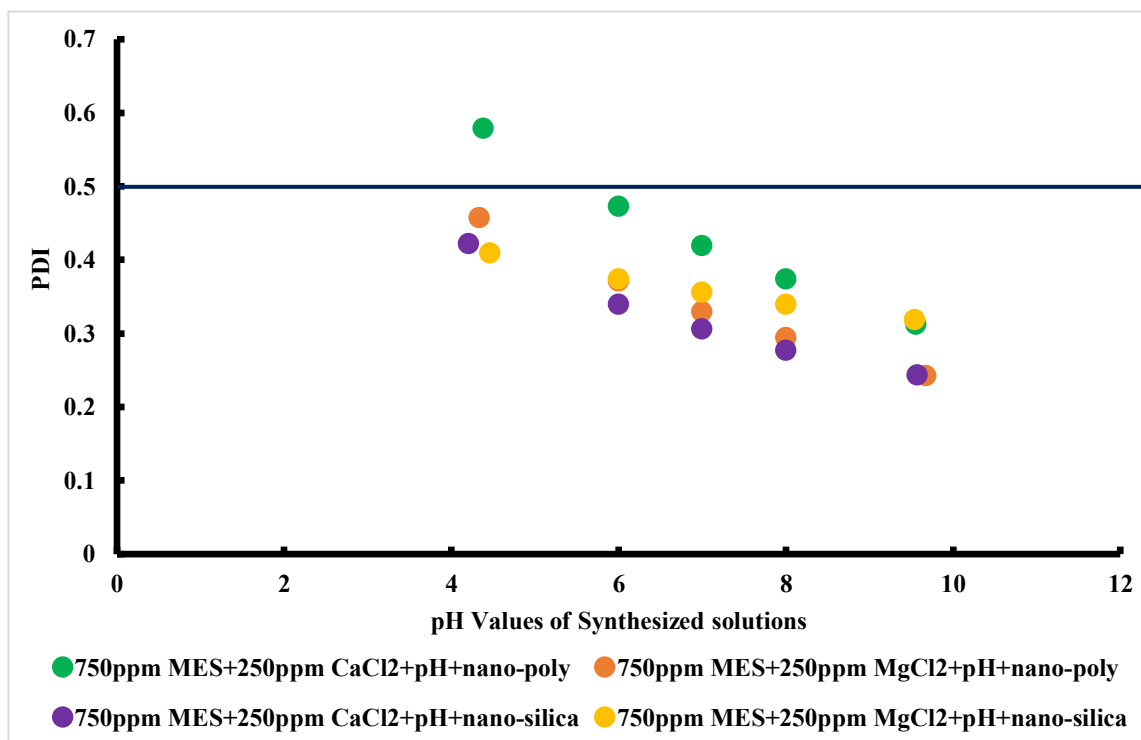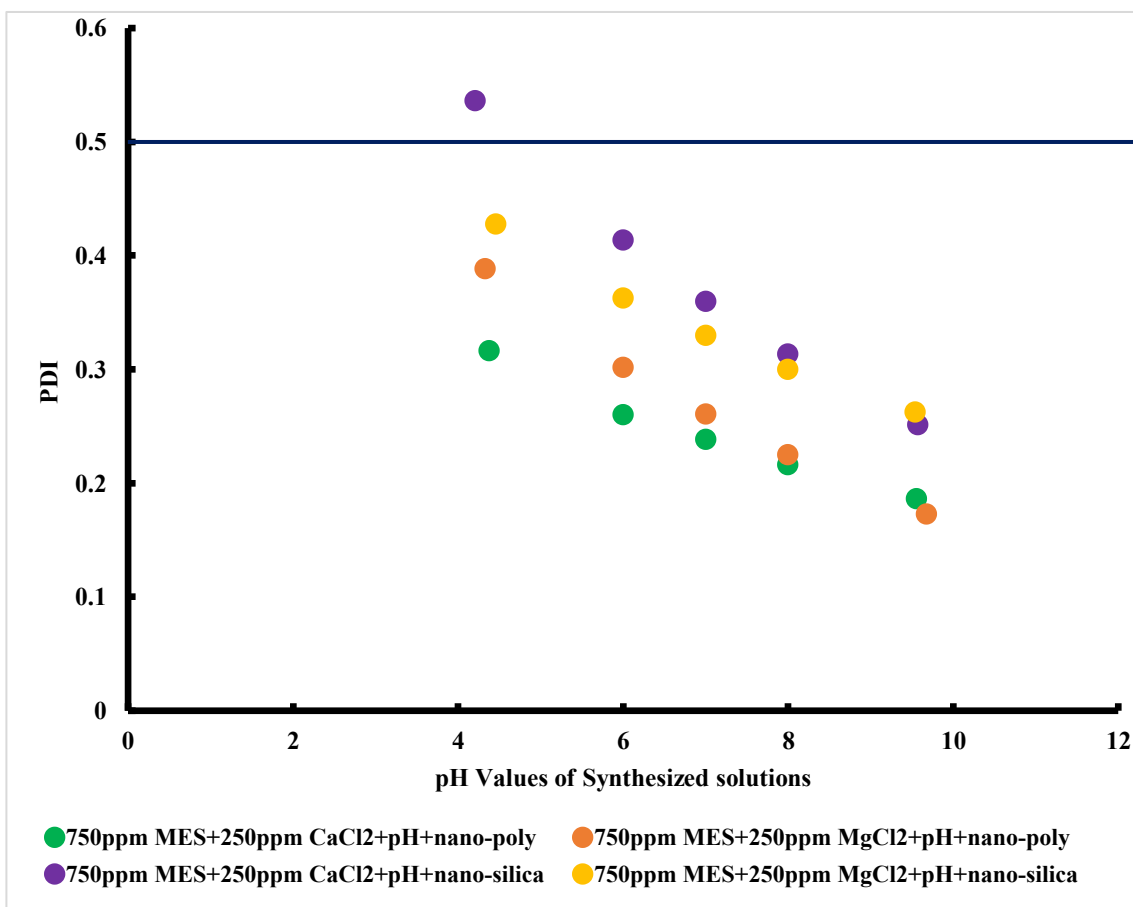|	
750ppm MES + 250ppm CaCl$_2$ + 25ppm Nano-silica + Acidic Condition	0.536
750ppm MES + 250ppm MgCl$_2$ + 25ppm Nano-silica + Alkaline Condition	0.263
750ppm MES + 250ppm MgCl$_2$ + 25ppm Nano-silica + Acidic Condition	0.428

Figure 4.6: PDI values of synthesized solutions presence with NPs at ambient temperature conditions (70°C)

4.3 Phase Behavior And IFT Measurement

The phase behavior study investigates the interaction between crude oil, brine, and synthesized solution and identifies the Winsor type behavior at the separation phase. Besides, the interfacial tension value can be estimated through the Chun Huh equation, which has been listed in Chapter 3. This study was conducted at reservoir temperature to achieve accurate results and only two types of synthesized solutions were applied which are (750ppm MES + 250ppm $CaCl_2$ + 25ppm Nano-polystyrene + Alkaline Condition) and (750ppm MES + 250ppm $MgCl_2$ + 25ppm Nano-polystyrene + Alkaline Condition). The result shown in Table 4.7 revealed that both synthesized solutions could achieve Winsor Type III, where there are micro-emulsions formed in the separation phase. The presence of high salinity water in the system increases the hydrophobicity of MES anionic surfactant. Thus, the surfactant will penetrate out from the brine to form a micro-emulsion in the separation phase (Phukan et al., 2020). Behera et al. 2022 mentioned that the occurrence of micro-emulsion between the oil and water phase is one of the main reasons for reducing the IFT in the oil-water system. In comparison, the synthesized solution with $CaCl_2$ showed a higher micro-emulsion volume, resulting in lower interfacial tension. Several studies mentioned that lower interfacial tension could result in a higher oil recovery factor (Kumar et al., 2018; Pal et al., 2018; Ahsaei et al., 2022). Experimental work from Pan et al., 2020 compared the IFT obtained from two types of surfactants. Their study mentioned that surfactant which achieved the lowest interfacial tension between water and oil resulted to the highest oil recovery. Thus, it is essential to achieve lower interfacial tension to enhance the oil recovery factor.

Table 4.7: Determination of Winsor types of the selected synthesized solutions

Synthesized solutions	Winsor Types	Separation phase behavior
750ppm MES + 250ppm $CaCl_2$ + 25ppm Nano-polystyrene + Alkaline Condition	Winsor Type III	
750ppm MES + 250ppm $MgCl_2$ + 25ppm Nano-polystyrene + Alkaline Condition	Winsor Type III	

Table 4.8 presented the calculation results by applying the Chun Huh equation and the data obtained from the phase behavior study. The IFT value obtained with the synthesized solution of (750ppm MES + 250ppm $CaCl_2$ + 25ppm Nano-polystyrene + Alkaline Condition) is lower than the synthesized solution of (750ppm MES + 250ppm $MgCl_2$ + 25ppm Nano-polystyrene + Alkaline Condition). Thus, this result further prove that a synthesized solution with $CaCl_2$ could lead to lower interfacial tension in the system. This statement agrees with the experimental work from (Nezhad et al., 2021), where the IFT values obtained by the researchers for $CaCl_2$ and $MgCl_2$ at 1000ppm are 2.5 mN/m and 5 mN/m, respectively. Also, study from Pillai et al. (2018) highlighted that increasing

pH value toward alkaline condition could reduce the IFT in the oil/water system. Thus, the alkaline condition of the synthesized solution aided in the IFT reduction. Furthermore, increasing temperature from 70°C to 100°C will only cause minor changes in the IFT between brine and oil (Aggelopoulos et al., 2011). Thus, temperature ranges 60 to 70°C is optimum condition for IFT reduction.

Table 4.8: Interfacial tension results calculated by Chun Huh Equation

Synthesized solutions	V_o (ml)	V_w (ml)	V_s (ml)	σ_o	σ_w	$\sigma *$	$\gamma *$ (IFT) (mN/m)
750ppm MES + 250ppm $CaCl_2$ + 25ppm Nano-polystyrene + Alkaline Condition	1.6	2.2	0.6	2.67	3.67	3.09	0.0315
750ppm MES + 250ppm $MgCl_2$ + 25ppm Nano-polystyrene + Alkaline Condition	0.8	1.4	0.6	1.33	2.33	1.70	0.1042

In comparison with the results in Table 4.9, the IFT values obtained from this study are considered acceptable and low. Even though the synthesized solutions could not achieve ultra-low IFT value, it achieved a favorable result which is similar or even lower than the results obtained from the other literature studies. The lowest IFT value obtained from the present study is 0.0315 mN/m with the synthesized solution (750ppm MES + 250ppm CaCl2 + 25ppm Nano-polystyrene + Alkaline Condition). Study from Ramos et al., (2020) mentioned that chemical materials that achieved IFT values below 0.1 mN/m have a high opportunity to be applied for field operation for c-EOR. The synthesized solution of (750ppm MES + 250ppm MgCl2 + 25ppm Nano-polystyrene + Alkaline Condition) is slightly exceeds 0.1 mN/m, which still achieve better results compared to other previous experimental works. Thus, it is worth further investigating the application and feasibility of the selected synthesized solution with wettability, adsorption and c-EOR studies.

Table 4.9: Summary IFT results obtained from different previous experimental work

Literatures	Chemicals	Temperatures (℃)	Crude Oil Gravity (API°)	IFT values (mN/m)
Behera et al., 2022	Low salinity water + Dioctyl Sodium Sulfosuccinate (AOT) anionic surfactant + polymer + nanoparticles	60	43.3	0.27
Joshi et al., 2022	Cocamidopropyl betaine (CAPB) surfactant +nano-silica	90	23.3	0.095
Phukan et al., 2020	Sodium Dodecyl Sulfate (SDS) Surfactant + alkaline + brine	70	31	0.0068
Winanda et al., 2021	Low salinity water + Linear Alkylbenzene Sulfonate (LAS) anionic surfactant	70	31.9	0.108
Xu et al., 2022	Betaine-type Zwitterionic surfactant	25	28.5	0.077

4.4   Effect Of Surfactant Concentration On Wettability Alteration

Based on the results in Figure 4.7, the contact angle is significantly undergoing declination trend starting from the concentration of MES with 100ppm up to 1000ppm. The contact angle measurement for the formation water (FW) for Grey and Buff Berea sandstone rocks are 91.7° and 98.4° respectively. The reduction of contact angle reached the minimum point at 1000ppm of MES. Meanwhile, the contact angle gradually increased as concentration of MES increased from 1250ppm to 5000ppm.
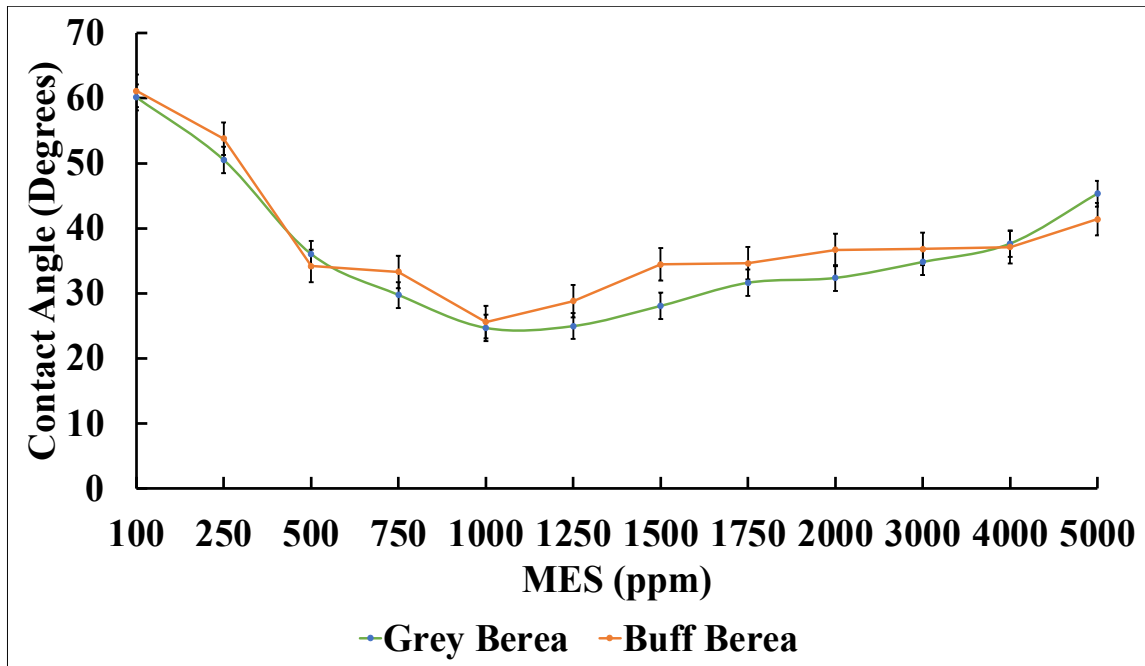
Figure 4.7: Effect of MES Concentration on Contact Angle Measurement (Grey and Buff Berea)

The results in Figure 4.7 revealed that the concentration of MES surfactant at 1000ppm reached the Critical Micelle Concentration (CMC) point. The CMC point is approximately at 1150ppm as shown in Appendix B.1. It is shown that the contact angle obtained at 1000ppm is the lowest. The adsorption of MES surfactant onto the rock surface will continue with the rising concentration via the electrostatic interaction between the rock surface and the hydrophilic head group of MES surfactant. Hence, a monolayer is formed at the rock-fluid interface. Meanwhile, the interaction between hydrophobic part of MES surfactant molecule and the adsorbed Tapis crude oil molecule on the mineral surface caused the wettability shift towards water-wet state (Youssif et al., 2018). The hydrophobic tail groups of the MES surfactant are attracted to the rock surface, which causes the hydrophilic part of the MES surfactant to be exposed to the interface between rock and fluid. However, any increment of the concentration of MES surfactant will no longer contribute to wettability alteration, but it will cause the formation and aggregation of micelles (Massarweh et al., 2020). Therefore, the contact angle will gradually increase when the concentration of MES surfactant is beyond the CMC point. The formation of the micelles restricts the release of surfactant molecule to the solid-liquid interface. Moreover,

the large amount of surface hydrophobicity also causes contact angle to increase beyond the CMC point.

Figure 4.7 shows the contact angle measurement results for Buff Berea. Apparently, the results from Buff Berea have similar trend with the results from Grey Berea. The lowest contact angle obtained at 1000ppm is 25.59° which is slightly higher than Grey Berea (24.68°). This can be attributed to the clay content of the Buff Berea which is slightly higher than Grey Berea. The clay content could affect the results of wettability alteration due to the repulsive forces created from the rock with higher clay content is lower as presence of greater number of co-ions. Therefore, the activity of detachment of oil molecules tends to reduce. However, the contact angle difference between both rock types are negligible. Besides, both conditions could shift the wettability from oil-wet toward strong water-wet state. Furthermore, MES anionic surfactant could achieve lowest excessive surfactant losses when applied on the sandstone rock due to the presence of same charged of the ions. Thus, the repulsive force between the MES anionic surfactant and the negatively charged rock surface could reduce the excessive surfactant adsorbed onto the rock surface. Therefore, it is proven that the MES anionic surfactant reduce contact angle for Grey Berea and Buff Berea sandstone rock effectively.

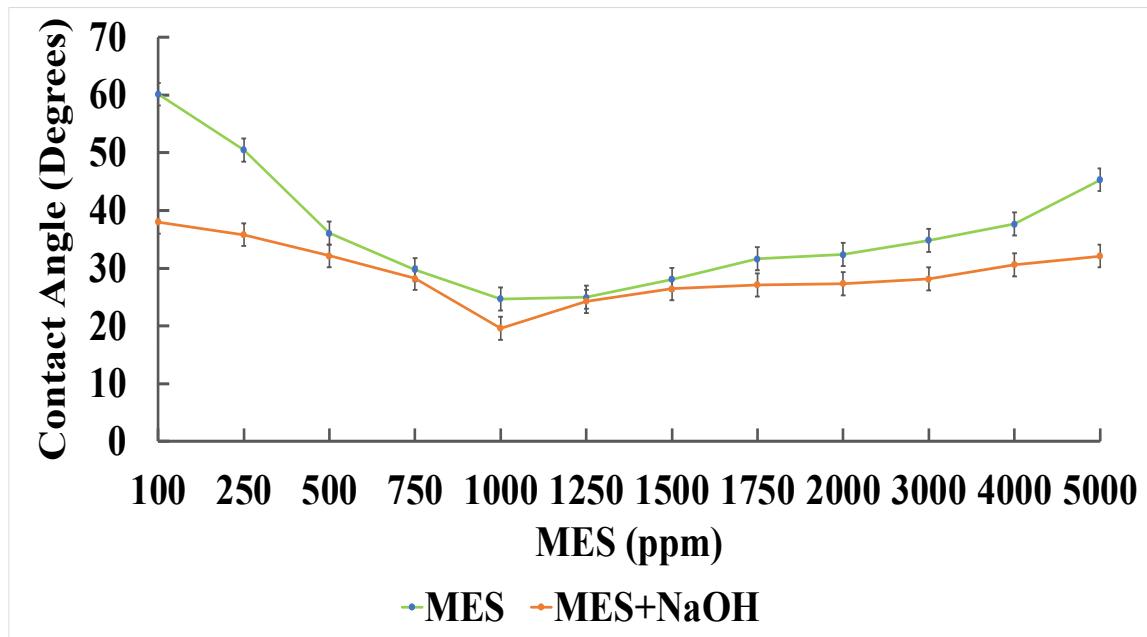**4.5   Effect Of Alkaline pH On Wettability Alteration**

Figure 4.8: Effect of pH on Contact Angle Measurement (Grey Berea)

MES surfactant under different concentrations is maintained at 9.5 to 10 pH value to create an alkaline condition. Based on the contact angle results shown in Figure 4.8, a similar trend can be observed from the results of MES surfactant under alkaline condition compared to the result in Figure 4.7, as the alkaline condition is absent. Nevertheless, a significant contact angle reduction can be observed in the low concentration of MES surfactant under alkaline condition. This indicated that the alkaline condition has a significant impact at low concentration of MES surfactant. For instance, the contact angle obtained from both conditions, 100 ppm of MES surfactant and 100 ppm under alkaline conditions, are 60.14° and 38.01° respectively. An approximately 36.8% of reduction was achieved with the alkaline condition. Besides, for the cases in 1000ppm of MES surfactant, a reduction of 5.5% (24.68° to 19.61°) was obtained for the alkaline condition. Alkaline condition can provide better wettability alteration towards the water-wet state. The optimum concentration of MES surfactant under alkaline condition is the same as that of MES surfactant alone, which is 1000ppm. According to Figure 4.8, the measured contact angle gradually increased as the concentration increased, similar to both conditions. However, the overall data obtained from the alkaline condition were lower

than the MES surfactant alone, which indicated that the alkaline condition could further improve the wettability alteration of the rock towards the water-wet state.

The result in Figure 4.8 revealed that the rock surface is sensitive to the surrounding environment changes, such as the changes in pH to alkaline medium. This can be further explained with the result in Figure 4.8. The Buff and Grey Berea contained approximately 16% to 20% of clay particles, especially Kaolinite and Montmorillonite, leading to more positively charged ions present on the rock surfaces. Nonetheless, the alkaline condition could turn the positively charged rock surface into negatively charged rock surface. Therefore, the sandstone rock surface would become more negatively charged under alkaline flooding. The surface of clay particles would become negatively charged as the pH of the solution is within the range of 9.5 to 10, which can alter the pH toward negatively charged rock surface. This is because the presence of Hydroxyl group (OH^-) in the interface between the solution and rock surface has increased. Electrostatic repulsion force between the negatively charged rock surface and the negatively charged oil components become higher, further releasing the oil components from the rock surface. Meanwhile, the clay particles will have a lower attraction towards the negatively charged oil components, which could also mitigate the wettability alteration towards the water-wet state.
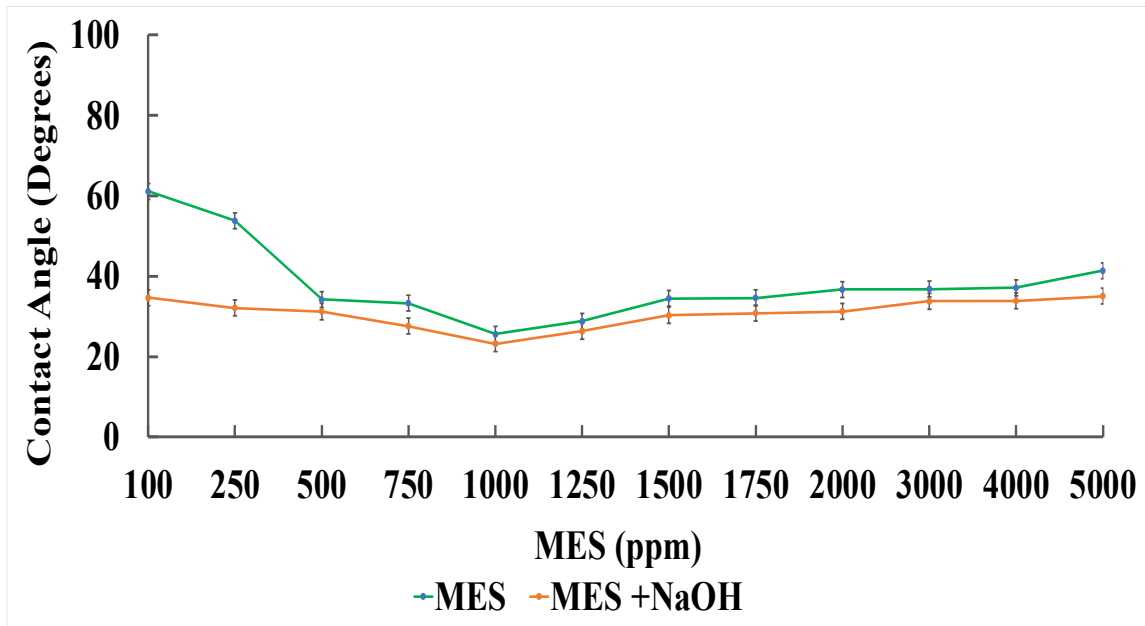
Figure 4.9: Effect of pH on Contact Angle Measurement (Buff Berea)

The optimum concentration of MES surfactant solution under alkaline condition is still the same at 1000ppm. This is because the CMC point under alkaline solution is also verified at 1050ppm refer to Appendix B.2. In addition, the effect of pH value on wettability alteration is proven, which indicates that alkaline condition can enhance additional oil recovery. By referring to Figure 4.8 and 4.9, both the graphs showed the similar trend. Meaning that, the alkaline MES surfactant worked on both situations and further reduced the contact angle.

4.6   Effect Of Salinity On Wettability Alteration

In this study, contact angle of different concentrations of divalent cation ($CaCl_2$ and $MgCl_2$) low salinity water was measured. Figure 4.10 presents the contact angle between the synthetic solution (different low salinity water/MES surfactant/alkaline condition) and the mineral rock surface. According to the results in Figure 4.10, it can be seen that the synthesized alkaline MES surfactant with 250ppm $CaCl_2$ achieved the lowest contact angle measurement recorded at 12.2°. Notably, the MES surfactant achieved the lowest contact angle at 750ppm with 250ppm of $CaCl_2$. This could be due to the lower CMC point when divalent cation is added to the alkaline MES surfactant at 750ppm. The CMC point is shown in Appendix B.3. This revealed that the low salinity water, especially

with divalent cations, could further alter the wettability to a more water-wet state. The lowest contact angle obtained from different concentration of divalent cations ($CaCl_2$) for 100ppm, 250ppm, 500ppm and 1000ppm are 14.1° , 12.2° , 17.3° , and 19.62° , respectively. The LSWF could reduce the contact angle measurement which could be verified with the previous experimental works (Duffy et al., 2019; Wang et al., 2020; Farhadi et al., 2021).

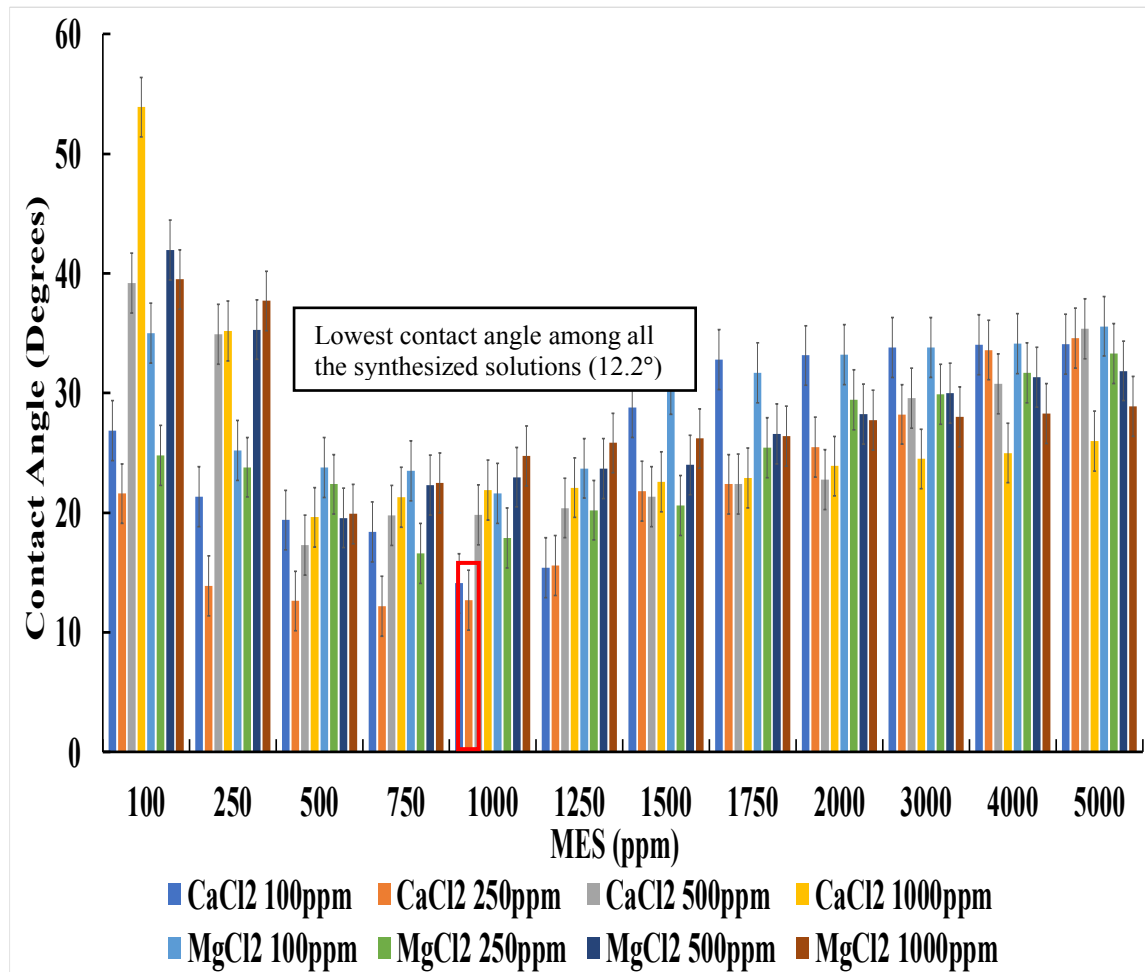Figure 4.10: Effect of Salinity with MES on Contact Angle Measurement (Grey Berea)

The concentration of MES surfactant that achieved the lowest contact angle at salinity of 100ppm of $CaCl_2$ is at 1000ppm, which is similar to the MES surfactant and alkaline MES surfactant conditions. Hence, this indicated that the concentration of $CaCl_2$ at 100ppm is not capable to lower the CMC point. However, the concentration of MES

surfactant can be reduced to 750ppm in 250ppm of CaCl$_2$. The concentration of MES surfactant could be reduced to 500ppm in the situation of 500ppm and 1000ppm of CaCl$_2$. On the other hand, the divalent cations (MgCl$_2$) also presented a similar trend. The lowest contact angle achieved by various concentration of MgCl$_2$ for 100ppm, 250ppm, 500ppm and 1000ppm are $21.63°$, $16.6°$, $19.57°$ and $19.9°$, respectively. However, the concentration of MgCl$_2$ with 250ppm could provide significant contact angle reduction compared to the lowest contact angle obtained from 1000ppm of alkaline MES surfactant. This indicates that the CaCl$_2$ could significantly cause wettability alteration towards the water-wet state. Among all the different concentrations of divalent cations applied to the alkaline MES surfactant, 250ppm of CaCl$_2$ could attain the lowest contact angle.

Previously, the contact angle obtained between formation water with 19000ppm (NaCl equivalent) and the Grey Berea rock surface is noted as 91.7°. This also indicated that high salinity water would negatively impact wettability alteration. Throughout this study, it is proven that low salinity water could alter the wettability towards a more water-wet state. Besides, synthesizing low salinity water with surfactant under alkaline condition could further alter the wettability towards water-wet state. However, it is noteworthy that the lowest concentration of salinity water might not lead to the lowest contact angle. From the result, it is notable that 250ppm of divalent cations provide lower contact angle measurement compared to 100ppm of divalent cation.

Low salinity water with MES anionic surfactant solution in alkaline medium reduced the contact angle, this reduction can be explained by several driving mechanisms such as multi-ions exchange, electrical double layer expansion (EDLE), and salting-in effect (Xie et al., 2019). Low salinity water would generate the substitution between Ca^{2+} and H$^+$. Therefore, the local pH value increases due to the desorption of cation from the clay particles in the rock. This substitution has occurred to re-achieve the chemical equilibrium disturbed during low salinity water injection. The local pH increased because of OH$^-$ ions released during the segregation of water molecule into the H$^+$ and OH$^-$. The H$^+$ ions have a high potential to attract the clay particles as the ions have the most affinity to the clay particles (Chen et al., 2018). Meanwhile, the water molecules contained in the

solution could facilitate and enhance the process. Besides, the presence of divalent cations such as Ca^{2+} could form the cation bridging between the negatively charged rock surface and the organic material from the crude oil. This is a fragile connection, and therefore, the monovalent ions from the solution could easily be released from the rock surface together with the functional groups. As a result, the wettability on the rock surface would further shift towards a water-wet state. The electric double layer expansion is one of the driving mechanisms behind the low salinity water injection (Mehraban et al., 2021). The electrostatic repulsive force continues to increase due to the substitution of divalent ions by the monovalent ions. The desorption of oil from the clay particle occurs as the electrostatic repulsive force are greater than the binding force between the rock surface and the organic functional group of oil molecule. This could lead to the wettability alteration of the oil-wet rock surface towards the water-wet state.
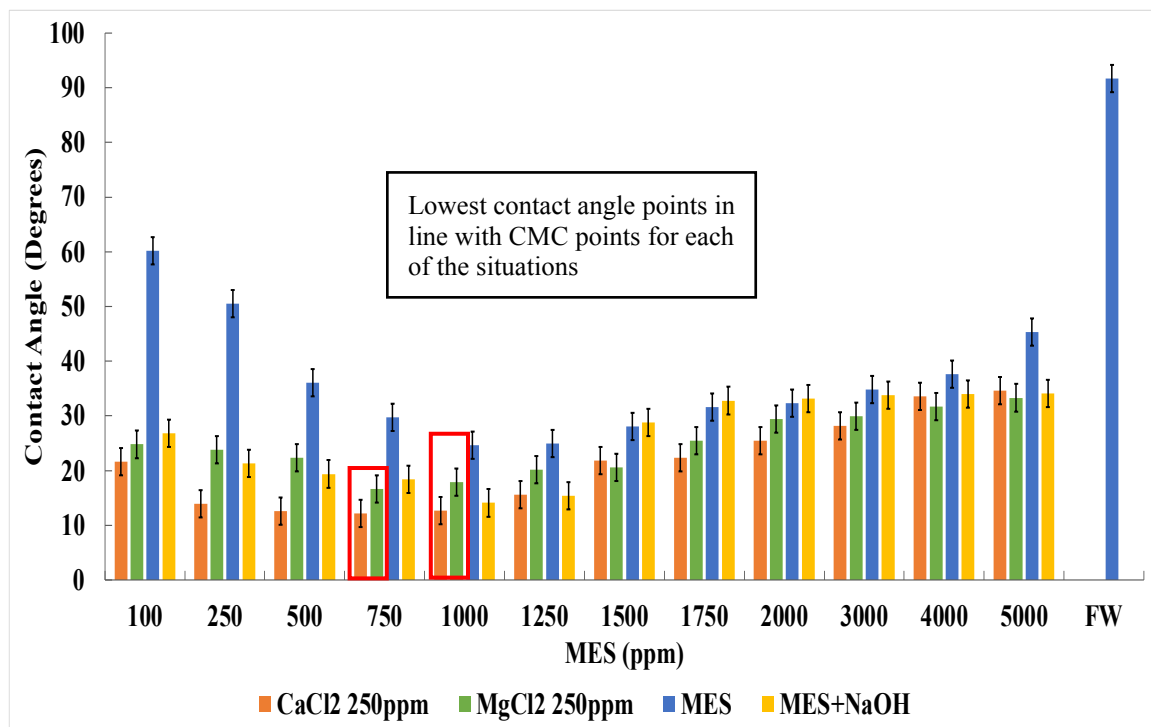

Figure 4.11: Comparison of Different Best Cases (Grey Berea)

Among the different best cases (MES surfactant alone/alkaline MES surfactant/alkaline MES surfactant with divalent cation), the contact angle obtained with 750ppm MES/250ppm of $CaCl_2$ under alkaline condition is the lowest contact angle. This

can be clearly observed from the Figure 4.11. From the results, it showed that alkaline condition and divalent cations provide positive impact to the wettability alteration. Thus, it is crucial to synergize MES anionic surfactant with divalent cation under alkaline conditions to enhance oil recovery further. The Figures in 4.7, 4.8, 4.10 and 4.11 also showed the percentage error which are within the range of 2% to 4%. Therefore, the contact angle measurements obtained from the Grey Berea under different effects are reliable.
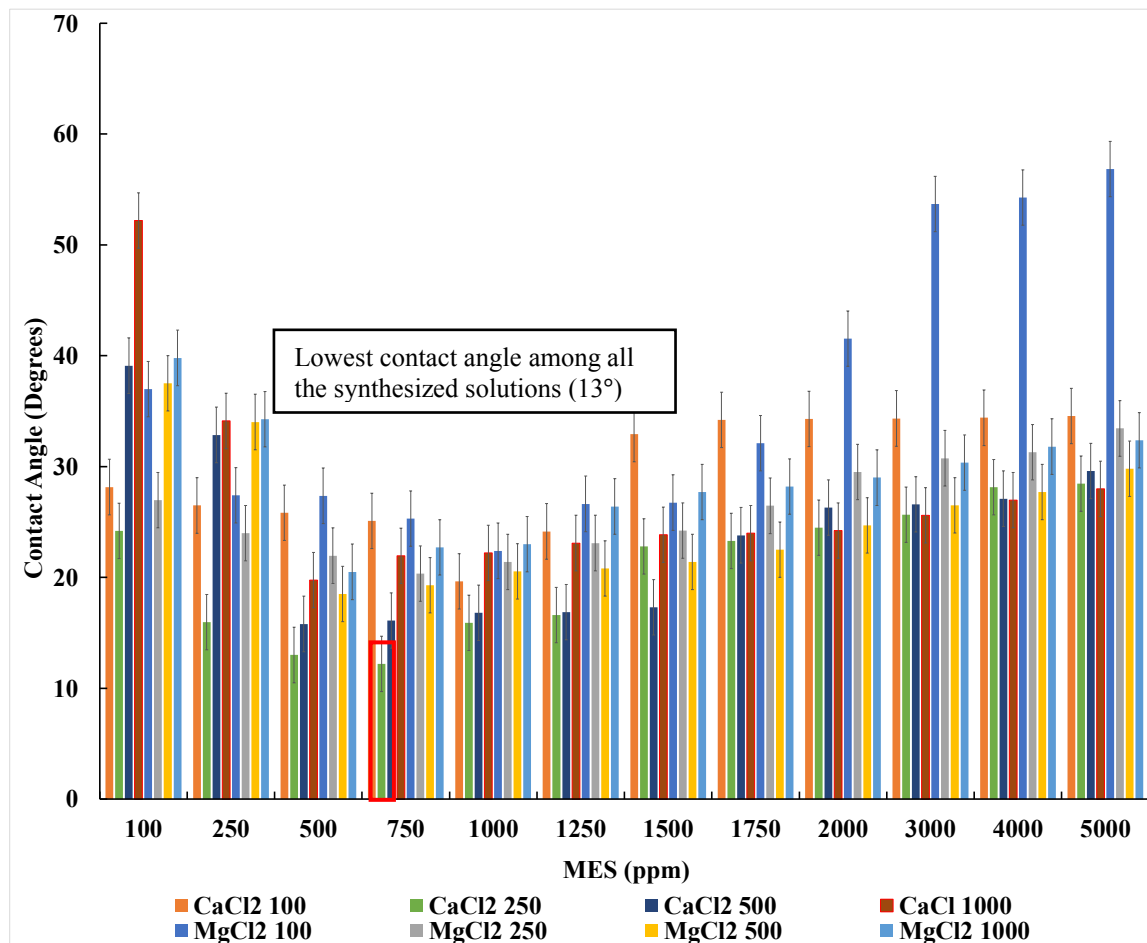
Figure 4.12: Effect of Salinity with MES on Contact Angle Measurement (Buff Berea)

The trend of the result for Buff Berea in Figure 4.12 follows the trend of Grey Berea in Figure 4.11. Therefore, this indicates that the synthesized solutions could provide positive impact on wettability alteration of Buff Berea and Grey Berea. The lowest contact angle obtained with Buff Berea is 13° where 87.6% of contact angle reduction is achieved.

This could further prove that the synthesized solutions could be applied for different sandstone reservoir.
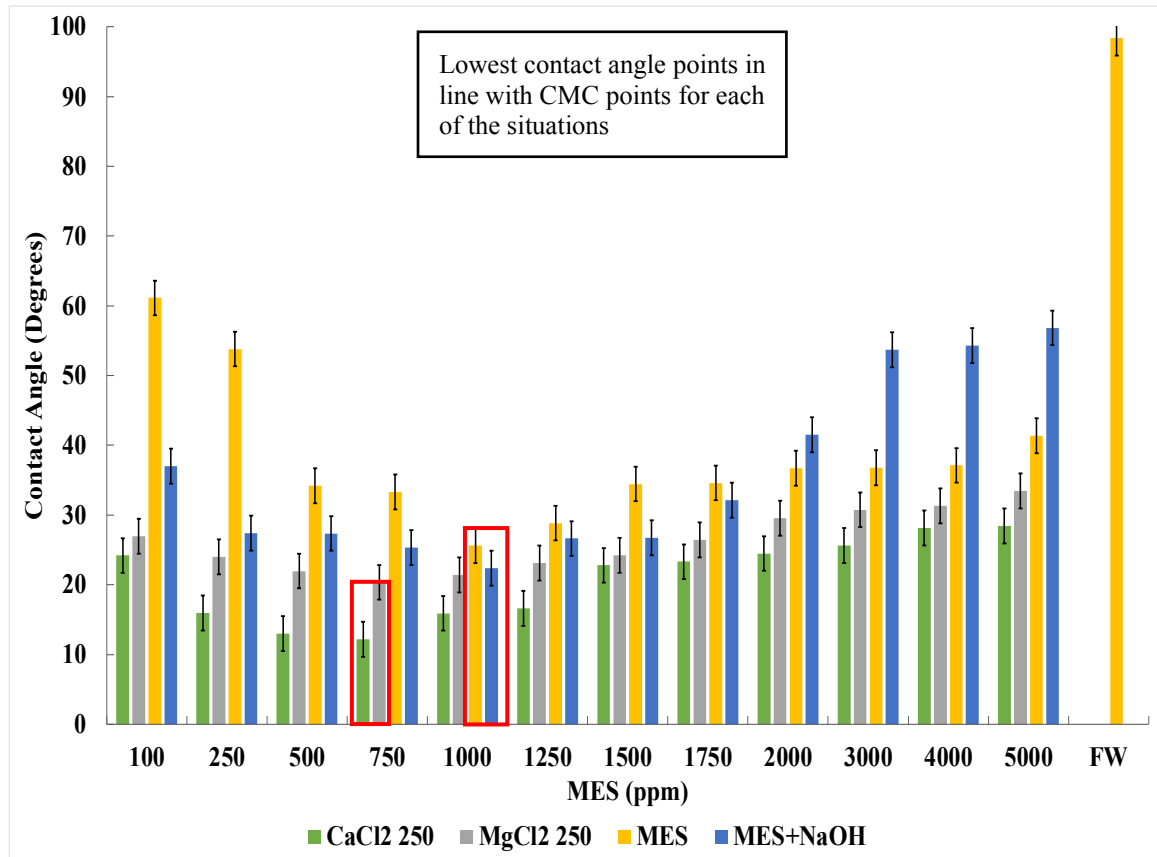
Figure 4.13: Comparison of Different Best Cases (Buff Berea)

Figure 4.13 presents contact angle measurement best case scenario obtained for Buff Berea. Apparently, there is only slight difference compared to the results obtained from Grey Berea. Both rocks showed that with 750ppm MES/250ppm of $CaCl_2$ under alkaline condition could effectively shift the oil-wet rocks toward strong water-wet state. Thus, there is high potential of using the synthesized solution to enhance additional oil recovery. The percentage of the error for Buff Berea is very similar to Grey Berea which is within the range of 2.5% to 4%. Therefore, the contact angle measurements obtained from the Buff Berea under different conditions are also applicable and reliable.

Table 4.10: Summary of best contact angle measurement results

Synthesized solutions	Contact angle (°), Grey Berea	Contact angle (°), Buff Berea
1000ppm MES	24.68	25.55
1000ppm MES + Alkaline condition	19.61	23.22
750ppm MES + Alkaline condition + 250ppm $CaCl_2$	12.20	13
750ppm MES + Alkaline condition + 250ppm $MgCl_2$	16.60	20.35

Table 4.11: Summary of best contact angle results from the literatures

Literatures	Designed c-EOR Fluid	Contact Angle Measurement	Experiment Condition
Joshi et al., 2022	Cocamidopropyl Betaine (CAPB) surfactant + PHPA polymer + Nano-silica	16.2°	Room temperature
Pal et al., 2019	Anionic surfactant derived from Jatropha Oil + alkaline	24.9°	Room temperature
Fan et al., 2021	Polymer + Nano-silica	20°	Room temperature

Table 4.10 shows the summary of the best contact angle results from the present study in different conditions and Table 4.11 shows the summary of the best contact angle measurement results from literatures. The experimental works showed in Table 4.11 are from sandstone rock and under room temperature which is similar to the present study. Therefore, the comparison works is reliable and feasible. Pal et al., (2019) obtained 24.9° of contact angle measurement with anionic surfactant derived from Jatropha Oil. Comparing the result with the present study, MES anionic surfactant showed a slightly lower contact angle measurement. For the comparison between the combinations of chemical materials, (MES + Alkaline condition + $CaCl_2$) showed the best results among

the studies. However, experimental work from Joshi et al., (2022) still obtained a significant contact angle reduction while combining the different types of chemical materials (nanoparticles/surfactant/polymer). Therefore, combination of optimum chemical materials presents a better result on wettability alteration towards water-wet state.

4.7   Effect Of NPs On Wettability Alteration

The results presented in Figure 4.14 indicate that the trend of the wettability alteration is still following the trend in Figure 4.7. In the case of (25ppm nano-polystyrene + alkaline + 1000ppm MES), it achieved a contact angle reduction of 75.8% (from 91.7° to 22.2°). For the case (25ppm nano-silica + alkaline + 1000ppm MES) showed a further contact angle reduction which is from 91.7° to 21.1°. These are the lowest contact angle measured without divalent cations. Therefore, the results indicated that the CMC point is around 1000ppm where 25ppm nano-polystyrene and 25ppm nano-silica could not significantly affect the CMC point. The result is slightly higher than the case of MES under alkaline condition. However, it is still showing a favorable result since the primary purpose of NPs is to reduce the excessive surfactant loss. The combination with nano-silica showed a slightly lower contact angle measurement due to the nano-polystyrene has lower negative charge. Therefore, combination with nano-silica could create larger electrostatic repulsion force which could aid on the wettability alteration.
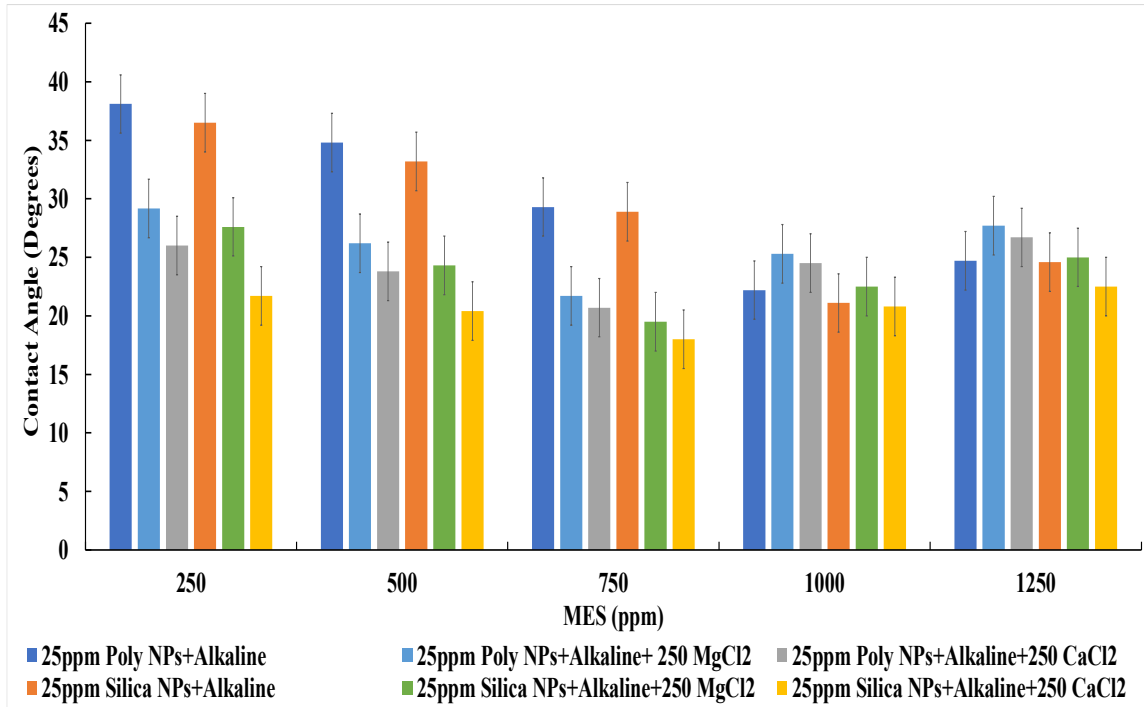
Figure 4.14: Effect of NPs with best cases on Contact Angle Measurement (Grey Berea)

The lowest contact angle obtained from the synthesized solution of nano-silica with $CaCl_2$ and $MgCl_2$ are 18° and 19.5° respectively, a significant contact angle reduction was achieved. For the nano-polystyrene with $CaCl_2$ and $MgCl_2$, the contact angle measured as 20.7° and 21.7°, respectively. However, the overall results are slightly higher than the cases without adding NPs into the synthesized solution. Nevertheless, the obtained contact angles with NPs are still below 22°. Therefore, this indicate that utilizing NPs in the synthesized solution can reverse wettability from oil-wet state to a strong water-wet state. Besides, the efficiency of NPs can be further verified during flowing situation because the structural disjoining pressure is more effective during flowing situation.
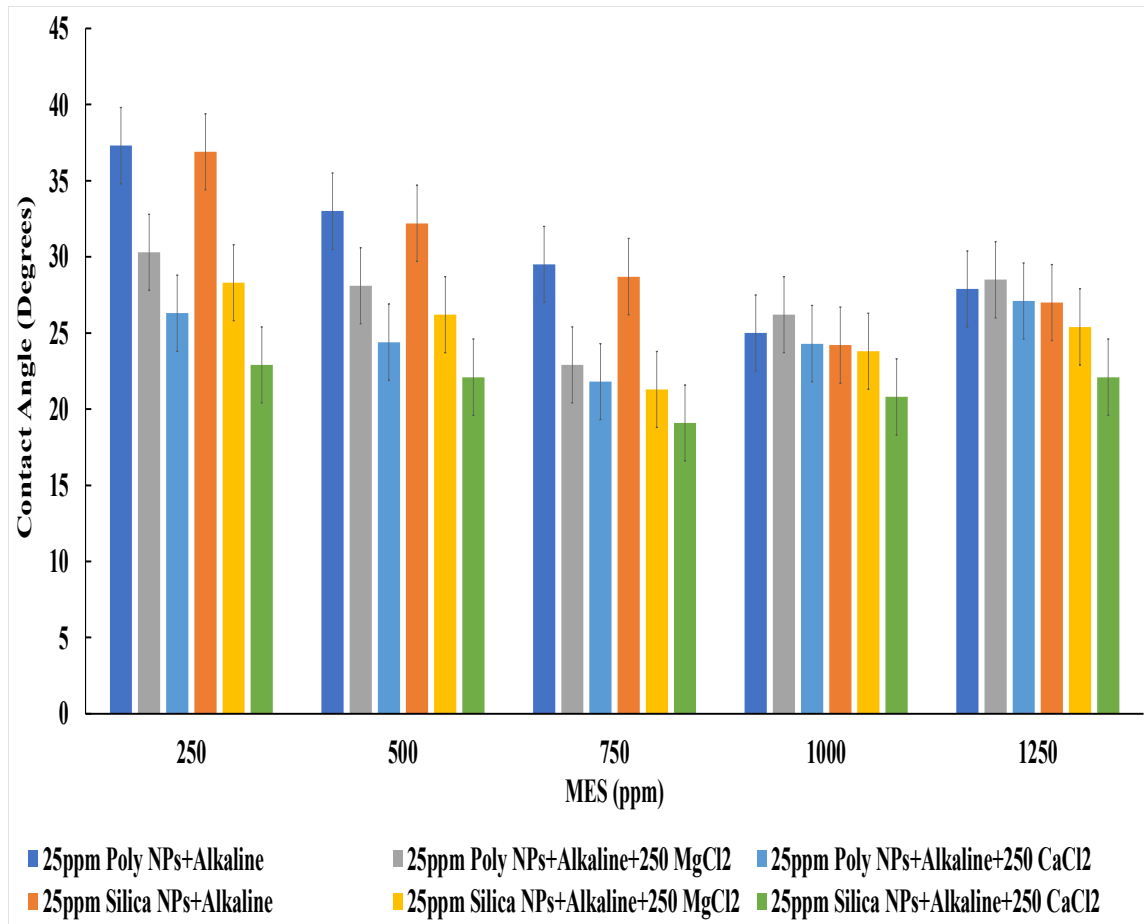
Figure 4.15: Effect of NPs with best cases on Contact Angle Measurement (Buff Berea)

According to Figure 4.15, the contact angle measurement for Buff Berea showed similar outcome with Grey Berea. The lowest contact angle obtained among the different cases (25ppm nano-silica + 1000ppm MES, 25ppm nano-silica + 750ppm MES + 250ppm $CaCl_2$ and 25ppm nano-silica + 750ppm MES + 250ppm $MgCl_2$, 25ppm nano-polystyrene + 1000ppm MES, 25ppm nano-polystyrene + 750ppm MES + 250ppm $CaCl_2$ and 25ppm nano-polystyrene + 750ppm MES + 250ppm $MgCl_2$) all in alkaline medium are 24.2°, 19.1°and 21.3°, 25°, 21.8°and 22.9°, respectively. These results prove that the designed nanofluid induced wettability alteration towards a strong water-wet state.

4.8 Adsorption Study

Based on the result from wettability, MES surfactant concentration 250ppm to 1250ppm were considered suitable for adsorption study. Adsorption capacity of low salinity/MES/ surfactant/NP results is presented in Figure 4.16. The results are specified for the MES concentrations of 750ppm and 1000ppm at room temperature.
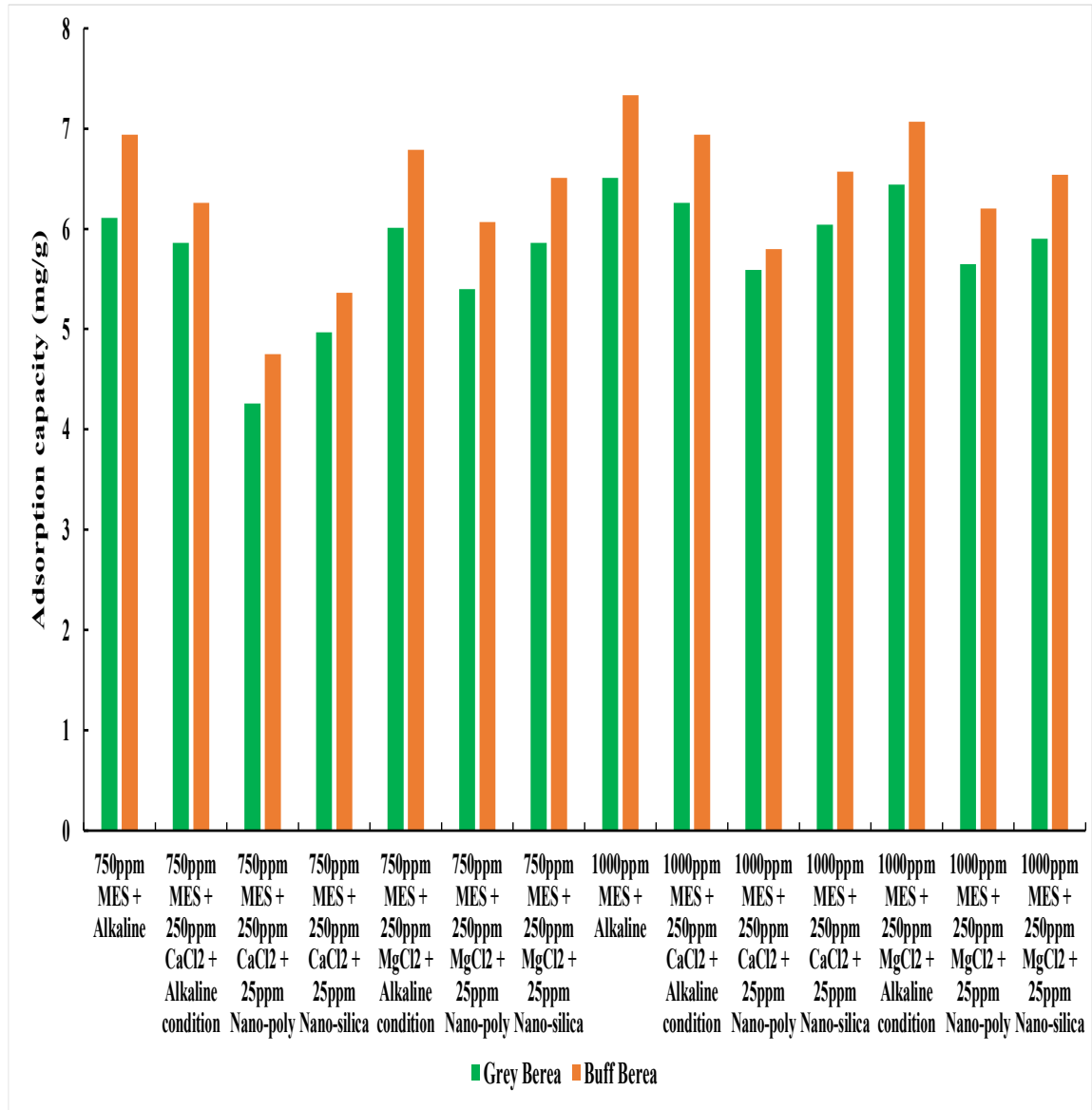

Figure 4.16: Adsorption capacity of Grey and Buff Berea at room temperature condition

Based on Table 4.12, the overall amount of adsorbed surfactant for 1000ppm of MES surfactant in all conditions is higher than 750ppm of MES surfactant. For the alkaline MES surfactant, a 6.15% reduction was achieved by reducing the concentration of MES surfactant from 1000ppm to 750ppm. Combination of 250ppm $CaCl_2$ with 750ppm and 1000ppm in alkaline medium, MES surfactant reduced the adsorption of surfactant by 3% and 4%, respectively. The amount of adsorbed MES surfactant was reduced while adding the nanoparticle into the solution. Adding 25ppm of nano-silica into the 750ppm of MES surfactant and 250ppm of $CaCl_2$ achieved an approximately 18.66% reduction. The nanoparticle is acting as sacrificial agent. Presence of nanoparticles could create competitive condition with anionic surfactant (Liu et al., 2020c). Therefore, the nano-silica would compete with anionic surfactant to adsorb onto the rock surface. However, changing the nanoparticles from 25ppm of nano-silica to 25ppm of nano-polystyrene led to larger adsorption capacity reduction. The difference of the adsorption capacity reduction between nano-silica and nano-polystyrene is up to 0.71 mg/g which is approximately 11.62%. This shows that nano-polystyrene performed better on surfactant adsorption reduction. This is attributed to the less negative charge of the nano-polystyrene. Hence, the polystyrene prompt to adsorb onto the rock surface compared to nano-silica. The combination of 250ppm $MgCl_2$ with 750ppm MES and 1000ppm MES in alkaline medium only led to slight reduction of surfactant adsorption. Only 4.10% and 11.62% of MES surfactant adsorption reduction was achieved while adding the solution with 25ppm of nano-silica and 25ppm of nano-polystyrene respectively. As a result, the combination of MES surfactant and $CaCl_2$ in alkaline medium significantly reduced the amount of adsorbed surfactant. In contrast, $MgCl_2$ resulted to minor reduction of surfactant adsorption in both conditions.

Table 4.12: Adsorption capacity of Grey Berea at room temperature condition

Synthesized solutions	Adsorption Capacity (mg/g)	Langmuir Model R^2	Freundlich Model R^2
750ppm MES + Alkaline	6.11	0.9237	0.7344
750ppm MES + 250ppm $CaCl_2$ + Alkaline condition	5.86	0.9628	0.9338
750ppm MES + 250ppm $CaCl_2$ + 25ppm Nano-silica	4.97	0.9753	0.6245
750ppm MES + 250ppm $CaCl_2$ + 25ppm Nano-polystyrene	4.26	0.9477	0.8948
750ppm MES + 250ppm $MgCl_2$ + Alkaline condition	6.01	0.9555	0.8709
750ppm MES + 250ppm $MgCl_2$ + 25ppm Nano-silica	5.86	0.9441	0.7307
750ppm MES + 250ppm $MgCl_2$ + 25ppm Nano-polystyrene	5.40	0.9788	0.9745
1000ppm MES + Alkaline	6.51	0.9237	0.7344
1000ppm MES + 250ppm $CaCl_2$ + Alkaline condition	6.26	0.9628	0.9338
1000ppm MES + 250ppm $CaCl_2$ + 25ppm Nano-silica	6.04	0.9753	0.6245
1000ppm MES + 250ppm $CaCl_2$ + 25ppm Nano-polystyrene	5.59	0.9477	0.8949
1000ppm MES + 250ppm $MgCl_2$ + Alkaline condition	6.44	0.9555	0.8709
1000ppm MES + 250ppm $MgCl_2$ + 25ppm Nano-silica	5.90	0.9441	0.7307
1000ppm MES + 250ppm $MgCl_2$ + 25ppm Nano-polystyrene	5.65	0.9788	0.9745

The Langmuir and Freundlich isotherms were applied to further analyze the adsorption behavior of the MES surfactant which have been demonstrated through the graphs in Appendix C and D. The overall R^2 values obtained from Langmuir isotherm are higher than the Freundlich isotherm. This indicated that Langmuir isotherm is more suitable to validate the adsorption study. Thus, it indicates that monolayer adsorption occurred, and the possibility of multilayer adsorption was lower. In comparing the R2 values from Langmuir isotherm obtained from different conditions, they are overall larger than 0.95, further indicating the potential of the formation of monolayer adsorption. However, the adsorption capacity was significantly reduced as the nanoparticles (nano-polystyrene/nano-silica) were added to the solutions. Therefore, it is essential to consider the addition of nanoparticles into the synthesized solution in order to reduce surfactant adsorption significantly. As nanoparticles promptly adsorbed onto the rock surface and prevented excess surfactant from adsorbing onto the rock surface. As a result, the adsorption capacity is the primary factor to be considered during the adsorption study.

However, multilayer adsorption might occur in particular phases since the R^2 obtained from Freundlich model is considered high for some of the situations. The synthesized solution (1000ppm MES + 250ppm $MgCl_2$ + 25ppm Nano-polystyrene) obtained high R^2 with Langmuir and Freundlich isotherms, indicating that multilayer adsorption might also occur instead of monolayer adsorption. Meanwhile, the synthesized solution (1000ppm MES + 250ppm $CaCl_2$ + 25ppm Nano-silica) shows the adsorption process following the Langmuir model as single-layer adsorption has occurred.

Table 4.13: Adsorption capacity of Buff Berea at room temperature condition

Synthesized solutions	Adsorption Capacity (mg/g)	Langmuir Model R^2	Freundlich Model R^2
750ppm MES + Alkaline	6.94	0.9899	0.9102
750ppm MES + 250ppm $CaCl_2$ + Alkaline condition	6.26	0.9563	0.8883
750ppm MES + 250ppm $CaCl_2$ + 25ppm Nano-silica	5.36	0.9505	0.7407
750ppm MES + 250ppm $CaCl_2$ + 25ppm Nano-polystyrene	4.75	0.9677	0.9183
750ppm MES + 250ppm $MgCl_2$ + Alkaline condition	6.79	0.9932	0.8560
750ppm MES + 250ppm $MgCl_2$ + 25ppm Nano-silica	6.51	0.9834	0.9185
750ppm MES + 250ppm $MgCl_2$ + 25ppm Nano-polystyrene	6.07	0.9953	0.9786
1000ppm MES + Alkaline	7.33	0.9899	0.9102
1000ppm MES + 250ppm $CaCl_2$ + Alkaline condition	6.94	0.9563	0.8883
1000ppm MES + 250ppm $CaCl_2$ + 25ppm Nano-silica	6.57	0.9505	0.7407
1000ppm MES + 250ppm $CaCl_2$ + 25ppm Nano-polystyrene	5.80	0.9677	0.9183
1000ppm MES + 250ppm $MgCl_2$ + Alkaline condition	7.07	0.9932	0.8560
1000ppm MES + 250ppm $MgCl_2$ + 25ppm Nano-silica	6.54	0.9834	0.9185
1000ppm MES + 250ppm $MgCl_2$ + 25ppm Nano-polystyrene	6.20	0.9953	0.9786

Comparing the results from Table 4.12 and 4.13, Buff and Grey Berea exhibited similar surfactant adsorption behavior. Grey and Buff Berea showed the lowest adsorption capacity for the solution (750ppm MES + 250ppm $CaCl_2$ + 25ppm Nano-polystyrene) which are 4.26mg/g and 4.75mg/g, respectively. The adsorption capacity for Buff Berea is slightly higher than Grey Berea. This could be due to the clay content in the rock samples are different and the amount of the clay content would also affect the adsorption capacity (Saxena et al., 2019).

Table 4.14: Adsorption capacity of Grey Berea at 70°C

Synthesized solution with 750ppm of MES	Adsorption capacity (mg/g)
750ppm MES + pH	4.66
750ppm MES + pH + 250ppm $CaCl_2$	2.58
750ppm MES + pH + 250ppm $CaCl_2$ + 25ppm silica	0.69
750ppm MES + pH + 250ppm $CaCl_2$ + 25ppm polystyrene	0.43
750ppm MES + pH + 250ppm $MgCl_2$	2.88
750ppm MES + pH + 250ppm $MgCl_2$ + 25ppm silica	0.93
750ppm MES + pH + 250ppm $MgCl_2$ + 25ppm polystyrene	0.71

Table 4. 15: Adsorption capacity of Buff Berea at 70°C

Synthesized solution with 750ppm of MES	Adsorption capacity (mg/g)
750ppm MES + pH	5.49
750ppm MES + pH + 250ppm $CaCl_2$	2.72
750ppm MES + pH + 250ppm $CaCl_2$ + 25ppm silica	0.85
750ppm MES + pH + 250ppm $CaCl_2$ + 25ppm polystyrene	0.63
750ppm MES + pH + 250ppm $MgCl_2$	3.03
750ppm MES + pH + 250ppm $MgCl_2$ + 25ppm silica	1.16
750ppm MES + pH + 250ppm $MgCl_2$ + 25ppm polystyrene	0.90

Table 4.14 and 4.15 shows the adsorption capacity of Grey and Buff Berea at 70℃. Comparing the results from room temperature with 70℃ showed a further reduction of MES surfactant adsorption. The amount of adsorbed surfactant was reduced from 6.1 mg/g to 4.66 mg/g for 750ppm alkaline MES surfactant. Alkaline MES surfactant with $CaCl_2$ showed reduction from 6.11 mg/g to 2.58 mg/g. The results obtained with the same solution at different temperatures of (25℃ and 70℃) are 5.86 mg/g and 2.58 mg/g, respectively. Adding 25 ppm of nano-silica to the solution resulted to a significant lower surfactant adsorption which is 0.69 mg/g. The surfactant adsorption reduction achieved up to 88.7% which is due to the presence of nanoparticles and higher temperature. Temperature increase could reduce the adsorption capacity due to the viscosity reduction and exothermic process (Saha et al., 2017). Meanwhile, synthesized solution with nano-polystyrene presented the lowest adsorption capacity which is 0.43 mg/g. This is because nano-polystyrene led to lower electrostatic repulsion force so the potential to adsorb onto the rock surface is higher than nano-silica. $MgCl_2$ also showed a similar trend with the divalent cation $CaCl_2$ at higher temperature. However, $CaCl_2$ provided a better result. Therefore, $CaCl_2$ synergy with nanoparticles and higher temperature is more suitable to be applied for EOR-process.
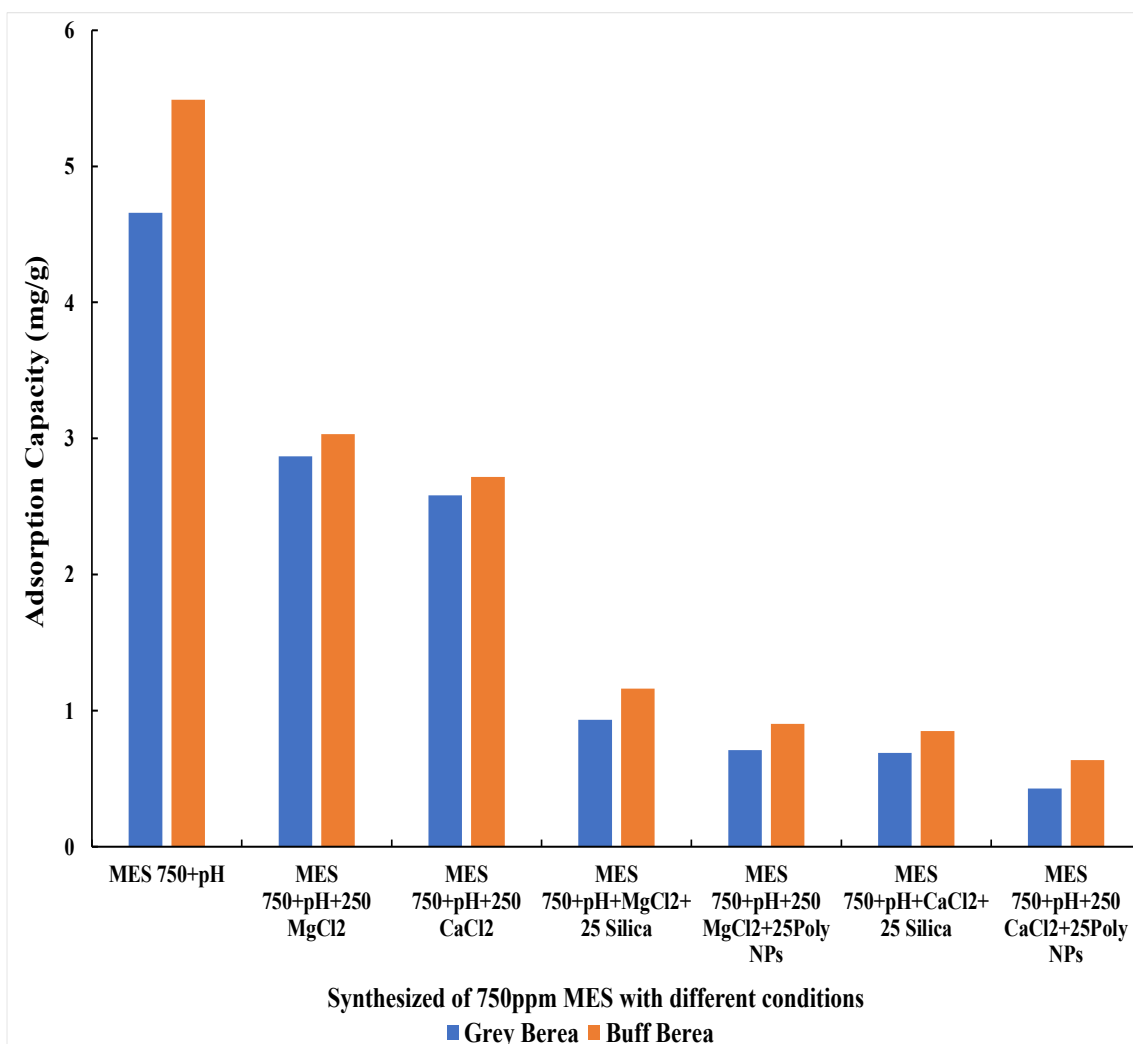
Figure 4.17: Comparison of adsorption capacity between Grey and Buff Berea with different synthesized solutions at 70°C

Overall result of adsorption capacity between Buff Berea and Grey Berea is shown in Figure 4.17, the Buff Berea showed higher adsorption capacity. This might be because Buff Berea has higher clay content than Grey Berea. However, both situations showed favorable adsorption capacity reduction when nanoparticle is added as a sacrificial agent. The lowest adsorption capacity obtained for both Grey and Buff Berea at 70°C are 0.43 mg/g and 0.63 mg/g, respectively. The synthesized solution with the lowest adsorption capacity is 250ppm of $CaCl_2$/750ppm of alkaline MES surfactant/25ppm of nano-polystyrene. As a result, nano-polystyrene is sufficient to minimize the excessive

surfactant adsorbed onto the rock surface. Higher temperature reduced the surfactant adsorption onto the rock. Therefore, the study indicated that the effect of temperature plays an important role to reduce excessive surfactant adsorbed onto the rock surface.

Table 4.16: Literatures studies with similar operating condition to the present study

Literatures	Designed c-EOR Fluid	Adsorption capacity (mg/g)	Experiment Condition
Ahmadi et al., 2015	Natural surfactant derived from Zyziphus Spina Christi leaves	6.8816	90°C
Chen et al., 2019	Biobased zwitterionic surfactant	0.43	45°C

Table 4.16 showed the previous experimental works with similar operating condition to the present study. Ahmadi et al. (2015) conducted the adsorption study at different temperature conditions with sandstone rock. The adsorption capacity decreased from 35.3597 mg/g to 6.8816 mg/g as the temperature increased up to 90°C. This indicate that increasing the temperature reduced the surfactant adsorption onto the rock surface significantly. The present adsorption study was conducted at 70°C due to the limitation of the equipment. Therefore, it is estimated that the adsorption capacity with the synthesized solutions would continue reducing as the temperature increases beyond 70°C.

4.9   Enhanced Oil Recovery Study

Core-flooding test was conducted to obtain the additional oil recovery from the core rock samples under reservoir condition. This phase of experimental work was only conducted with a few synthesized solutions, tabulated in Table 4.17. The selected optimum synthesized solutions can shift the oil-wet state toward a strong water-wet state and achieve significant surfactant adsorption reduction. The whole core-flooding process will be undergoing a steady-state flooding to achieve a high accurate and promising results.

Thus, 0.2 ml/min of injection rate was maintained throughout the core-flooding test. Both types of rock samples were used in the core-flooding test to verify further the potential and capability of the synthesized solution to achieve favorable oil recovery.

Table 4.17: Selected optimum synthesized solutions for core-flooding test

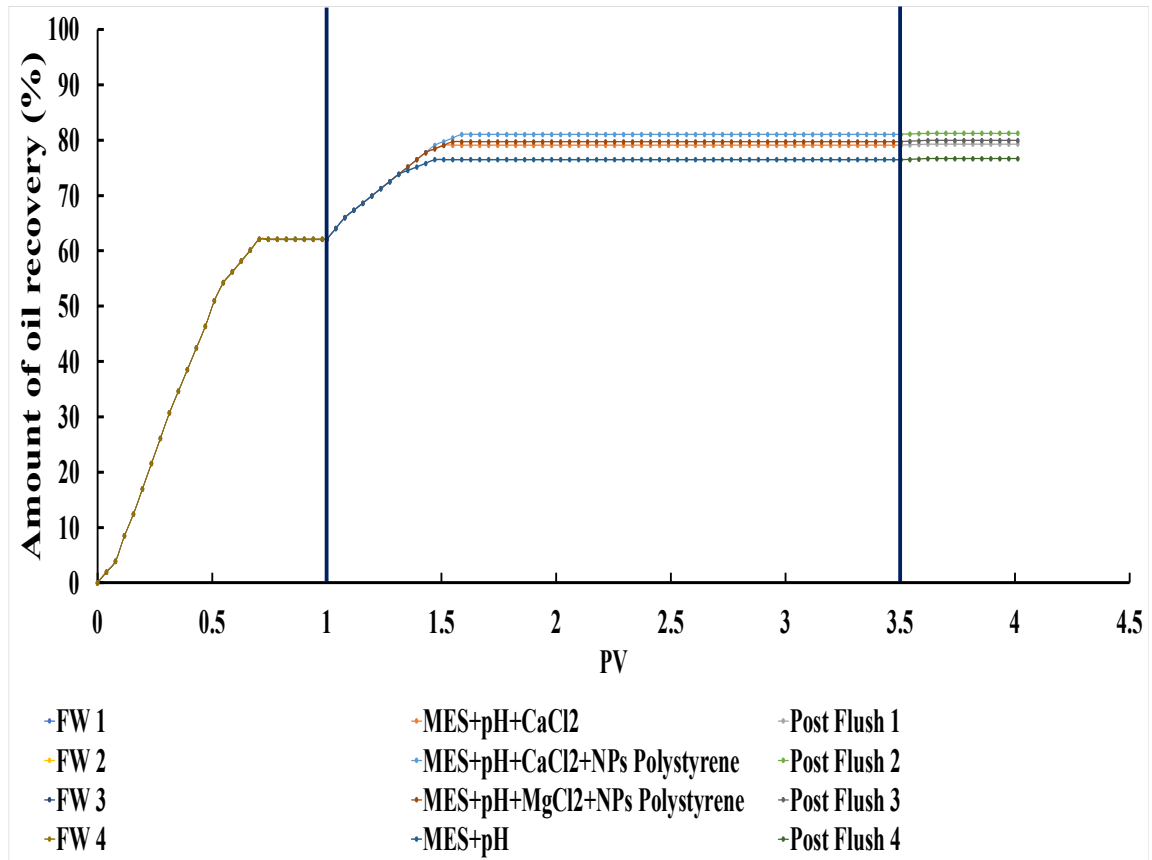| Core-flooding test	Selected optimum synthesized solutions
1	75ppm MES + Alkaline Condition
2	75ppm MES + Alkaline Condition + 250ppm $CaCl_2$
3	75ppm MES + Alkaline Condition + 250ppm $CaCl_2$ + 25ppm Nano-polystyrene
4	75ppm MES + Alkaline Condition + 250ppm $MgCl_2$ + 25ppm Nano-polystyrene

Figure 4.18: Oil recovery from Grey Berea under reservoir condition

According to the results in Figure 4.18, all the selected synthesized solutions achieved favorable amount of additional oil recovery. The increment of additional oil could be clearly observed after the 1 PV of formation water injection. Initially, the core-flooding test was started with secondary oil recovery method, which is water-flooding. All the Grey Berea obtained a similar oil recovery factor with the water-flooding, which is approximately 62.09%. A differential pressure was observed and increased gradually to mobilize the oil from the pore spaces by overcoming the capillary force. The differential pressure was within 2 psi to 10 psi. The water-flooding reached the maximum oil recovery at approximately 0.71 PV of water-flooding. The synthesized solution injection was conducted after 1 PV of water flooding was injected. 750ppm of MES surfactant under alkaline conditions was injected through the Grey Berea core sample. An additional 14.38% of oil recovery was observed. This indicated that MES surfactant under alkaline conditions could lead to favorable oil recovery factor from the sandstone reservoir. Experimental

work from Khayati et al., (2020) obtained an additional 8.4% of oil recovery with surfactant flooding from a sandstone rock. The results showed a better impact than several previous experimental works. Altering MES surfactant solution into an alkaline condition could create stronger electrostatic repulsive force between the organic compounds present in the crude oil and the rock surface. Therefore, the oil molecules could be removed from the rock surface easily. Furthermore, the alkaline condition could reduce the interfacial tension further by generating the reaction with natural acids content in the crude oil (Firozjaii et al., 2020).

The core-flooding test is then conducted with the synthesized solution (750ppm of MES surfactant/250ppm of $CaCl_2$) under alkaline conditions. This further enhanced the additional oil recovery, where 17% of additional oil recovery was achieved. The pressure difference along the 2.5 PV of the synthesized solution injection is considered low (below 30) and there is no significant pressure differential increment, indicating that no formation damage occurred (Joshi et al., 2022). The result also indicated that the presence of divalent cation ($CaCl_2$) could further enhance oil recovery. This can be attributed to the MIE, EDLE and salting effects. The wettability study elucidated that 250ppm of $CaCl_2$ could lead to a positive impact on wettability alteration significantly. According to several studies, wettability alteration would directly affect the oil recovery factor where the wettability shifted from oil-wet toward water-wet state which could significantly lead to a higher oil recovery (Xu et al., 2019; Esfandyari et al., 2020; Zargar et al., 2020). Meanwhile, this is verified in the present study, where 750 ppm of MES surfactant/250 ppm of $CaCl_2$ obtained a lower contact angle measurement and higher oil recovery factor.

Nano-polystyrene was introduced in the following core-flooding test. 25 ppm of nano-polystyrene was combined with the synthesized solution under two different conditions. Based on the results in Table 4.18, the combination of 25 ppm of nano-polystyrene/250 ppm of $CaCl_2$/750 ppm of MES surfactant under alkaline conditions showed a better result while compared to the combination of 25ppm of nano-polystyrene/250ppm of $MgCl_2$/750ppm of MES surfactant under the alkaline condition were 18.95% and 17.65% of residual crude oil were recovered, respectively. Apparently,

25 ppm of nano-polystyrene/250 ppm of $CaCl_2$/750 ppm of MES surfactant under alkaline condition showed the best result among the different synthesized solutions during the core-flooding test with Grey Berea. The synthesized solution with $CaCl_2$ provided higher additional oil recovery compared to synthesized solution with $MgCl_2$. This is because MES anionic surfactant and nano-polystyrene with $CaCl_2$ allowed the dispersion of nano-polystyrene to maintain high stability and maximize the disjoining pressure. The oil recovery study proves the capability and reliability of nano-polystyrene to achieve additional oil recovery. Several mechanisms could be attributed to enhancing the additional oil recovery, such as increasing disjoining pressure, penetration through the small pores, and enhanced macroscopic sweep efficiency (Aziz et al., 2019; Rostami et al., 2019; Nasr et al., 2021c). Study from Kumar et al., (2020b) achieved 13% of the additional oil recovery from chemical materials such as polymer, low salinity water and nanoparticles. An additional 10% of additional oil is recovered with the synthesized solution of seawater with an optimum concentration of nano-silica (Shakiba et al., 2020). Fan et al., (2021) revealed that 15% of the oil recovery factor is obtained with the synthesized solution of nano-silica/polymer/low salinity water. Meanwhile, this present study also obtained a positive impact with the implementation of nano-polystyrene. Therefore, the application of nanotechnology to enhance oil recovery is noteworthy.

Table 4.18: Additional oil recovery for Grey and Buff Berea

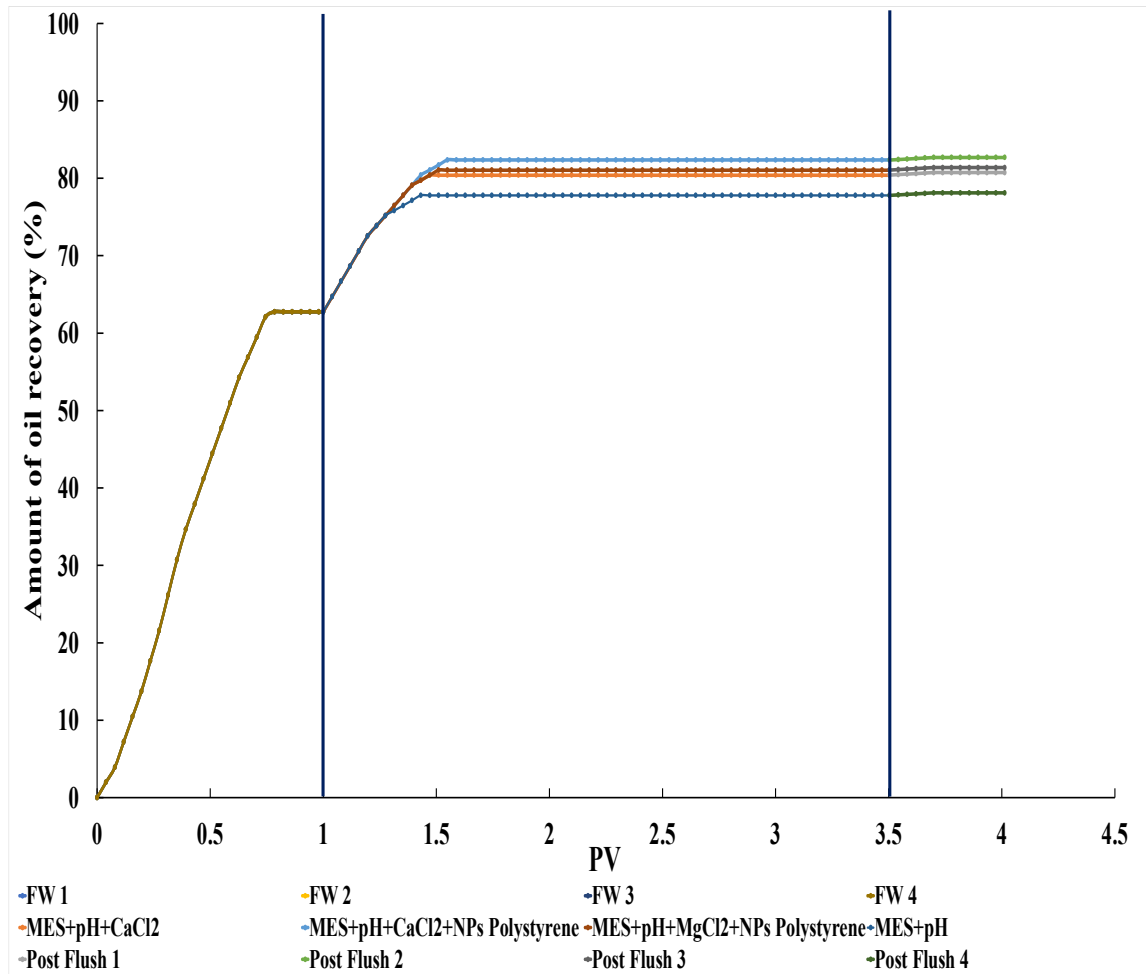| Selected synthesized solutions	Oil Recovery (%) Grey Berea	Oil Recovery (%) Buff Berea
75ppm MES + Alkaline Condition	14.38	15.03
75ppm MES + Alkaline Condition + 250ppm $CaCl_2$	17.00	17.65
75ppm MES + Alkaline Condition + 250ppm $CaCl_2$ + 25ppm Nano-polystyrene	18.95	19.61
75ppm MES + Alkaline Condition + 250ppm $MgCl_2$ + 25ppm Nano-polystyrene	17.65	18.30

Figure 4.19: Oil recovery from Buff Berea under reservoir condition

The core-flooding test was conducted for Buff Berea core samples with the selected optimum synthesized solution. The overall results showed in Figure 4.19 has a similar trend to the results from Grey Berea. However, the oil recovery factors are slightly higher during the secondary and tertiary oil recovery process. The highest oil recovery obtained for Buff Berea is up to 19.61%. The synthesized solution of (75ppm MES + Alkaline Condition + 250ppm $CaCl_2$ + 25ppm Nano-polystyrene) achieved the highest oil recovery for Grey and Buff Berea. Thus, this indicate that the synthesized solution is feasible for Grey and Buff Berea. A higher permeability in Buff Berea could be the reason for achieving higher additional oil recovery. Laboratory work from Joshi et al. (2022) revealed that nanoparticles could provide a better impact on the rock with higher permeability due to the larger structural disjoining pressure. Besides, the pressure

difference obtained from the Buff Berea are overall lower than the Grey Berea. This is because a lesser log jamming effect occurred in Buff Berea. Therefore, it is verified that nanoparticles could provide higher efficiency when applied to rock with higher permeability.

Table 4.19 compares the oil recovery achieved by the other researchers that conducted the core-flooding test with similar temperature conditions and rock types. The oil recovery obtained with a synthesized solution of (75ppm MES + Alkaline Condition + 250ppm $CaCl_2$ + 25ppm Nano-polystyrene) showed a better result than the oil recovery shown in Table 4.19. It is noticeable that the previous experimental works rarely applied the combination of different chemical materials under alkaline condition. From the wettability, adsorption, and oil recovery studies, it is crucial to apply the alkaline condition, especially for the synthesized solution with NPs. This is because the alkaline condition could stabilize the nanoparticles suspended in the fluid. Besides, the alkaline condition could relatively achieve wettability alteration toward a water-wet state and reduce the excessive surfactant loss. Most of the researchers investigated the application of nano-silica for the chemical-EOR process. Meanwhile, the investigation on nano-polystyrene to enhance oil recovery is very limited. However, the high additional oil recovery obtained from the synthesized solution with nano-polystyrene indicate the feasibility of nano-polystyrene to achieve high additional oil recovery and reduce excessive surfactant loss significantly.

Table 4.19: Summary of other previous experimental works on c-EOR method

Literatures	Rock Types	Types of injection fluid	Pressure (psi)	Temperature (℃)	Oil Recovery (%)
Zhou et al., 2019	Sandstone	Amino terminated Nano-silica + anionic surfactant (Soloterra 964)	1160	65	17.23
Zhou et al., 2020	Sandstone	Polymer + surfactant + NPs	1450	80	15.03
Sagala et al., 2020b	Sandstone	Low salinity water + surfaces modified pyroxene NPs	600	60	15
Olayiwola et al., 2020	Sandstone	Low salinity water + SDS surfactant + silica NPs	3000	70	18.46
Liu et al., 2020a	Sandstone	SDBS surfactant + Silica NPs	Ambient pressure	80	9.8

4.10   Analysis on Cost of Excessive Surfactant Losses for Field Application

The application of the c-EOR method not only to achieve the best performance on wettability alteration and oil recovery but the consideration of economic effectiveness is also essential. Therefore, an estimation of the cost with the optimum synthesized solution under different cases is listed in Table 4.20. The estimation is applied on the sandstone reservoir with the assumption of 1 acre (4048 m^2) size and 3m of depth. Besides, sandstone comprises 60% of solid material with 2.5 g/cm^3 of the average density (Park et al., 2015).

Thus, the total amount of the MES surfactant entitled to the sandstone adsorbent would be approximately 1.82×10^{10} g.

According to the current market price of the MES surfactant, it is about RM 11.50/kg. By multiplying the adsorption capacity (4.26 mg/g-adsorbent) with the total adsorbent weight which is (1.82×10^{10} g) and the current market price of MES surfactant, the cost of excessive surfactant losses can be estimated. Thus, the financial loss with the synthesized solution at the ambient temperature case would be approximately RM 891,618. The best case shows that the financial loss could be significantly reduced at reservoir temperature.

Table 4.20: Cost analysis with optimum synthesized solution

Different Cases with (750ppm MES + 250 CaCl$_2$ + 25ppm Nano-polystyrene + Alkaline Condition	Adsorption Capacity (mg/g)	Cost (RM)
Ambient temperature (Grey Berea Sandstone)	4.26	891,618
Ambient temperature (Buff Berea Sandstone)	4.75	994,175
Reservoir temperature (Buff Berea Sandstone)	0.43	899,99
Reservoir temperature (Buff Berea Sandstone)	0.63	131,859

CHAPTER FIVE
Conclusions and Recommendations

5.1   Conclusions

This study conducted a series of experimental works to investigate the feasibility and effectiveness of the synergy of low salinity water/MES anionic surfactant/nano-polystyrene to support additional oil recovery from sandstone reservoir. The polystyrene nanofluid is favorably stable for the chemical-EOR process, which has been confirmed with the zeta potential measurements. The zeta potential values obtained with the negative magnitude greater than -30mV in ambient or reservoir temperature conditions indicate that the nano-polystyrene particles repelled each other and prevented agglomeration in the fluid.

The results obtained from the wettability study confirms the potential of synthesize solutions (low salinity water/MES anionic surfactant/nano-polystyrene/alkaline condition) to shift the oil-wet rock toward a strong water-wet state. The contact angle decreased when MES surfactant is in alkaline medium, and combined with low salinity water and nano-polystyrene. The combination of 250ppm MES surfactant with divalent cation ($CaCl_2$) under alkaline conditions presented the lowest contact angle among the synthesized solutions. The tendency of nanoparticles to reduce the excessive surfactant loss during the chemical-EOR process was proven. The synergy of 25ppm of nano-polystyrene/250ppm of $CaCl_2$/750ppm of MES surfactant under alkaline conditions was able to achieve the lowest adsorption capacity as well as the lowest IFT value. Introducing nano-polystyrene into the synthesized solution reduced the surfactant adsorption capacity up to 92% at reservoir temperature condition. Thus, the synthesized solution has a high potential to be applied efficiently and economically at reservoir condition.

The application of nanofluid to enhance oil recovery is proven through the core-flooding test. The addition of nano-polystyrene supported recovery of 19.61% of additional oil with the synthesized solution of (25ppm nano-polystyrene/750ppm alkaline MES surfactant/250ppm $CaCl_2$). In conclusion, nano-polystyrene can be beneficial to the

synergy of low salinity water and MES anionic surfactant under alkaline conditions to achieve a strong water-wet state, significant surfactant adsorption reduction and maximize additional oil recovery.

5.2   Recommendations

One of the suggestions for the adsorption study is to conduct the adsorption test in dynamic conditions. This could provide more accurate results as the dynamic condition could simulate the reservoir condition. The adsorption of the MES surfactant could be affected by several factors, such as injection flow rate and pressure. Core-flooding equipment can be used for dynamic adsorption tests since it could simulate the real-life reservoir condition. The effluent obtained from the core-flooding test can be used for further analyses so that the accuracy of dynamic adsorption can be improved.

In addition, further investigation with core-flooding test should be applied with different parameters magnitude to validate the feasibility of the selected optimum synthesized solutions under different conditions. The core-flooding test could apply with a higher temperature since the reservoir temperature and pressure could be even higher for different reservoirs. Besides, the injection rates would affect the oil recovery factor and cause formation damage. Therefore, the core-flooding test should also consider different injection rates. Lastly, the cost estimation for the surfactant losses could be further improved by using the industrial simulation with the support of details field data.

References

Abbas, A. H., Abd Alsaheb, R. A., & Abdullah, J. K. 2022. Comparative study of natural chemical for enhanced oil recovery: Focus on extraction and adsorption at quartz sand surface. *Petroleum*.

Abbasi, S., Khamehchi, E. 2021. Experimental investigation of competitive mechanisms of precipitation and dissolution due to seawater and low salinity water injection in carbonate reservoirs. J. Mol. Liq. 324, 114767.

Ab Rasid, S. A., Mahmood, S. M., Kechut, N. I., & Akbari, S. 2021. A review on parameters affecting nanoparticles stabilized foam performance based on recent analyses. *Journal of Petroleum Science and Engineering*, 109475.

Adil, M., Zaid, H. M., Chuan, L. K. 2020. Electromagnetically-induced change in interfacial tension and contact angle of oil droplet using dielectric nanofluids. Fuel 259, 116274.

Afekare, D., Garno, J., Rao, D. 2021. Enhancing oil recovery using silica nanoparticles: Nanoscale wettability alteration effects and implications for shale oil recovery. J. Pet. Sci. Eng. 203, 108897.

Afekare, D., Gupta, I., Rao, D. 2020. Nanoscale investigation of silicon dioxide nanofluids and implications for enhanced oil recovery–An atomic force microscope study. J. Pet. Sci. Eng. 191, 107165.

Afzali, S., Rezaei, N., & Zendehboudi, S. 2018. A comprehensive review on enhanced oil recovery by water alternating gas (WAG) injection. Fuel, 227, 218-246.

Aggelopoulos, C., Robin, M., & Vizika, O. 2011. Interfacial tension between CO2 and brine (NaCl+ CaCl2) at elevated pressures and temperatures: The additive effect of different salts. *Advances in Water Resources, 34*(4), 505-511.

Agi, A., Junin, R., Jaafar, M. Z., Mohsin, R., Arsad, A., Gbadamosi, A., Gbonhinbor, J. 2020. Synthesis and application of rice husk silica nanoparticles for chemical enhanced oil recovery. J. Mater. Res. Technol. 9(6), 13054-13066.

Ahmadi, M. A., & Shadizadeh, S. R. 2015. Experimental investigation of a natural surfactant adsorption on shale-sandstone reservoir rocks: Static and dynamic conditions. *Fuel, 159*, 15-26.

Ahmadi, P., Asaadian, H., Khadivi, A., Kord, S. 2019a. A new approach for determination of carbonate rock electrostatic double layer variation towards wettability alteration. J. Mol. Liq. 275, 682-698.

Ahmadi, R., Farmani, Z., Osfouri, S., Azin, R. 2019b. Condensate blockage remediation in a gas reservoir through wettability alteration using natural $CaCO_3$ nanoparticles. Colloids Surf. A: Physicochem Eng. Asp. 579, 123702.

Ahsaei, Z., Nabipour, M., Azdarpour, A., Santos, R. M., Mohammadian, E., Babakhani, P., Esfandiarian, A. 2022. Application of commercial zwitterionic surfactants and ionic liquids to reduce interfacial tension and alter wettability in a carbonate reservoir. *Energy Sources, Part A: Recovery, Utilization, and Environmental Effects, 44*(2), 2811-2822.

Alhuraishawy, A. K., Bai, B., Wei, M., Geng, J., Pu, J. 2018. Mineral dissolution and fine migration effect on oil recovery factor by low-salinity water flooding in low-permeability sandstone reservoir. Fuel 220, 898-907.

Ali, J. A., Kalhury, A. M., Sabir, A. N., Ahmed, R. N., Ali, N. H., & Abdullah, A. D. 2020. A state-of-the-art review of the application of nanotechnology in the oil and gas

industry with a focus on drilling engineering. *Journal of Petroleum Science and Engineering, 191*, 107118.

Almahfood, M., Bai, B. 2018. The synergistic effects of nanoparticle-surfactant nanofluids in EOR applications. J. Pet. Sci. Eng. 171, 196-210.

Alnarabiji, M. S., Husein, M. M. 2020. Application of bare nanoparticle-based nanofluids in enhanced oil recovery. Fuel 267, 117262.

Alnarabiji, M. S., Yahya, N., Nadeem, S., Adil, M., Baig, M. K., Ghanem, O. B., Klemeš, J. J. 2018. Nanofluid enhanced oil recovery using induced ZnO nanocrystals by electromagnetic energy: Viscosity increment. *Fuel, 233*, 632-643.

Al-Saedi, H. N., Flori, R. E. 2018. Enhanced oil recovery of low salinity water flooding in sandstone and the role of clay. Pet. Explor. Dev. 45(5), 927-931.

Al-Saedi, H. N., Flori, R. E. 2019. Effect of divalent cations in low salinity water flooding in sandstone reservoirs. J. Mol. liq. 283, 417-426.

Aminian, A., ZareNezhad, B. 2019. Wettability alteration in carbonate and sandstone rocks due to low salinity surfactant flooding. J. Mol. Liq. 275, 265-280.

Amrouche, F., Blunt, M., Iglauer, S., Short, M., Crosbie, T., Cordero, E., & Xu, D. 2023. Using magnesium oxide nanoparticles in a magnetic field to enhance oil production from oil-wet carbonate reservoirs. *Materials Today Chemistry, 27*, 101342.

Apaydin, O. G., Kovscek, A. R. 2001. Surfactant concentration and end effects on foam flow in porous media. Transp Porous Media 43(3), 511-536.

Atta, D. Y., Negash, B. M., Yekeen, N., Habte, A. D. 2020. A state-of-the-art review on the application of natural surfactants in enhanced oil recovery. J. Mol. Liq. 321, 114888.

Aziz, H., Tunio, S. Q. 2019. Enhancing oil recovery using nanoparticles—A review. Adv. Nat. Sci.: Nanosci. Nanotechnol. 10(3), 033001.

Bashir, A., Haddad, A. S., Rafati, R. 2019. Nanoparticle/polymer-enhanced alpha olefin sulfonate solution for foam generation in the presence of oil phase at high temperature conditions. Colloids Surf. A: Physicochem Eng. Asp. 582, 123875.

Bashir, A., Haddad, A. S., & Rafati, R. 2021. A review of fluid displacement mechanisms in surfactant-based chemical enhanced oil recovery processes: analyses of key influencing factors. *Petroleum Science*.

Behera, U. S., & Sangwai, J. S. 2022. Silica nanofluid in low salinity seawater containing surfactant and polymer: Oil recovery efficiency, wettability alteration and adsorption studies. *Journal of Petroleum Science and Engineering, 211*, 110148.

Bera, A., & Belhaj, H. 2016. Application of nanotechnology by means of nanoparticles and nanodispersions in oil recovery-A comprehensive review. Journal of Natural Gas Science and Engineering, 34, 1284-1309.

Bhicajee, P., & Romero-Zerón, L. 2021. Effect of different low salinity flooding schemes and the addition of alkali on the performance of low-salinity waterflooding during the recovery of heavy oil from unconsolidated sandstone. *Fuel, 289*, 119981.

Bila, A., Stensen, J. Å., & Torsæter, O. Polymer-functionalized silica nanoparticles for improving water flood sweep efficiency in Berea sandstones. In: The 2019 International Symposium of the Society of Core Analyst. 2019.

Cacua, K., Ordoñez, F., Zapata, C., Herrera, B., Pabón, E., & Buitrago-Sierra, R. 2019. Surfactant concentration and pH effects on the zeta potential values of alumina nanofluids to inspect stability. *Colloids and Surfaces A: Physicochemical and Engineering Aspects, 583*, 123960.

Caldelas, F. M. 2010. Experimental parameter analysis of nanoparticle retention in porous media. (M.Sc. Thesis). The University of Texas at Austin, USA.

Chakraborty, S., & Panigrahi, P. K. 2020. Stability of nanofluid: A review. *Applied Thermal Engineering, 174*, 115259.

Chen, Q., Otaibi, M., Ayirala, S., Yousef, A. 2021. The prospects and potential opportunities of low salinity water flooding for offshore applications in sandstones. J. Pet. Sci. Eng. 199, 108260.

Chen, Y., Jha, N. K., Al-Bayati, D., Lebedev, M., Sarmadivaleh, M., Iglauer, S., Xie, Q. 2020. Geochemical controls on wettability alteration at pore-scale during low salinity water flooding in sandstone using X-ray micro computed tomography. *Fuel, 271*, 117675.

Chen, Y., Xie, Q., Pu, W., Saeedi, A. 2018. Drivers of pH increase and implications for low salinity effect in sandstone. Fuel, *218*, 112-117.

Chen, Z.-Z., Gang, H.-Z., Liu, J.-F., Mu, B.-Z., Yang, S.-Z. 2019. A thermal-stable and salt-tolerant biobased zwitterionic surfactant with ultralow interfacial tension between crude oil and formation brine. J. Pet. Sci. Eng. 181, 106181.

Choi, K.-O., Aditya, N., & Ko, S. 2014. Effect of aqueous pH and electrolyte concentration on structure, stability and flow behavior of non-ionic surfactant based solid lipid nanoparticles. *Food chemistry, 147*, 239-244.

Collins, I., Couves, J., Hodges, M., McBride, E., Pedersen, C., Salino, P., Zeng, H. Effect of low salinity waterflooding on the chemistry of the produced crude oil. In: Paper SPE 190191-MS presented at the SPE Improved Oil Recovery Conference. Tulsa Oklahoma, USA, April 14-18, 2018.

Da Costa, A. A., Mateo, J., Patel, R., Trivedi, J., Soares, J., Rocha, P., Embiruçu, M. 2021. Can low salinity water injection be an efficient option for the Recôncavo Basin? An experimental and simulation case study. *Journal of Petroleum Science and Engineering, 202*, 108557.

Da Costa, A. A., Soares, J., Rocha, P., Costa, G., & Embiruçu, M. 2020. An experimental evaluation of low salinity water mechanisms in a typical Brazilian sandstone and light crude oil with low acid/basic number. *Fuel, 273*, 117694.

Díez, R., Medina, O. E., Giraldo, L. J., Cortés, F. B., & Franco, C. A. 2020. Development of nanofluids for the inhibition of formation damage caused by fines migration: effect of the interaction of quaternary amine (CTAB) and MgO nanoparticles. *Nanomaterials, 10*(5), 928.

Doan, T. H. Y., Le, T. T., Nguyen, T. M. T., Chu, T. H., Pham, T. N. M., Nguyen, T. A. H., & Pham, T. D. 2021. Simultaneous adsorption of anionic alkyl sulfate surfactants onto alpha alumina particles: Experimental consideration and modeling. *Environmental Technology & Innovation, 24*, 101920.

Duffy, T. S., Raman, B., Hall, D. M., Machesky, M. L., Johns, R. T., Lvov, S. N. 2019. Experimentation and modeling of surface chemistry of the silica-water interface for low salinity waterflooding at elevated temperatures. Colloids Surf. A: Physicochem Eng. Asp. *570*, 233-243.

Elochukwu, H., Gholami, R., & Dol, S. S. 2017. An approach to improve the cuttings carrying capacity of nanosilica based muds. *Journal of Petroleum Science and Engineering, 152*, 309-316.

Enerdata. Accessed 21 December 2022. Malaysia Energy Information. https://www.enerdata.net/estore/energy-market/malaysia/.

Esfandyari, H., Shadizadeh, S. R., Esmaeilzadeh, F., Davarpanah, A. 2020. Implications of anionic and natural surfactants to measure wettability alteration in EOR processes. Fuel, 278, 118392.

Fan, G., Li, M., Chen, X., Palyanitsina, A., & Timoshin, A. 2021. Polymer-Nanosilica-assisted to evaluate oil recovery performances in sandstone reservoirs. *Energy Reports, 7*, 2588-2593.

Farhadi, H., Fatemi, M., Ayatollahi, S. 2021. Experimental investigation on the dominating fluid-fluid and rock-fluid interactions during low salinity water flooding in water-wet and oil-wet calcites. J. Pet Sci. Eng, 204, 108697.

Firozjaii, A. M., & Saghafi, H. R. 2020. Review on chemical enhanced oil recovery using polymer flooding: Fundamentals, experimental and numerical simulation. *Petroleum, 6*(2), 115-122.

Foroozesh, J., Kumar, S. 2020. Nanoparticles behaviors in porous media: application to enhanced oil recovery. J. Mol. Liq. 316, 113876.

Gbadamosi, A. O., Junin, R., Manan, M. A., Agi, A., Oseh, J. O., Usman, J. 2019. Effect of aluminium oxide nanoparticles on oilfield polyacrylamide: Rheology, interfacial tension, wettability and oil displacement studies. J. Mol. Liq. 296, 111863.

Hanamertani, A. S., Pilus, R. M., Idris, A. K., Irawan, S., & Tan, I. M. 2018. Ionic liquids as a potential additive for reducing surfactant adsorption onto crushed Berea sandstone. *Journal of Petroleum Science and Engineering, 162*, 480-490.

Hashemi, S., Saien, J. 2020. Highly efficient [C8mim][Cl] ionic liquid accompanied with magnetite nanoparticles and different salts for interfacial tension reduction. Chin. J. Chem. Eng. 28(1), 46-53.

Hassan, Y. M., Guan, B. H., Chuan, L. K., Hamza, M. F., & Sikiru, S. 2023. Effect of Silica-based Hybrid Nano-Surfactant on Interfacial Tension Reduction for Enhanced Oil Recovery. *Chemical Engineering Research and Design*. 195, 370-377.

He, J., Jia, H., Wang, Q., Xu, Y., Zhang, L., Jia, H., Xie, Q. 2022. Investigation on pH and redox-trigged emulsions stabilized by ferrocenyl surfactants in combination with Al2O3 nanoparticles and their application for enhanced oil recovery. *Colloids and Surfaces A: Physicochemical and Engineering Aspects, 655*, 130303.

Hendraningrat, L., Li, S., Torsaeter, O. Enhancing oil recovery of low-permeability Berea sandstone through optimized nanofluids concentration. In: Paper SPE 165283-MS presented at the SPE enhanced oil recovery conference. Kuala Lumpur, Malaysia, July 2-4 2013.

Hirasaki, G. J., Miller, C. A., Puerto, M. 2011. Recent advances in surfactant EOR. Soc. Pet. Eng. J. 16(04), 889-907.

Hutchinson, J., Lee, J., Eigley, T., Krueger, R. 2006. Method of making methyl ester surfactants. US Patent: US20060142602A1

Jaafar, M., Vinogradov, J., & Jackson, M. 2009. Measurement of streaming potential coupling coefficient in sandstones saturated with high salinity NaCl brine. *Geophysical Research Letters, 36*(21).

Jafarbeigi, E., Salimi, F., Kamari, E., & Mansouri, M. 2022. Effects of modified graphene oxide (GO) nanofluid on wettability and IFT changes: Experimental study for EOR applications. *Petroleum Science, 19*(4), 1779-1792.

Joshi, D., Maurya, N. K., Kumar, N., & Mandal, A. 2022. Experimental investigation of silica nanoparticle assisted Surfactant and polymer systems for enhanced oil recovery. *Journal of Petroleum Science and Engineering, 216*, 110791.

Kalam, S., Abu-Khamsin, S. A., Kamal, M. S., Patil, S. 2021. A review on surfactant retention on rocks: mechanisms, measurements, and influencing factors. Fuel 293, 120459.

Katende, A., Sagala, F. 2019. A critical review of low salinity water flooding: mechanism, laboratory and field application. J. Mol. Liq. 278, 627-649.

Kazemzadeh, Y., Shojaei, S., Riazi, M., Sharifi, M. 2019. Review on application of nanoparticles for EOR purposes: A critical review of the opportunities and challenges. Chin. J. Chem. Eng. 27(2), 237-246.

Khayati, H., Moslemizadeh, A., Shahbazi, K., Moraveji, M. K., Riazi, S. H. 2020. An experimental investigation on the use of saponin as a non-ionic surfactant for chemical enhanced oil recovery (EOR) in sandstone and carbonate oil reservoirs: IFT, wettability alteration, and oil recovery. Chem. Eng. Res. Des. 160, 417-425.

Keykhosravi, A., & Simjoo, M. 2019. Insights into stability of silica nanofluids in brine solution coupled with rock wettability alteration: An enhanced oil recovery study in oil-wet carbonates. *Colloids and Surfaces A: Physicochemical and Engineering Aspects, 583*, 124008.

Khishvand, M., Kohshour, I. O., Alizadeh, A. H., Piri, M., Prasad, S. 2019. A multi-scale experimental study of crude oil-brine-rock interactions and wettability alteration during low-salinity waterflooding. Fuel 250, 117-131.

Kim, I., Taghavy, A., DiCarlo, D., Huh, C. 2015. Aggregation of silica nanoparticles and its impact on particle mobility under high-salinity conditions. J. Pet. Sci. Eng. 133, 376-383.

Kim, I., Worthen, A. J., Johnston, K. P., DiCarlo, D. A., & Huh, C. 2016. Size-dependent properties of silica nanoparticles for Pickering stabilization of emulsions and foams. *Journal of Nanoparticle Research, 18*(4), 82.

Kim, Y., Kim, C., Kim, J., Kim, Y., & Lee, J. 2020. Experimental investigation on the complex chemical reactions between clay minerals and brine in low salinity water-flooding. *Journal of Industrial and Engineering Chemistry, 89*, 316-333.

Koparal, G. B., Sharma, H., Liyanage, P. J., Panthi, K. K., & Mohanty, K. K. 2021. Reducing surfactant retention using polyacrylate in Berea sandstone. *Journal of Petroleum Science and Engineering*, 109228.

Kumar, N., & Mandal, A. 2018. Surfactant stabilized oil-in-water nanoemulsion: stability, interfacial tension, and rheology study for enhanced oil recovery application. *Energy & Fuels, 32*(6), 6452-6466.

Kumar, N., Mandal, A. 2020a. Wettability alteration of sandstone rock by surfactant stabilized nanoemulsion for enhanced oil recovery—A mechanistic study. Colloids Surf. A: Physicochem Eng. Asp. 601, 125043.

Kumar, R. S., Chaturvedi, K. R., Iglauer, S., Sharma, T. 2020b. Impact of anionic surfactant on stability, viscoelastic moduli, and oil recovery of silica nanofluid in saline environment. J. Pet. Sci. Eng. 195, 107634.

Kumar, S., Mandal, A. 2016. Studies on interfacial behavior and wettability change phenomena by ionic and nonionic surfactants in presence of alkaline and salt for enhanced oil recovery. Appl. Surf. Sci. 372, 42-51.

Lager, A., Webb, K. J., Black, C., Singleton, M., Sorbie, K. S. 2008. Low salinity oil recovery-an experimental investigation. Petrophysics-The SPWLA Journal of Formation Evaluation and Reservoir Description, 49(01).

Li, Y.-l., Chen, Z., Liu, X.-m., Wang, L., Cui, Z.-G. 2020. 1, 3-Dialkyl glyceryl ethers derivatives as surfactants for enhanced oil recovery in high salinity and high temperature reservoir conditions. Colloids Surf. A: Physicochem Eng. Asp. 589, 124425.

Lin, Q., Xu, M., Cui, Z., Pei, X., Jiang, J., & Song, B. 2019. Structure and stabilization mechanism of diesel oil-in-water emulsions stabilized solely by either positively or negatively charged nanoparticles. *Colloids and Surfaces A: Physicochemical and Engineering Aspects, 573*, 30-39.

Lin, Y., Nan, G., Li, Y., Fan, W. 2020. Synthesis of sulfonate of alkylated extract of FCC slurry for enhancing oil recovery. Fuel 260, 116299.

Liu, P., Yu, H., Niu, L., Ni, D., Zhao, Q., Li, X., & Zhang, Z. 2020a. Utilization of Janus-silica/surfactant nanofluid without ultra-low interfacial tension for improving oil recovery. *Chemical Engineering Science, 228*, 115964.

Liu, Z., Bode, V., Hadayati, P., Onay, H., & Sudhölter, E. J. 2020b. Understanding the stability mechanism of silica nanoparticles: The effect of cations and EOR chemicals. *Fuel, 280*, 118650.

Liu, Z., Hedayati, P., Ghatkesar, M. K., Sun, W., Onay, H., Groenendijk, D., Sudhölter, E. J. 2021. Reducing anionic surfactant adsorption using polyacrylate as sacrificial agent investigated by QCM-D. J. Colloid Interface Sci. 585, 1-11.

Liu, Z., Hedayati, P., Sudhölter, E. J., Haaring, R., Shaik, A. R., Kumar, N. 2020c. Adsorption behavior of anionic surfactants to silica surfaces in the presence of calcium ion and polystyrene sulfonate. Colloids Surf. A: Physicochem Eng. Asp.602, 125074.

Liu, Z., Rios-Carvajal, T., Andersson, M., Ceccato, M., Stipp, S., & Hassenkam, T. 2018. Insights into the pore-scale mechanism for the low-salinity effect: implications for enhanced oil recovery. *Energy & Fuels, 32*(12), 12081-12090.

Madani, M., Zargar, G., Takassi, M. A., Daryasafar, A., Wood, D. A., Zhang, Z. 2019. Fundamental investigation of an environmentally-friendly surfactant agent for chemical enhanced oil recovery. Fuel 238, 186-197.

Ma, K., Cui, L., Dong, Y., Wang, T., Da, C., Hirasaki, G. J., & Biswal, S. L. 2013. Adsorption of cationic and anionic surfactants on natural and synthetic carbonate materials. Journal of Colloid and Interface Science, 408, 164-172.

Mahmoudi, S., Jafari, A., & Javadian, S. 2019. Temperature effect on performance of nanoparticle/surfactant flooding in enhanced heavy oil recovery. *Petroleum Science, 16*(6), 1387-1402.

Manshad, A. K., Rezaei, M., Moradi, S., Nowrouzi, I., Mohammadi, A. H. 2017. Wettability alteration and interfacial tension (IFT) reduction in enhanced oil recovery (EOR) process by ionic liquid flooding. J. Mol. Liq. 248, 153-162.

Mansouri, M., Nakhaee, A., & Pourafshary, P. 2019. Effect of SiO2 nanoparticles on fines stabilization during low salinity water flooding in sandstones. *Journal of Petroleum Science and Engineering, 174*, 637-648.

Massarweh, O., Abushaikha, A. S. 2020. The use of surfactants in enhanced oil recovery: A review of recent advances. Energy Rep. 6, 3150-3178.

Mehraban, M. F., Ayatollahi, S., Sharifi, M. 2021. Experimental investigation on synergic effect of salinity and pH during low salinity water injection into carbonate oil reservoirs. J. Pet. Sci. Eng. 202, 108555.

Mehraban, M. F., Farzaneh, S. A., Sohrabi, M., Sisson, A. 2022. Fluid-Fluid Interactions Inducing Additional Oil Recovery during Low Salinity Water Injection in Inefficacious Presence of Clay Minerals. Fuel 308, 121922.

Minakov, A., Pryazhnikov, M., Suleymana, Y., Meshkova, V., Guzei, D. 2021. Experimental study of nanoparticle size and material effect on the oil wettability characteristics of various rock types. J. Mol. Liq. 327, 114906.

Moghadasi, R., Rostami, A., & Hemmati-Sarapardeh, A. 2019. Application of nanofluids for treating fines migration during hydraulic fracturing: Experimental study and mechanistic understanding. *Advances in Geo-Energy Research, 3*(2), 198-206.

Nasr, M. S., Esmaeilnezhad, E., Choi, H. J. 2021a. Effect of Carbon-Based and Metal-Based nanoparticles on Enhanced Oil Recovery: A Review. J. Mol. Liq. 338, 116903.

Nasr, M. S., Esmaeilnezhad, E., Choi, H. J. 2021b. Effect of silicon-based nanoparticles on enhanced oil recovery. J. Taiwan Inst. Chem. Eng. 122, 241-259.

Nasr, M. S., Esmaeilnezhad, E., Allahbakhsh, A., & Choi, H. J. 2021c. Nitrogen-doped graphene quantum dot nanofluids to improve oil recovery from carbonate and sandstone oil reservoirs. *Journal of Molecular Liquids, 330*, 115715.

Negi, G., Anirbid, S., Sivakumar, P. 2021. Applications of silica and titanium dioxide nanoparticles in enhanced oil recovery: Promises and challenges. Pet. Res. 6(3), 224-246.

Negin, C., Ali, S., Xie, Q. 2017. Most common surfactants employed in chemical enhanced oil recovery. Petroleum 3(2), 197-211.

Nelson, R. 1981. Further studies on phase relationships in chemical flooding. In Surface phenomena in enhanced oil recovery 73-104: Springer.

Nezhad, M. S., Wood, D. A., Sadatshojaei, E., & Esmaeilzadeh, F. 2021. New insight to experimental study of ionic solutions with a non-ionic surfactant on wettability, interfacial tension and micro-model flooding. *Fuel, 285*, 119126.

Olayiwola, S. O., Dejam, M. 2019. A comprehensive review on interaction of nanoparticles with low salinity water and surfactant for enhanced oil recovery in sandstone and carbonate reservoirs. Fuel 241, 1045-1057.

Olayiwola, S. O., Dejam, M. 2020. Synergistic interaction of nanoparticles with low salinity water and surfactant during alternating injection into sandstone reservoirs to improve oil recovery and reduce formation damage. J. Mol. Liq. 317, 114228.

Omidi, A., Manshad, A. K., Moradi, S., Ali, J. A., Sajadi, S. M., Keshavarz, A. 2020. Smart-and nano-hybrid chemical EOR flooding using Fe3O4/eggshell nanocomposites. J. Mol. Liq. 316, 113880.

Pal, N., Kumar, S., Bera, A., & Mandal, A. 2019. Phase behaviour and characterization of microemulsion stabilized by a novel synthesized surfactant: Implications for enhanced oil recovery. *Fuel, 235*, 995-1009.

Pal, N., Saxena, N., Laxmi, K. D., & Mandal, A. 2018. Interfacial behaviour, wettability alteration and emulsification characteristics of a novel surfactant: Implications for enhanced oil recovery. *Chemical Engineering Science, 187*, 200-212.

Pan, F., Zhang, Z., Zhang, X., & Davarpanah, A. 2020. Impact of anionic and cationic surfactants interfacial tension on the oil recovery enhancement. *Powder Technology, 373*, 93-98.

Panchal, H., Patel, H., Patel, J., Shah, M. 2021. A systematic review on nanotechnology in enhanced oil recovery. Pet. Res. 6(3), 204-212.

Park, S., Lee, E. S., & Sulaiman, W. R. W. 2015. Adsorption behaviors of surfactants for chemical flooding in enhanced oil recovery. *Journal of Industrial and Engineering Chemistry, 21*, 1239-1245.

Paternina, C. A., Londono, A. K., Rondon, M., Mercado, R., Botett, J. 2020. Influence of salinity and hardness on the static adsorption of an extended surfactant for an oil recovery purpose. J. Pet. Sci. Eng. 195, 107592.

Phukan, R., Gogoi, S. B., & Tiwari, P. 2020. Effects of CO_2-foam stability, interfacial tension and surfactant adsorption on oil recovery by alkaline-surfactant-alternated-gas/CO_2 flooding. *Colloids and Surfaces A: Physicochemical and Engineering Aspects, 597*, 124799.

Pillai, P., Kumar, A., & Mandal, A. 2018. Mechanistic studies of enhanced oil recovery by imidazolium-based ionic liquids as novel surfactants. *Journal of Industrial and Engineering Chemistry, 63*, 262-274.

Pooryousefy, E., Xie, Q., Chen, Y., Sari, A., Saeedi, A. 2018. Drivers of low salinity effect in sandstone reservoirs. J. Mol. Liq. 250, 396-403.

Purswani, P., Tawfik, M. S., Karpyn, Z. T. 2017. Factors and mechanisms governing wettability alteration by chemically tuned waterflooding: a review. Energy Fuels. 31(8), 7734-7745.

Qiao, L., Cheng, J., Meng, N., Qian, Y., Yuan, Y., Li, Y., Ding, C. 2021. An isothermal adsorption model for adsorption of substrates by anammox extracellular polymeric substance proteins: Establishment, verification, and determination of adsorption capacity. *Journal of Water Process Engineering, 43*, 102233.

Radnia, H., Rashidi, A., Nazar, A. R. S., Eskandari, M. M., & Jalilian, M. 2018. A novel nanofluid based on sulfonated graphene for enhanced oil recovery. *Journal of Molecular Liquids, 271*, 795-806.

Rahimi, A., Honarvar, B., Safari, M. 2020. The role of salinity and aging time on carbonate reservoir in low salinity seawater and smart seawater flooding. J. Pet. Sci. Eng. 187, 106739.

Ramos, G. A., Akanji, L. T., & Afzal, W. 2020. A novel surfactant–polymer/alkaline–surfactant–polymer formulation for enhanced oil recovery (eor) processes. *Energy & Fuels, 34*(2), 1230-1239.

Rasid, S. A., Mahmood, S. M., Kechut, N. I., Akbari, S. 2021b. A review on parameters affecting nanoparticles stabilized foam performance based on recent analyses. J. Pet. Sci. Eng. 208, 109475.

Rezvani, H., Khalilnezhad, A., Ganji, P., Kazemzadeh, Y. 2018. How ZrO_2 nanoparticles improve the oil recovery by affecting the interfacial phenomena in the reservoir conditions? J. Mol. Liq. 252, 158-168.

Riswati, S. S., Bae, W., Park, C., Permadi, A. K., Efriza, I., & Min, B. 2019. Experimental analysis to design optimum phase type and salinity gradient of alkaline surfactant polymer flooding at low saline reservoir. *Journal of Petroleum Science and Engineering, 173*, 1005-1019.

Rostami, P., Sharifi, M., Aminshahidy, B., & Fahimpour, J. 2019. Enhanced oil recovery using silica nanoparticles in the presence of salts for wettability alteration. *Journal of Dispersion Science and Technology*.

Sadatshojaei, E., Jamialahmadi, M., Esmaeilzadeh, F., Wood, D. A., & Ghazanfari, M. H. 2019. The impacts of silica nanoparticles coupled with low-salinity water on

wettability and interfacial tension: experiments on a carbonate core. *Journal of Dispersion Science and Technology.*

Sagala, F., Hethnawi, A., Nassar, N. N. 2020a. Hydroxyl-functionalized silicate-based nanofluids for enhanced oil recovery. Fuel 269, 117462.

Sagala, F., Hethnawi, A., & Nassar, N. N. 2020b. Integrating silicate-based nanoparticles with low-salinity water flooding for enhanced oil recovery in sandstone reservoirs. *Industrial & Engineering Chemistry Research, 59*(37), 16225-16239.

Saha, R., Uppaluri, R. V., & Tiwari, P. 2017. Effect of mineralogy on the adsorption characteristics of surfactant—Reservoir rock system. *Colloids and Surfaces A: Physicochemical and Engineering Aspects, 531*, 121-132.

Sangwook, L., Zhang, H., Wu, P., Nikolov, A., Wasan, D., 2016. The dynamic spreading of nanofluids on solid surfaces – Role of the nanofilm structural disjoining pressure. Journal of Colloid and Interface Science 470, 22-30.

Saxena, N., Kumar, A., Mandal, A. 2019. Adsorption analysis of natural anionic surfactant for enhanced oil recovery: The role of mineralogy, salinity, alkalinity and nanoparticles. J. Pet. Sci. Eng. 173, 1264-1283.

Shakiba, M., Khamehchi, E., Fahimifar, A., & Dabir, B. 2020. A mechanistic study of smart water injection in the presence of nanoparticles for sand production control in unconsolidated sandstone reservoirs. *Journal of Molecular Liquids, 319*, 114210.

Sharma, T., Suresh Kumar, G., Sangwai, J. S. 2014. Enhanced oil recovery using oil-in-water (O/W) emulsion stabilized by nanoparticle, surfactant and polymer in the presence of NaCl. Geosystem Eng. 17(3), 195-205.

Shirazi, M., Kord, S., Tamsilian, Y. 2019. Novel smart water-based titania nanofluid for enhanced oil recovery. J. Mol. Liq. 296, 112064.

Singh, R., Mohanty, K. K. 2020. Study of nanoparticle-stabilized foams in harsh reservoir conditions. Transp. Porous Media, 131(1), 135-155.

Sofla, S. J. D., James, L. A., Zhang, Y. 2018. Insight into the stability of hydrophilic silica nanoparticles in seawater for Enhanced oil recovery implications. Fuel 216, 559-571.

Southwick, J. G., van den Pol, E., van Rijn, C. H., van Batenburg, D. W., Boersma, D., Svec, Y., Raney, K. 2016. Ammonia as alkali for alkaline/surfactant/polymer floods. SPE J. 21(01), 10-21.

Sun, Q., Liu, W., Li, S., Zhang, N., Li, Z. 2021. Interfacial Rheology of Foam Stabilized by Nanoparticles and Their Retention in Porous Media. Energy Fuels, 35(8), 6541-6552.

Taborda, E. A., Franco, C. A., Lopera, S. H., Castro, R. H., Maya, G. A., Idrobo, E. A., Cortes, F. B. 2021. Effect of surface acidity of SiO_2 nanoparticles on thermal stability of polymer solutions for application in EOR processes. J. Pet. Sci. Eng. 196, 107802.

Tai, X.-m., Song, J.-y., Du, Z.-p., Liu, X., Wang, T., Wang, G. 2018. The performance test of fatty acid methyl ester sulfonates and application in the dishwashing liquid detergent. J. Dispers. Sci. Technol. 39(10), 1422-1426.

Torrijos, I. D. P., Puntervold, T., Strand, S., Austad, T., Bleivik, T. H., Abdullah, H. I. 2018. An experimental study of the low salinity Smart Water-Polymer hybrid EOR effect in sandstone material. J. Pet. Sci. Eng. 164, 219-229.

Udoh, T. H. 2021. Improved insight on the application of nanoparticles in enhanced oil recovery process. Sci. Afr. 13, e00873.

Venancio, J. C. C., Nascimento, R. S. V., & Pérez-Gramatges, A. 2020. Colloidal stability and dynamic adsorption behavior of nanofluids containing alkyl-modified silica nanoparticles and anionic surfactant. Journal of Molecular Liquids, 308, 113079.

Vinogradov, J., Jackson, M. D., & Chamerois, M. 2018. Zeta potential in sandpacks: Effect of temperature, electrolyte pH, ionic strength and divalent cations. *Colloids and Surfaces A: Physicochemical and Engineering Aspects, 553*, 259-271.

Wang, H., Alvarado, V., Bagdonas, D. A., McLaughlin, J. F., Kaszuba, J. P., Grana, D., Ng, K. 2021. Effect of CO2-brine-rock reactions on pore architecture and permeability in dolostone: Implications for CO2 storage and EOR. Int. J. Greenh. Gas Control, 107, 103283.

Wang, Y., Pan, M., Mayanna, S., Schleicher, A. M., Spangenberg, E., Schicks, J. M. 2020. Reservoir formation damage during hydrate dissociation in sand-clay sediment from Qilian Mountain permafrost, China. Appl. Energy, 263, 114619.

Winanda, D. F., & Adisasmito, S. 2021. Addition of surfactants to Low Salinity Waterflooding in microfluidics system to increase oil recovery. *Petroleum Research*.

Wu, Y., Chen, W., Dai, C., Huang, Y., Li, H., Zhao, M., Jiao, B. 2017. Reducing surfactant adsorption on rock by silica nanoparticles for enhanced oil recovery. J. Pet. Sci. Eng. 153, 283-287.

Xu, G., Chang, J., Wu, H., Shao, W., Li, G., Hou, J., Yang, J. 2023. Enhanced oil recovery performance of surfactant-enhanced janus SiO2 nanofluid for high temperature and salinity reservoir. *Colloids and Surfaces A: Physicochemical and Engineering Aspects, 657*, 130545.

Yakasai, F., Jaafar, M. Z., Bandyopadhyay, S., Agi, A., Sidek, M. A. 2022. Application of iron oxide nanoparticles in oil recovery–A critical review of the properties, formulation, recent advances and prospects. J. Pet. Sci. Eng. 208, 109438.

Yang, K., Li, S., Zhang, K., Wang, Y. 2021. Synergy of hydrophilic nanoparticle and nonionic surfactant on stabilization of carbon dioxide-in-brine foams at elevated temperatures and extreme salinities. Fuel 288, 119624.

Yao, Y., Wei, M., & Kang, W. 2021. A review of wettability alteration using surfactants in carbonate reservoirs. Adv. Colloid Interface Sci. 294, 102477.

Yekeen, N., Malik, A. A., Idris, A. K., Reepei, N. I., Ganie, K. 2020. Foaming properties, wettability alteration and interfacial tension reduction by saponin extracted from soapnut (Sapindus Mukorossi) at room and reservoir conditions. J. Pet. Sci. Eng. 195, 107591.

Youssif, M. I., El-Maghraby, R. M., Saleh, S. M., Elgibaly, A. 2018. Silica nanofluid flooding for enhanced oil recovery in sandstone rocks. Egypt. J. Pet. 27(1), 105-110.

Yu, H., Kotsmar, C., Yoon, K. Y., Ingram, D. R., Johnston, K. P., Bryant, S. L., Huh, C. Transport and retention of aqueous dispersions of paramagnetic nanoparticles in reservoir rocks. In: Paper SPE 129887 presented at the SPE improved oil recovery symposium. Tulsa, Oklahoma, USA, April 24-28, 2010.

Yuan, B., Moghanloo, R. G., & Wang, W. 2018. Using nanofluids to control fines migration for oil recovery: Nanofluids co-injection or nanofluids pre-flush?-A comprehensive answer. *Fuel, 215*, 474-483.

Yue, L., Pu, W., Zhao, S., Zhang, S., Ren, F., Xu, D. 2020. Insights into mechanism of low salinity water flooding in sandstone reservoir from interfacial features of oil/brine/rock via intermolecular forces. J. Mol. Liq. 313, 113435.

Zargar, G., Arabpour, T., Manshad, A. K., Ali, J. A., Sajadi, S. M., Keshavarz, A., & Mohammadi, A. H. 2020. Experimental investigation of the effect of green TiO2/Quartz nanocomposite on interfacial tension reduction, wettability alteration, and oil recovery improvement. *Fuel, 263*, 116599.

Zargartalebi, M., Barati, N., Kharrat, R. 2014. Influences of hydrophilic and hydrophobic silica nanoparticles on anionic surfactant properties: Interfacial and adsorption behaviors. J. Pet. Sci. Eng. 119, 36-43.

Zhao, M., Cheng, Y., Wu, Y., Dai, C., Gao, M., Yan, R., & Guo, X. 2022. Enhanced oil recovery mechanism by surfactant-silica nanoparticles imbibition in ultra-low permeability reservoirs. *Journal of Molecular Liquids, 348*, 118010.

Zhong, C., Yang, Y., & Wu, X. 2021. Water-wettability reduction of an anionic hybrid fluorinated surfactant and depressurizing behavior in super-low permeability sandstone reservoirs. *Journal of Petroleum Science and Engineering, 201*, 108483.

Zhou, Y., Wu, X., Zhong, X., Reagen, S., Zhang, S., Sun, W., Zhao, J. X. 2020. Polymer nanoparticles based nano-fluid for enhanced oil recovery at harsh formation conditions. *Fuel, 267*, 117251.

Zhou, Y., Wu, X., Zhong, X., Sun, W., Pu, H., & Zhao, J. X. 2019. Surfactant-augmented functional silica nanoparticle based nanofluid for enhanced oil recovery at high temperature and salinity. *ACS applied materials & interfaces, 11*(49), 45763-45775.

Appendices

Appendix A: Results of Contact Angle Measurement

Table A.1: Contact angle measurement for Grey Berea

Concentration of MES (ppm)	MES	MES+NaOH
100	60.14°	38.01°
250	50.50°	27.79°
500	36.04°	32.12°
750	29.75°	28.23°
1000	24.68°	19.61°
1250	24.96°	24.27°
1500	28.07°	26.41°
1750	31.62°	27.11°
2000	32.37°	27.34°
3000	34.82°	28.13°
4000	37.65°	30.59°
5000	45.33°	32.11°
Formation water	91.7°	

Table A.2: Contact angle measurement for Grey Berea

Concentration of MES (ppm)	MES+NaOH +CaCl$_2$ (100ppm)	MES+NaOH+ CaCl$_2$ (250ppm)	MES+NaOH+ CaCl$_2$ (500ppm)	MES+NaOH+ CaCl$_2$ (1000ppm)
100	26.85°	21.60°	39.19°	53.90°
250	17.68°	13.90°	34.90°	35.20°
500	19.39°	12.63°	17.30°	19.62°
750	18.39°	12.20°	19.79°	21.30°
1000	14.10°	12.70°	19.83°	21.90°
1250	15.40°	15.58°	20.40°	22.10°

1500	28.80°	21.80°	21.34°	22.60°
1750	32.80°	22.38°	22.39°	22.90°
2000	33.15°	25.49°	22.76°	23.90°
3000	33.80°	28.22°	29.58°	24.50°
4000	34.03°	33.60°	30.79°	25.00°
5000	34.10°	34.60°	35.39°	22.50°

Table A. 3: Contact angle measurement for Grey Berea

Concentration of MES	MES+NaOH+MgCl$_2$ (100ppm)	MES+NaOH+ MgCl$_2$ (250ppm)	MES+NaOH+ MgCl$_2$ (500ppm)	MES+NaOH+MgCl$_2$ (1000ppm)
100	35.00°	24.80°	41.96°	39.50°
250	25.21°	23.80°	35.30°	37.70°
500	23.77°	22.38°	19.57°	19.90°
750	23.50°	16.60°	22.30°	22.50°
1000	21.63°	17.88°	22.97°	24.76°
1250	23.71°	20.21°	23.70°	25.83°
1500	30.74°	20.60°	23.99°	26.20°
1750	31.69°	25.45°	26.60°	26.40°
2000	33.20°	29.44°	28.23°	27.73°
3000	33.80°	29.90°	30.00°	28.00°
4000	34.12°	31.70°	31.34°	28.30°
5000	35.58°	33.32°	31.85°	28.90°

Table A. 4: Contact angle measurement for Buff Berea

Concentration of MES	MES	MES+NaOH
100	61.13°	34.66°
250	53.8°	32.11°
500	34.20°	31.2°

750	33.31°	27.6°
1000	25.59°	23.22°
1250	28.83°	26.33°
1500	34.45°	30.32°
1750	34.6°	30.80°
2000	36.7°	31.27°
3000	36.8°	33.80°
4000	37.12°	33.90°
5000	41.37°	35.04°
Formation water	98.4°	

Table A. 5: Contact angle measurement for Buff Berea

Concentration of MES	**MES+NaOH+ CaCl2 (100ppm)**	**MES+NaOH+ CaCl2 (250ppm)**	**MES+NaOH+ CaCl2 (500ppm)**	**MES+NaOH +CaCl2 (1000ppm)**
100	28.15°	24.19°	39.10°	52.20°
250	26.49°	15.96°	32.85°	34.11°
500	25.82°	13.00°	15.80°	19.76°
750	25.10°	12.20°	16.10°	21.95°
1000	19.64°	15.90°	16.80°	22.20°
1250	24.15°	16.60°	16.86°	23.10°
1500	32.93°	22.79°	17.31°	23.84°
1750	34.21°	23.30°	23.80°	24.00°
2000	34.30°	24.48°	26.30°	24.23°
3000	34.34°	25.65°	26.60°	25.60°
4000	34.40°	28.14°	27.10°	26.97°
5000	34.55°	28.45°	29.60°	22.18°

Table A. 6: Contact angle measurement for Buff Berea

Concentration of MES	MES+NaOH +MgCl$_2$ (100ppm)	MES+NaOH +MgCl$_2$ (250ppm)	MES+NaOH+ MgCl$_2$ (500ppm)	MES+NaOH+ MgCl$_2$ (1000ppm)
100	36.99°	26.97°	37.50°	39.80°
250	27.40°	24.00°	34.02°	34.27°
500	27.36°	21.96°	18.50°	20.50°
750	25.31°	20.35°	19.30°	22.70°
1000	22.40°	21.40°	20.55°	23.00°
1250	28.83°	23.10°	20.81°	26.40°
1500	34.45°	24.23°	21.40°	27.70°
1750	34.60°	26.46°	22.50°	28.20°
2000	36.70°	29.52°	24.70°	29.00°
3000	36.80°	30.75°	26.50°	30.35°
4000	37.12°	31.30°	27.70°	31.80°
5000	36.97°	33.44°	29.80°	32.36°

Appendix B: CMC Point Of The Solutions
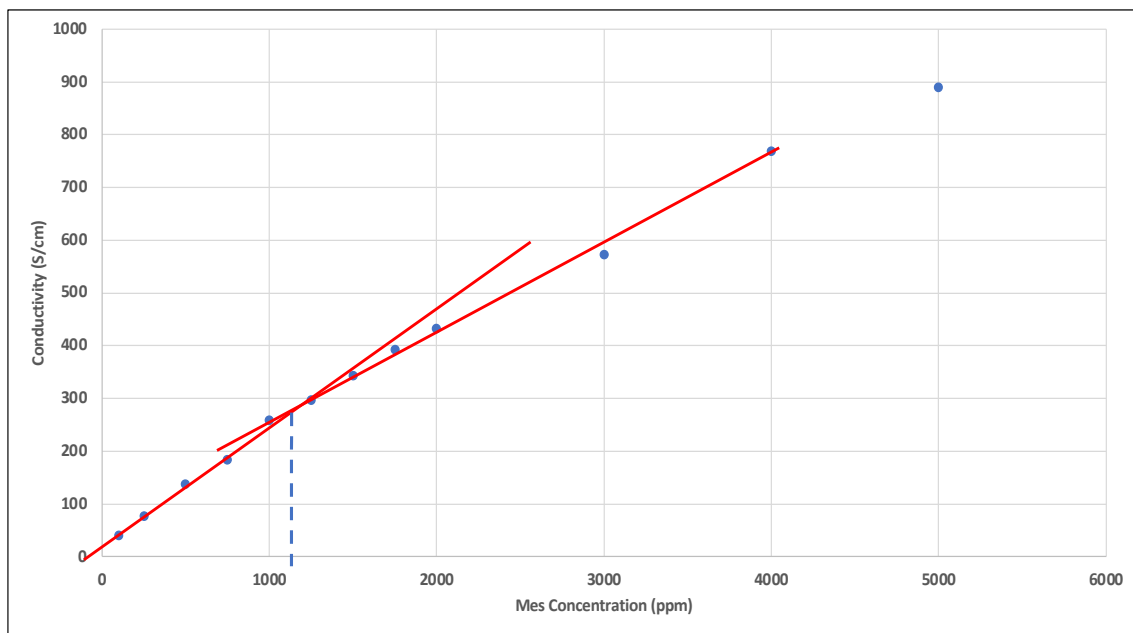
Figure B. 1: CMC point of MES surfactant
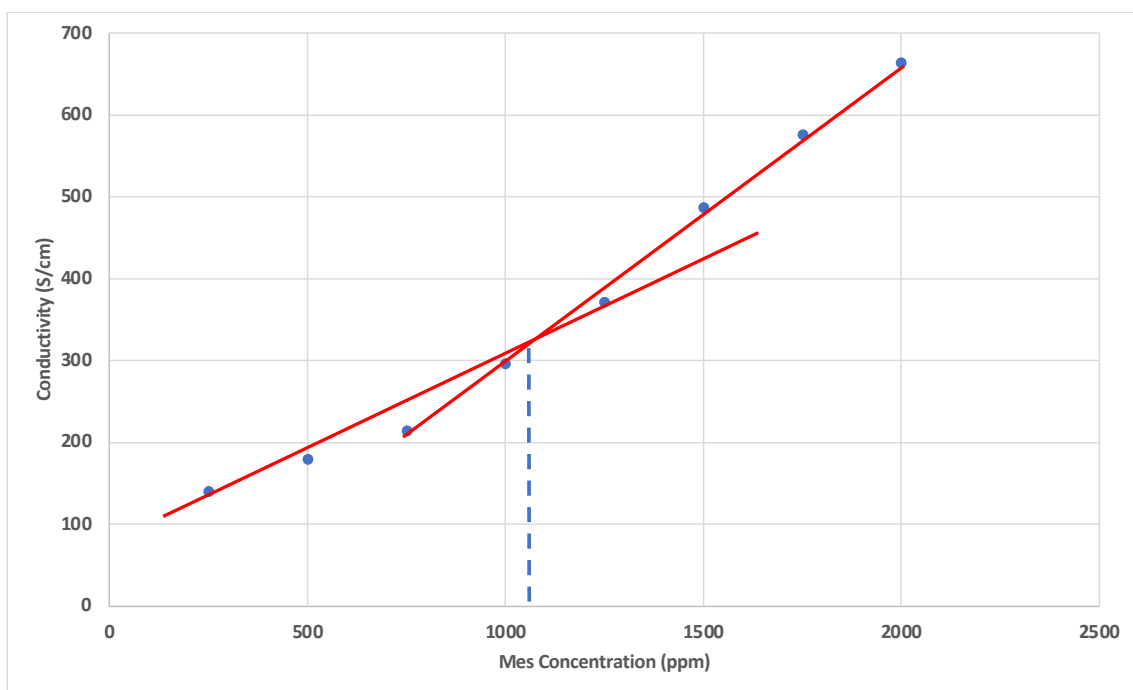
Figure B. 2: CMC point of alkaline MES surfactant
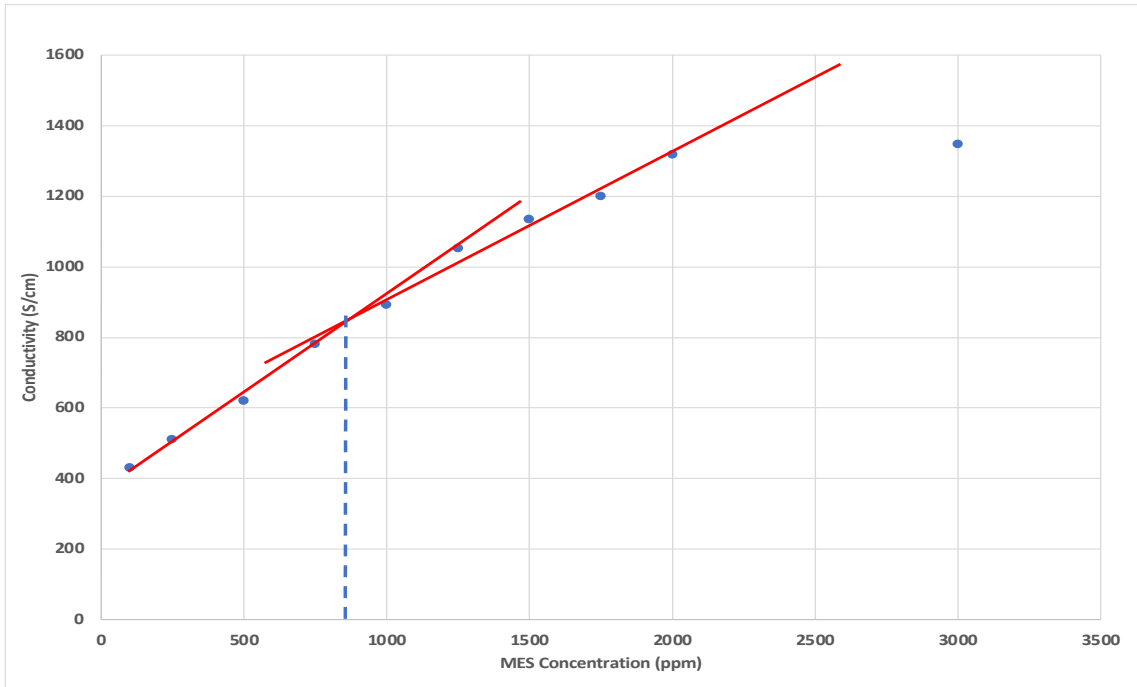
Figure B. 3: CMC point of alkaline MES surfactant + 250ppm of CaCl2
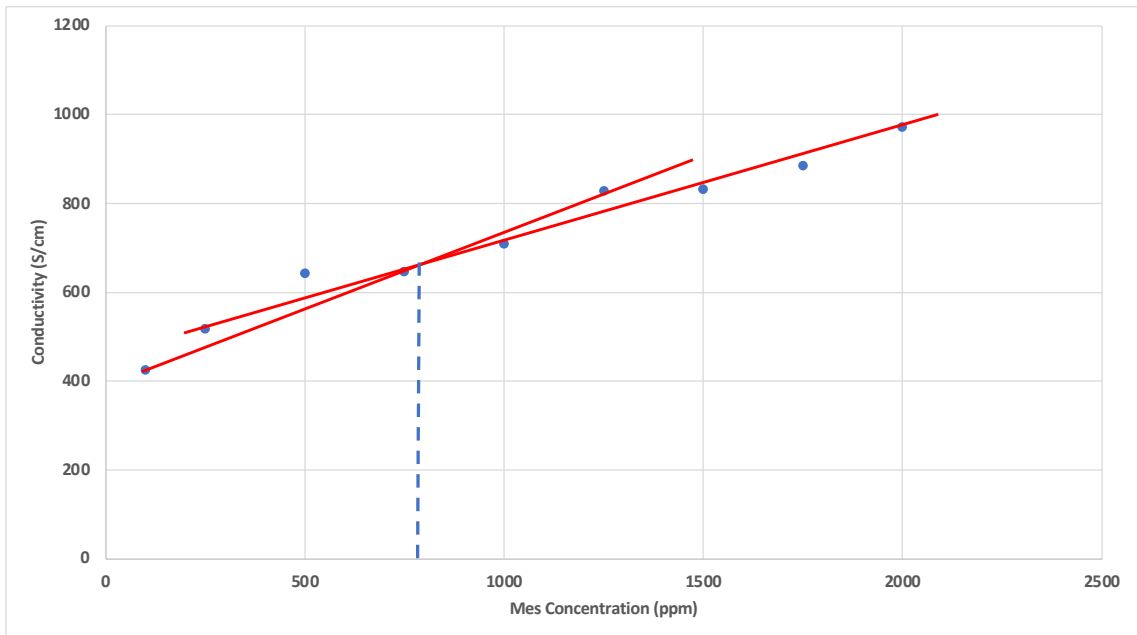
Figure B. 4: CMC point of alkaline MES surfactant + 250ppm of MgCl2

Appendix C: Graph Of Langmuir Model
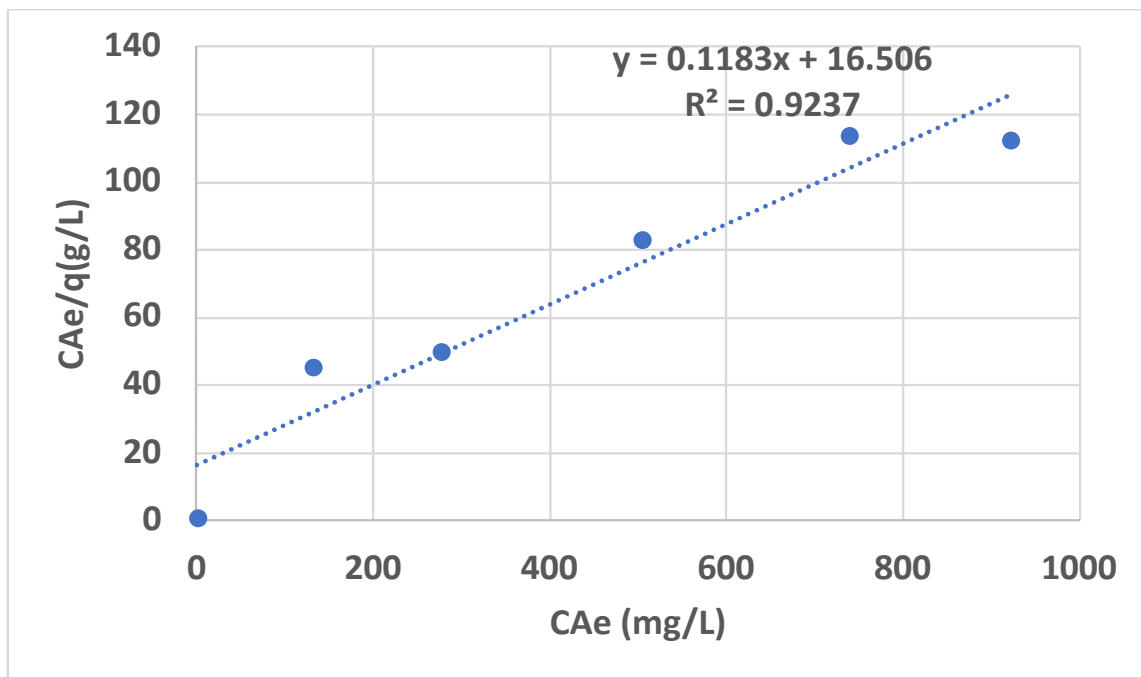
Figure C. 1: Langmuir model of alkaline MES surfactant (Grey Berea)
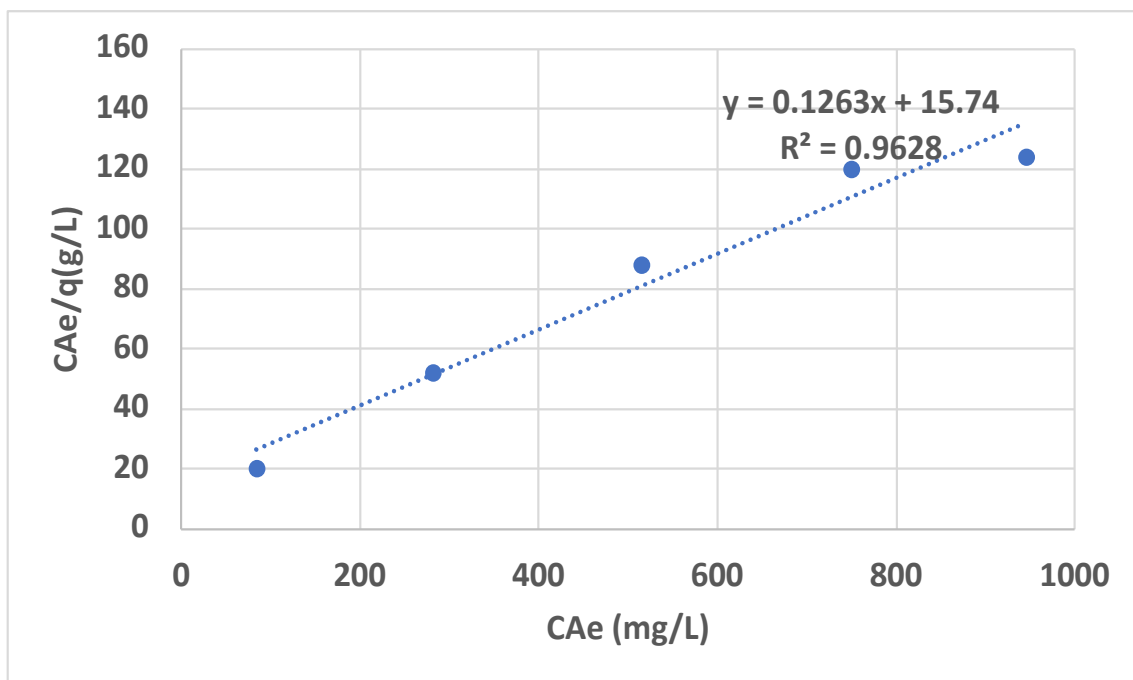
Figure C. 2: Langmuir model of alkaline MES surfactant + CaCl2 (Grey Berea)
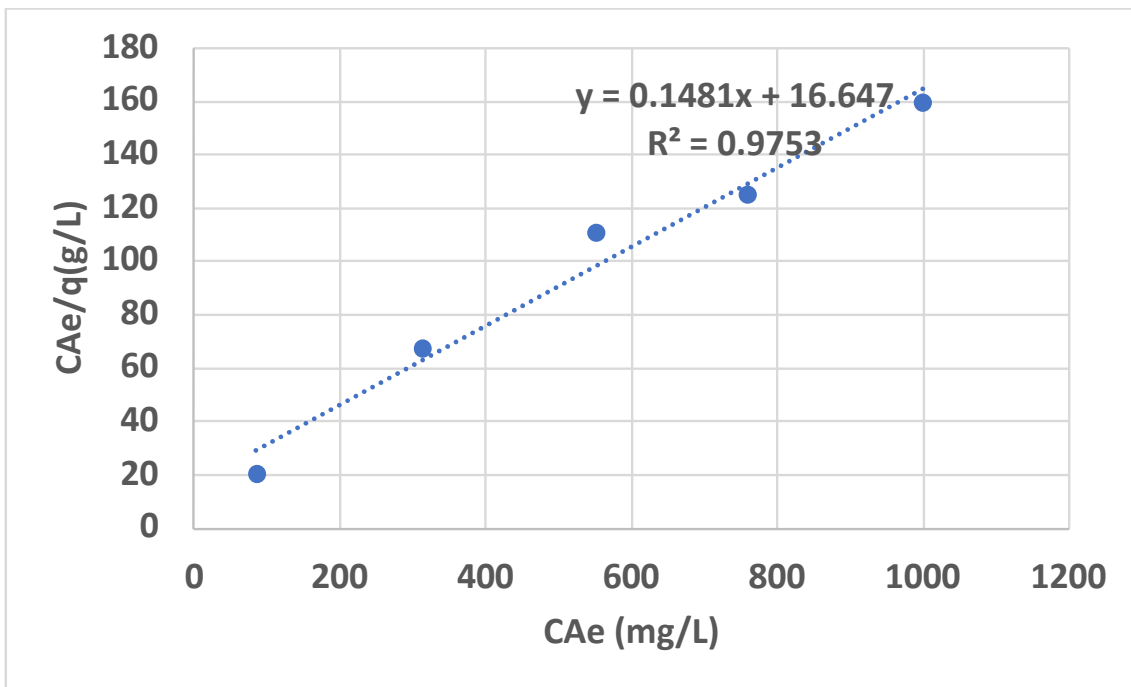
Figure C. 3: Langmuir model of alkaline MES surfactant + CaCl2 + nano-silica (Grey Berea)
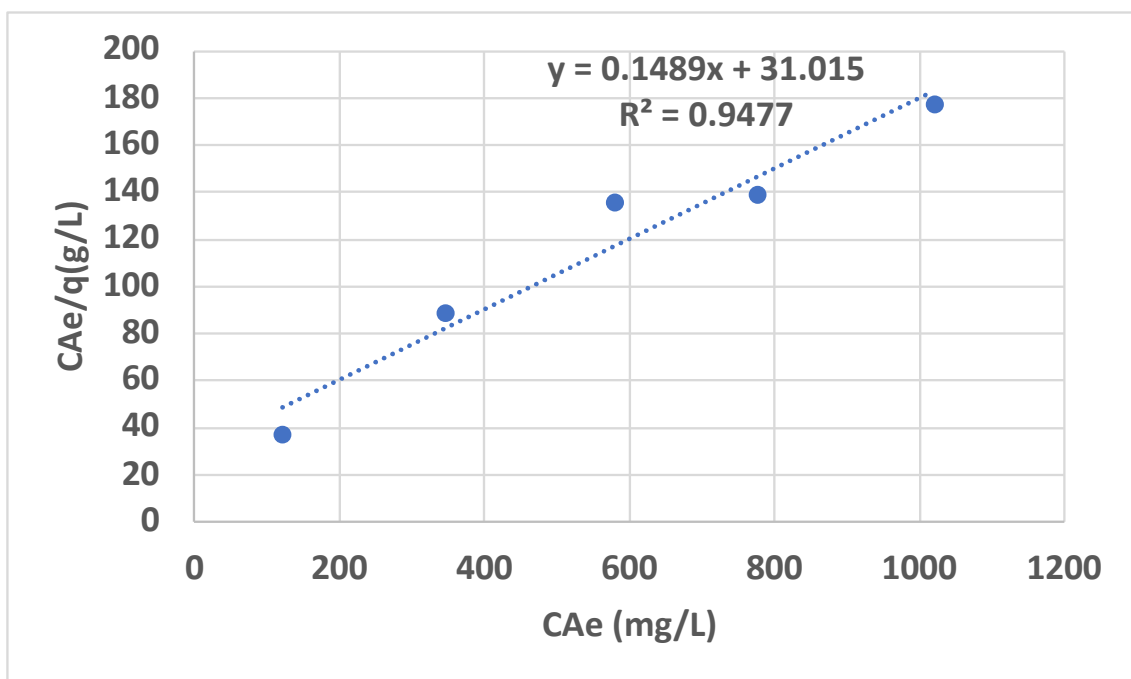
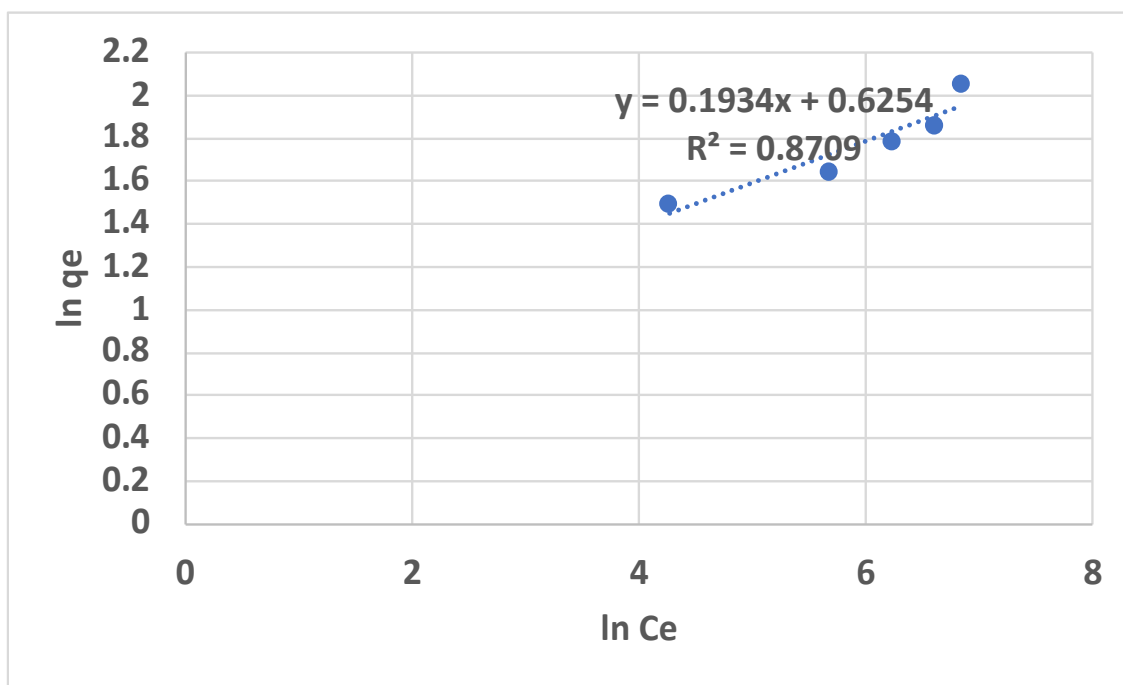Figure C. 4: Langmuir model of alkaline MES surfactant + CaCl2 + nano-polystyrene (Grey Berea)
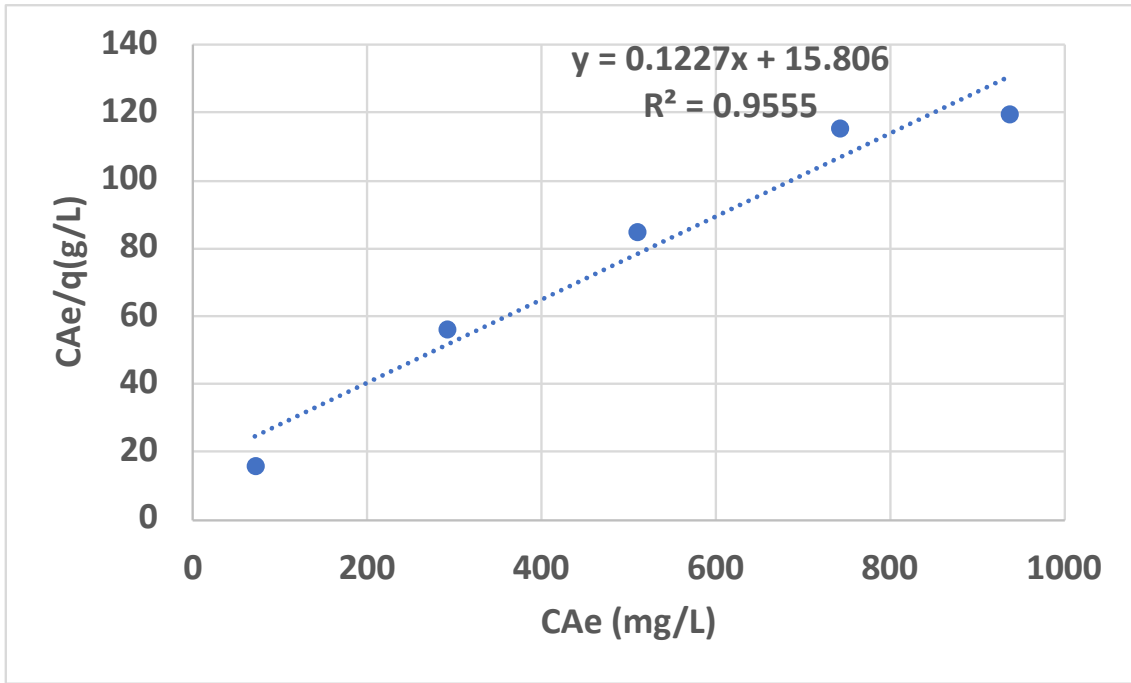
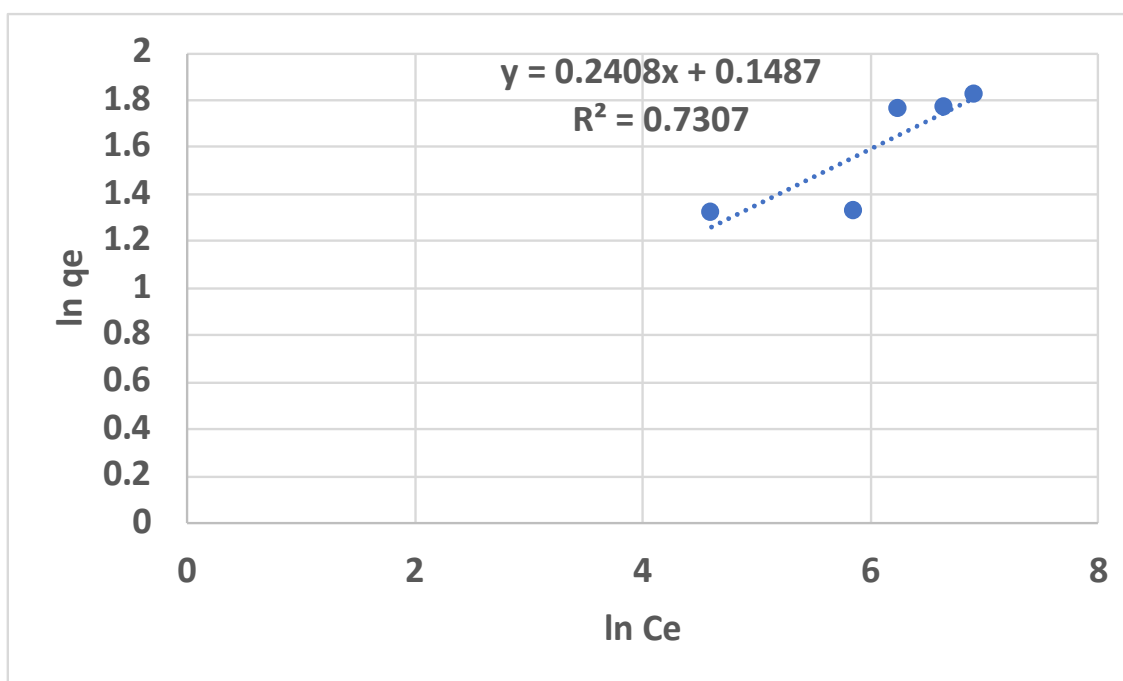Figure C. 5: Langmuir model of alkaline MES surfactant + MgCl2 (Grey Berea)
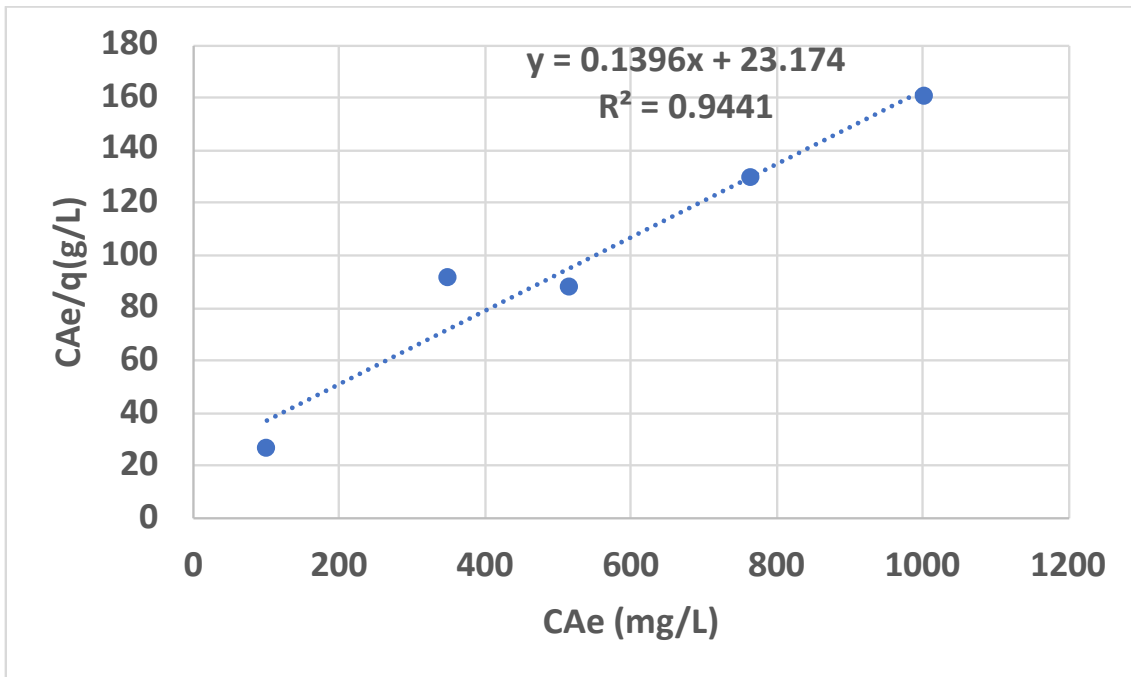
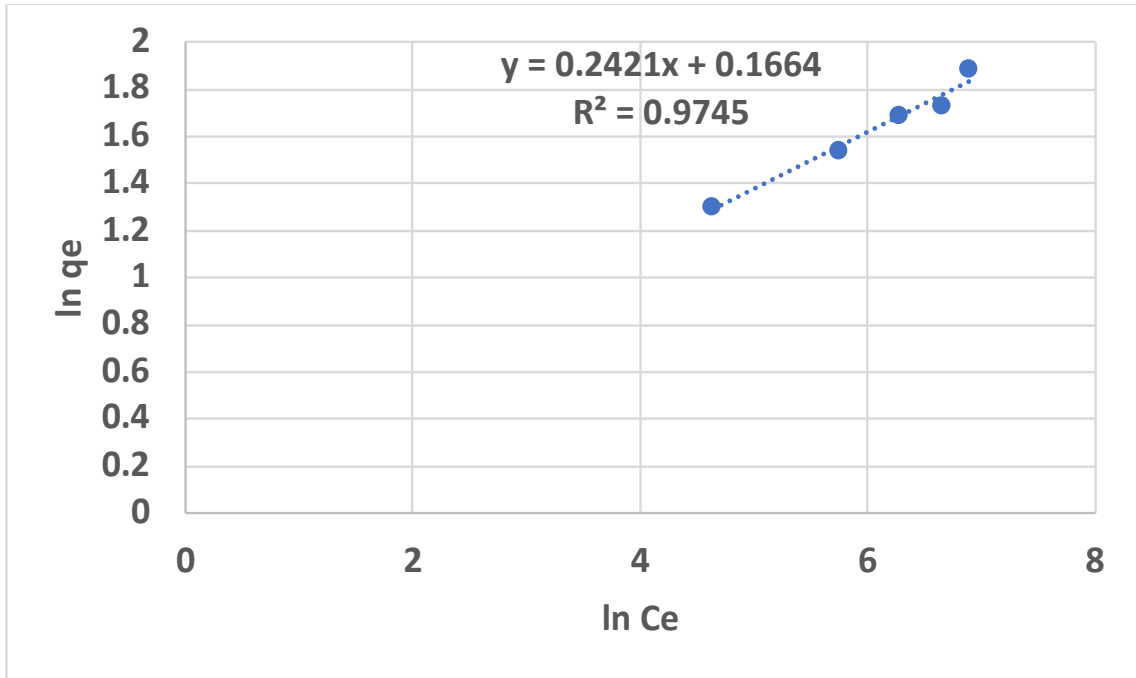Figure C. 6: Langmuir model of alkaline MES surfactant + MgCl2 + nano-silica (Grey
Berea)
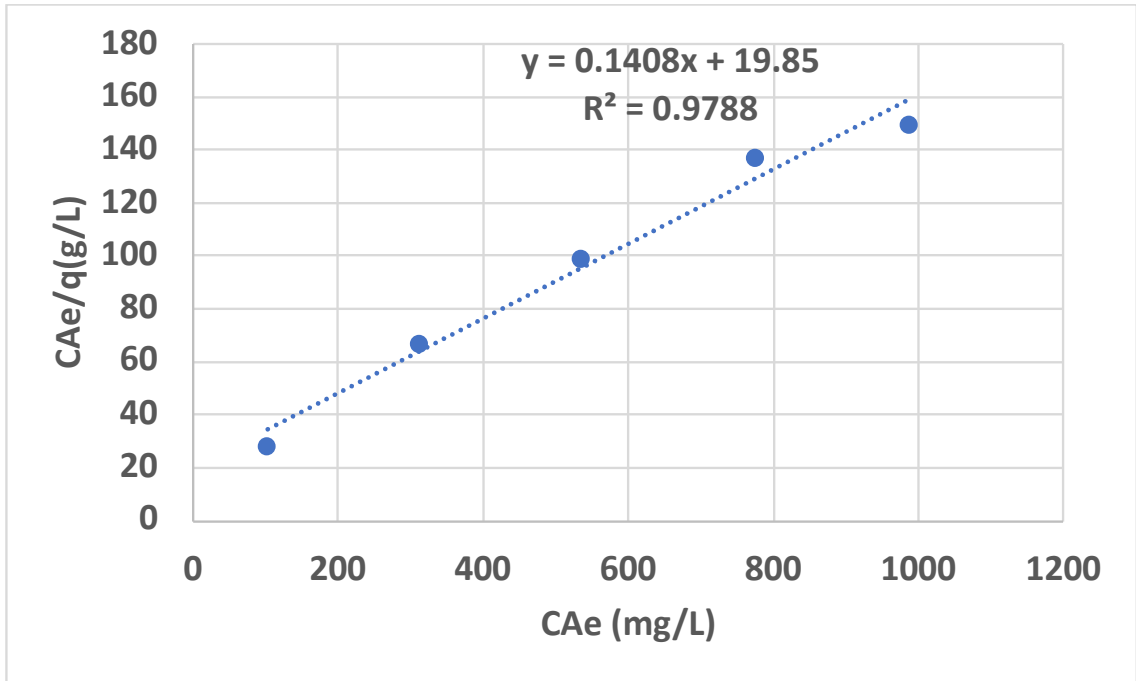
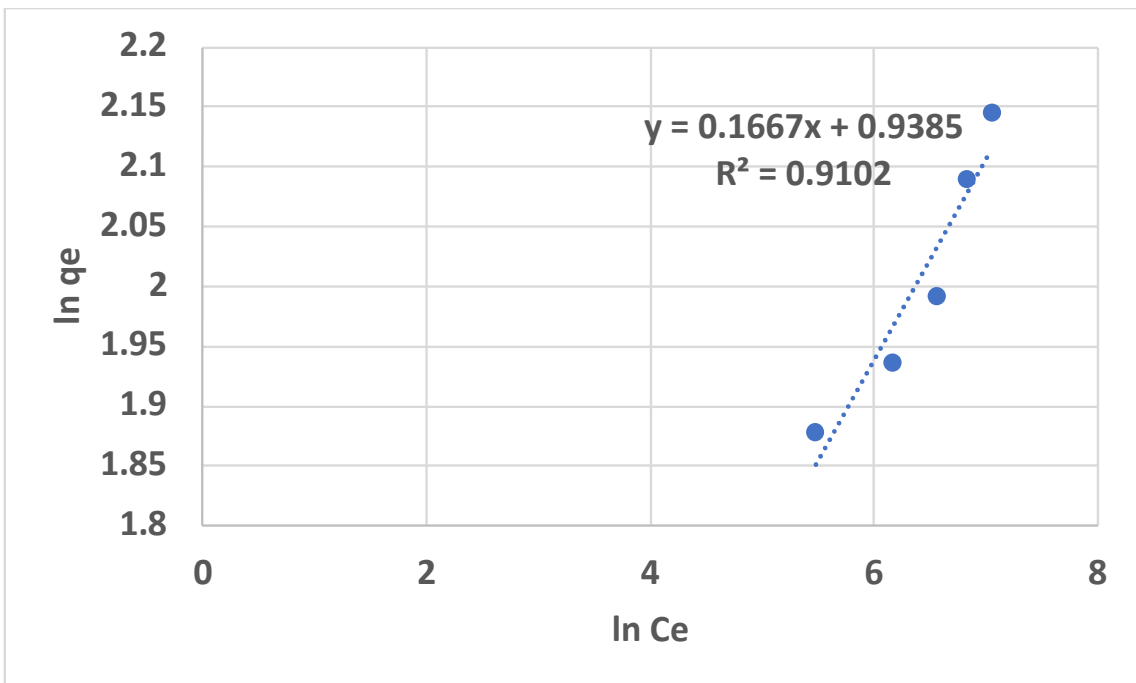Figure C. 7: Langmuir model of alkaline MES surfactant + MgCl2 + nano-polystyrene
(Grey Berea)
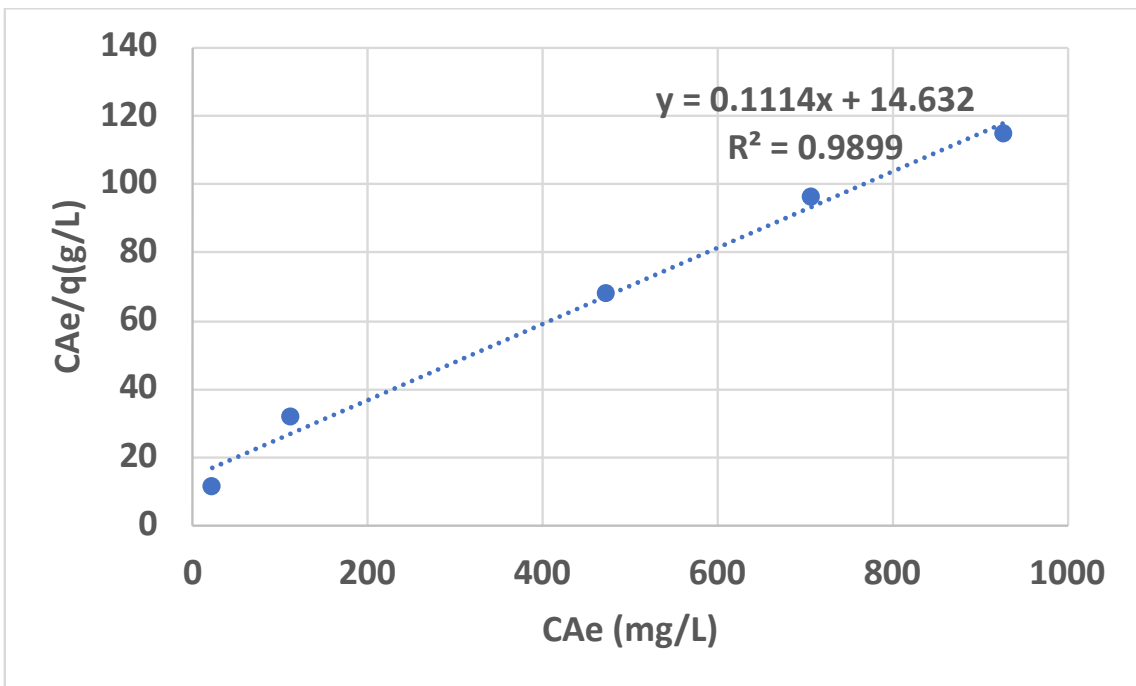
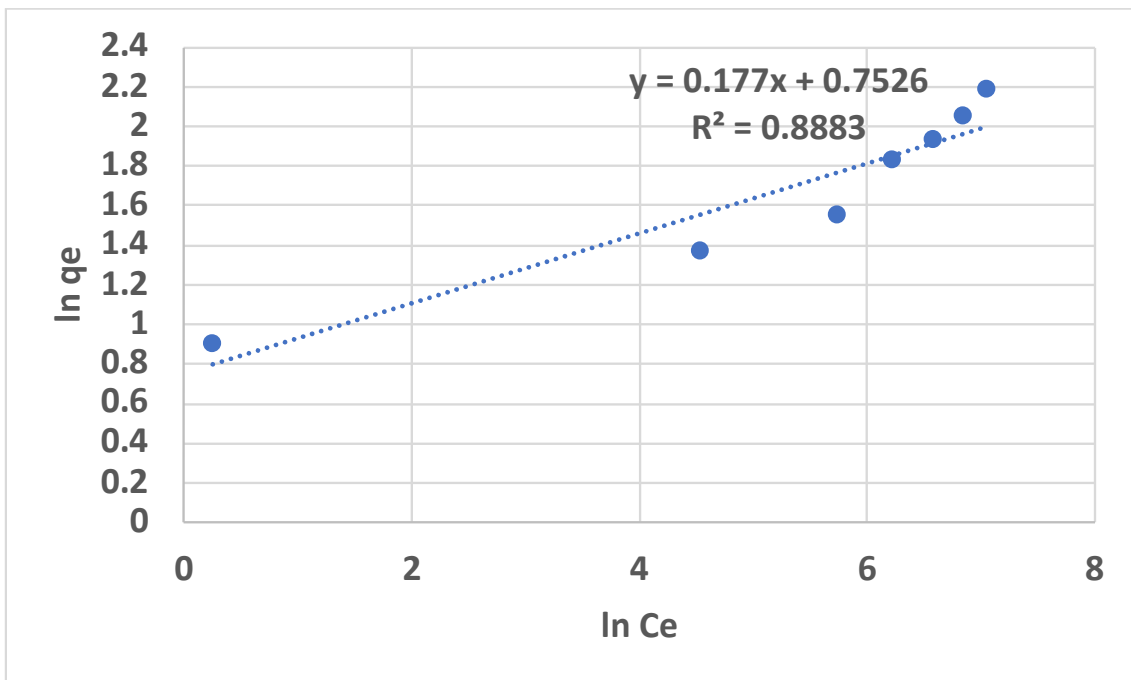Figure C. 8: Langmuir model of alkaline MES surfactant (Buff Berea)
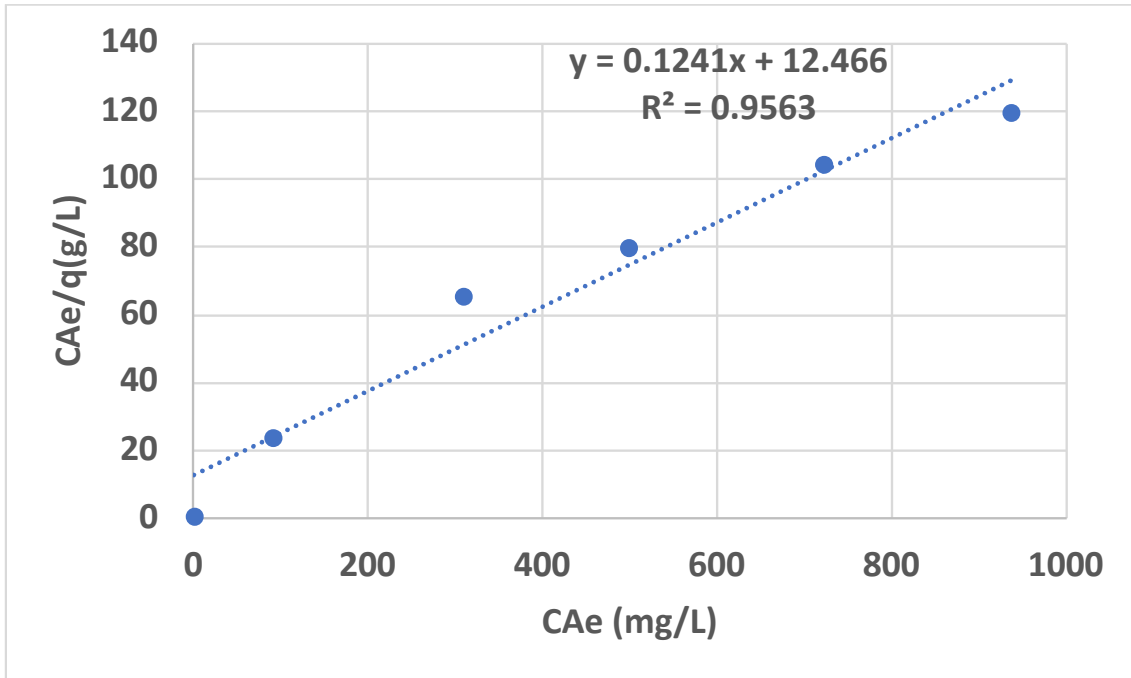
Figure C. 9: Langmuir model of alkaline MES surfactant + CaCl2 (Buff Berea)
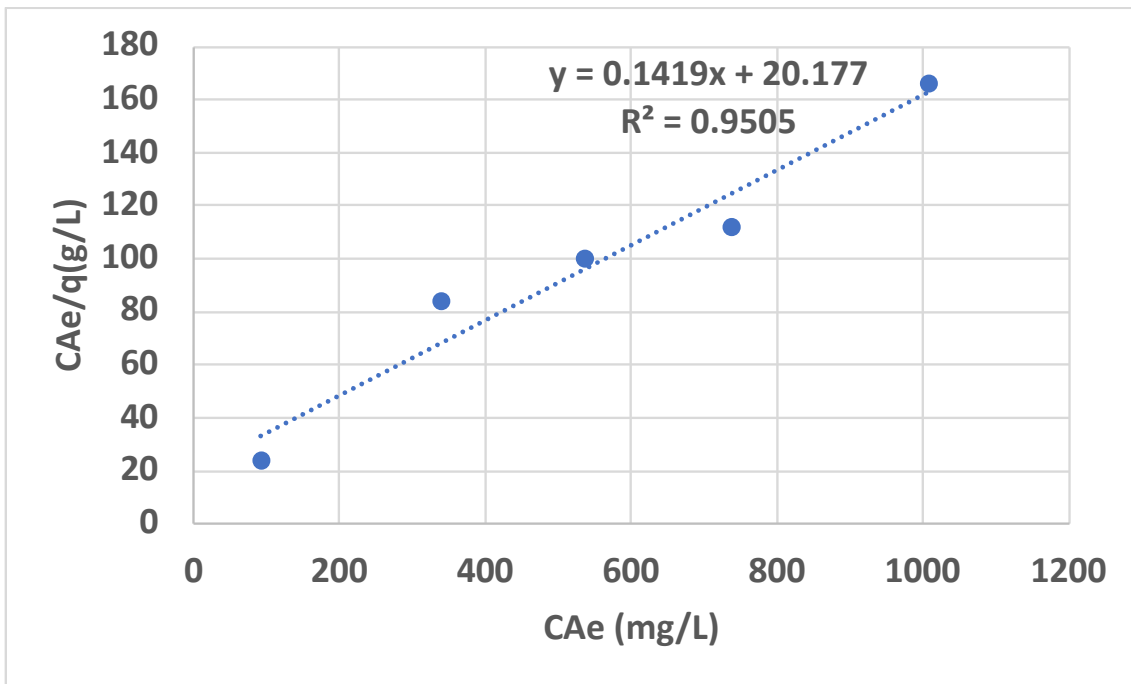
Figure C. 10: Langmuir model of alkaline MES surfactant + CaCl2 + nano-silica (Buff Berea)
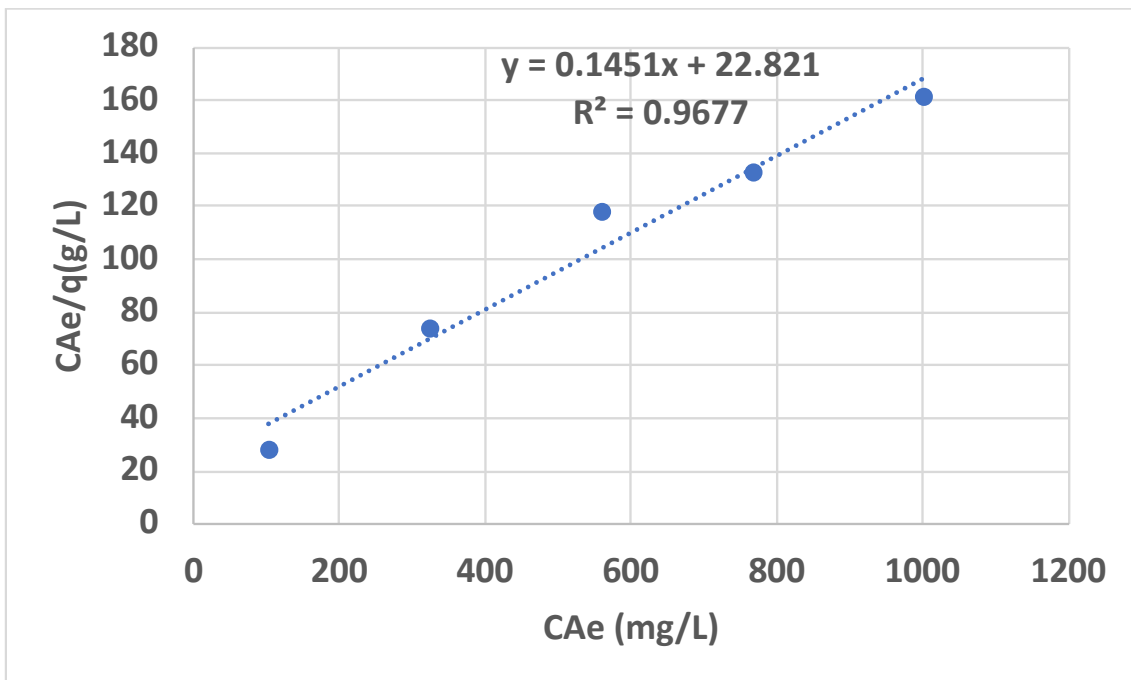
Figure C. 11: Langmuir model of alkaline MES surfactant + CaCl2 + nano-polystyrene
(Buff Berea)
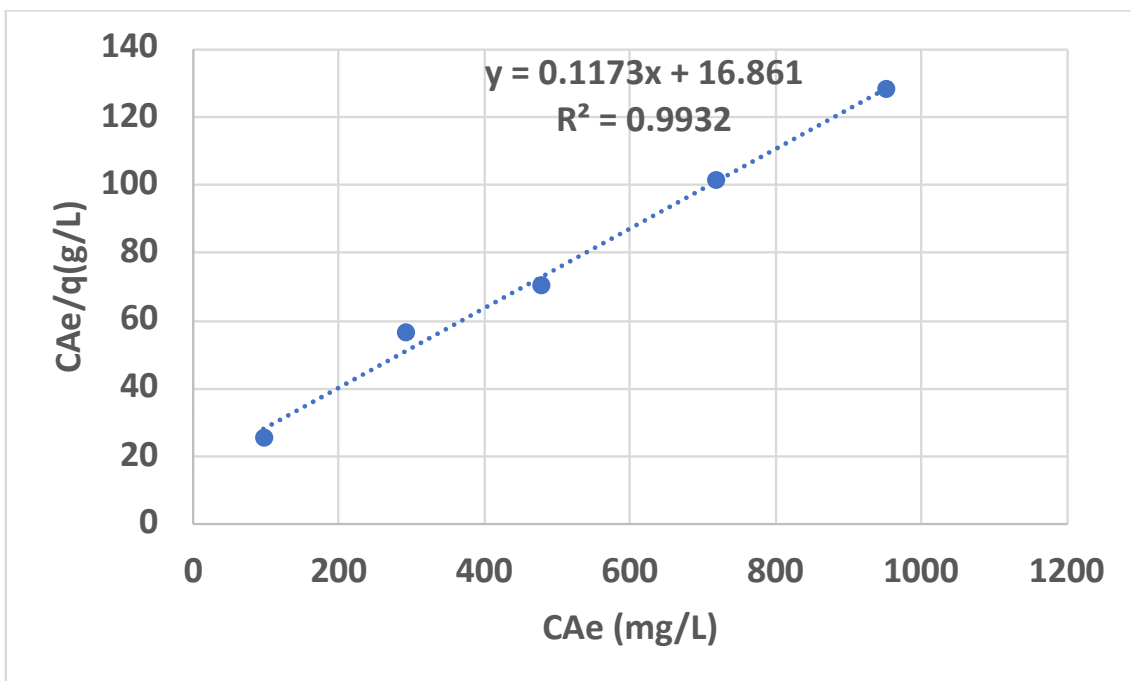
Figure C. 12: Langmuir model of alkaline MES surfactant + MgCl2 (Buff Berea)
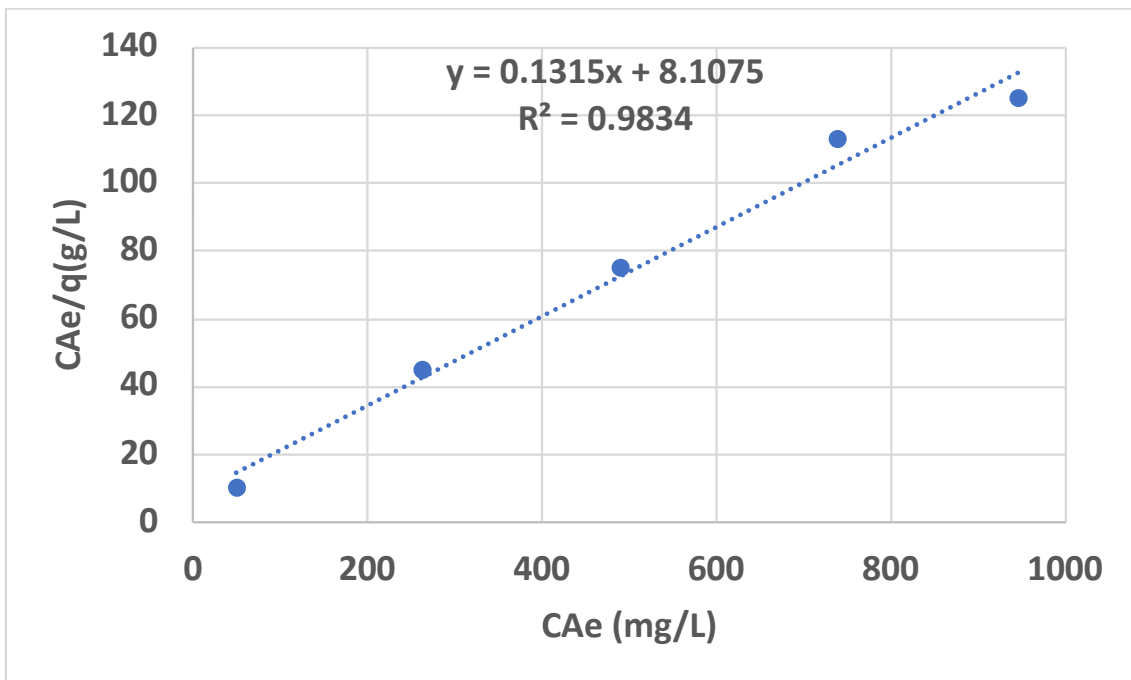
Figure C. 13: Langmuir model of alkaline MES surfactant + MgCl2 + nano-silica (Buff Berea)
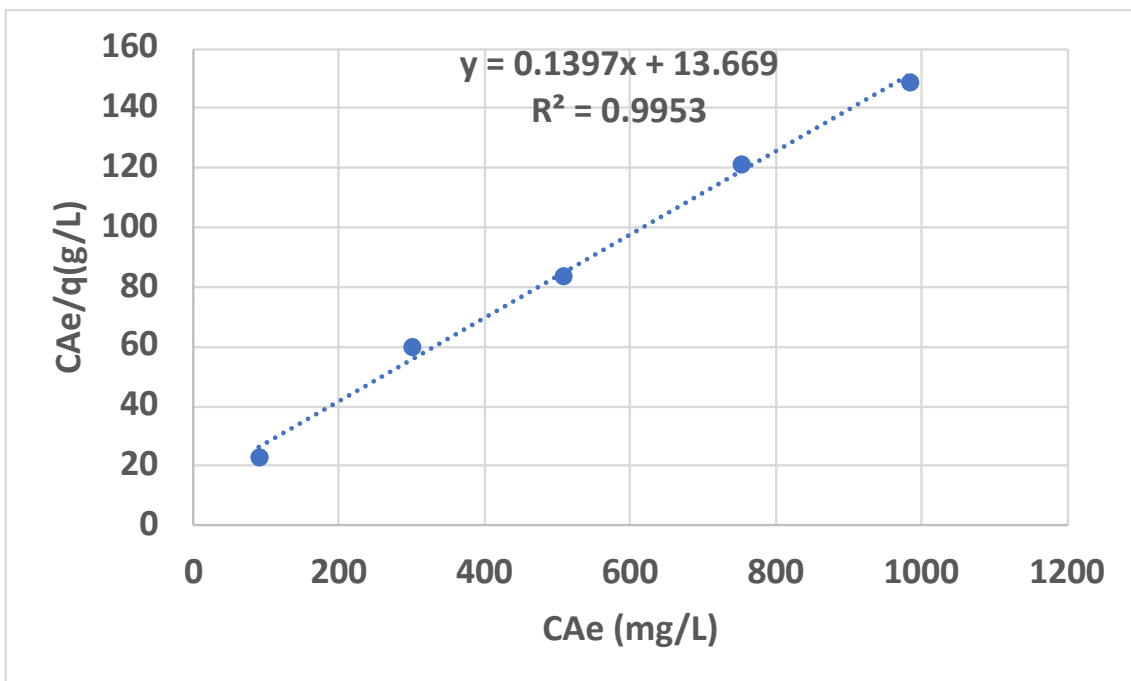
Figure C. 14: Langmuir model of alkaline MES surfactant + MgCl2 + nano-polystyrene (Buff Berea)

Appendix D: Graph Of Freundlich Model
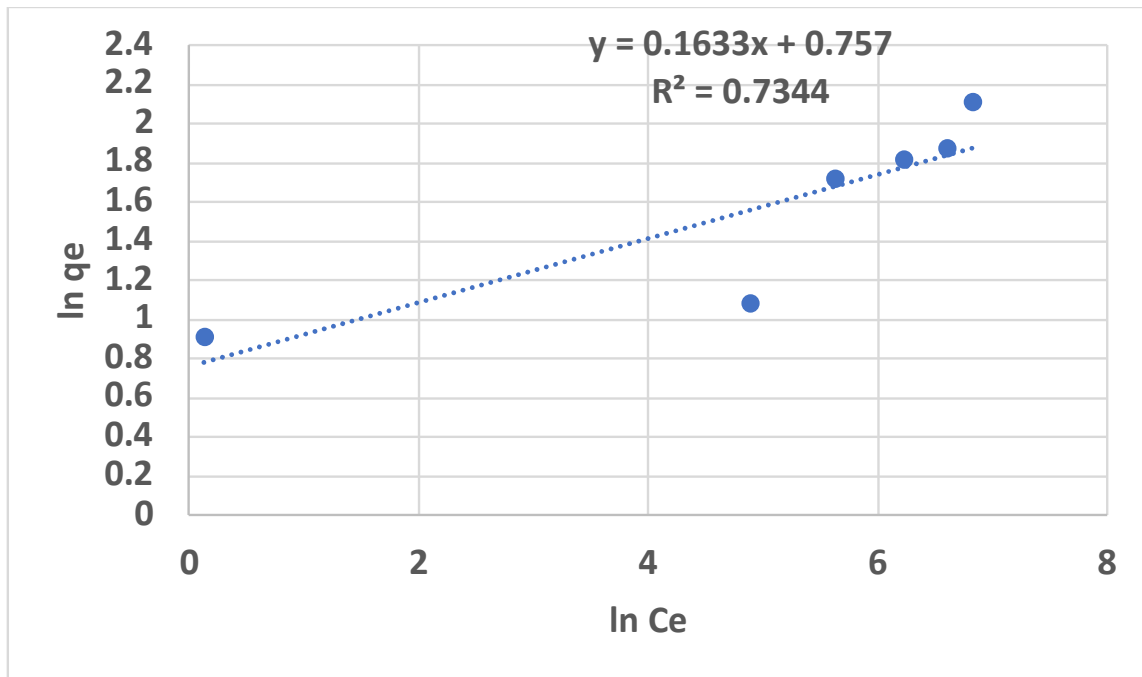
Figure D. 1: Freundlich model of alkaline MES surfactant (Grey Berea)
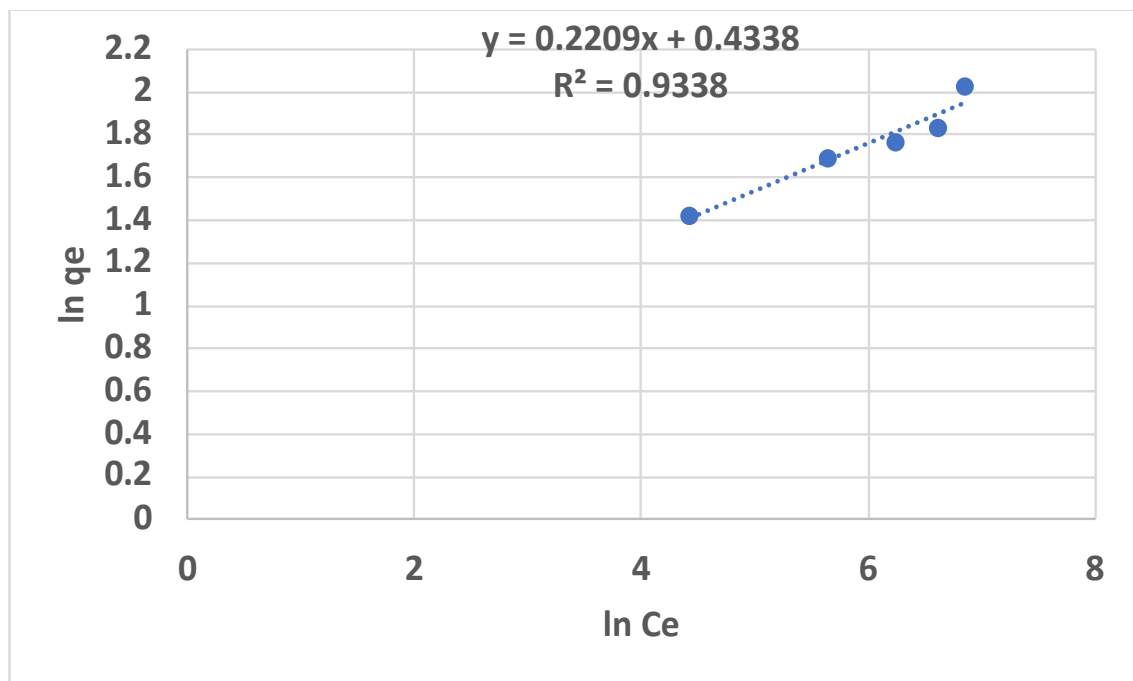
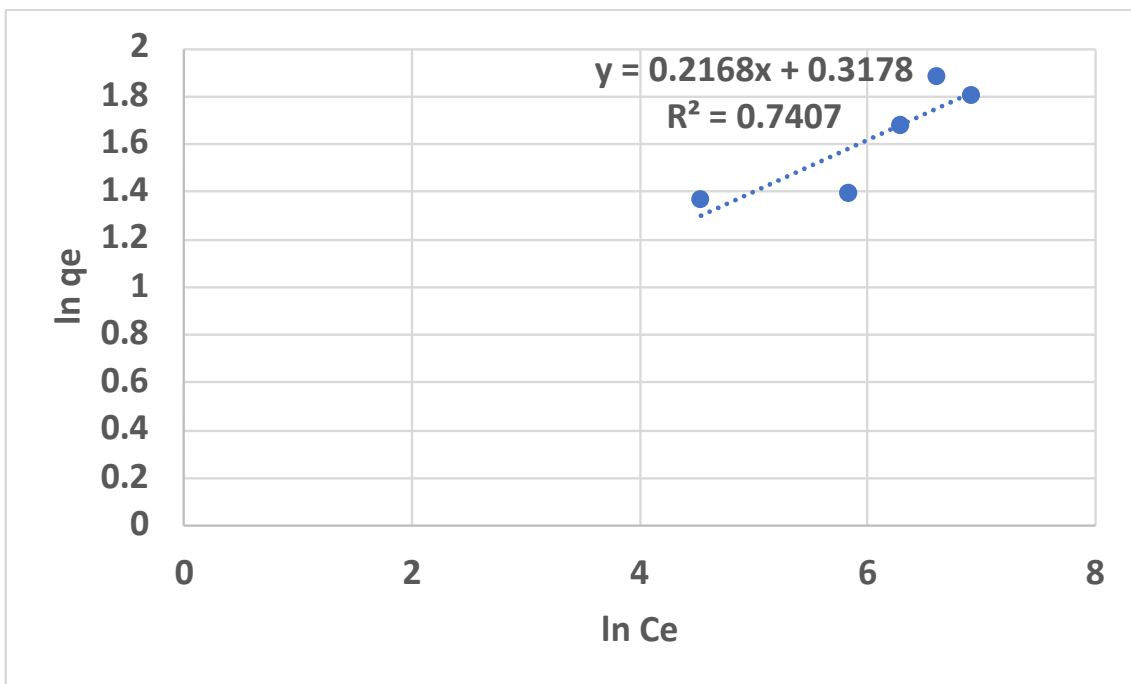Figure D. 2: Freundlich model of alkaline MES surfactant + CaCl2 (Grey Berea)
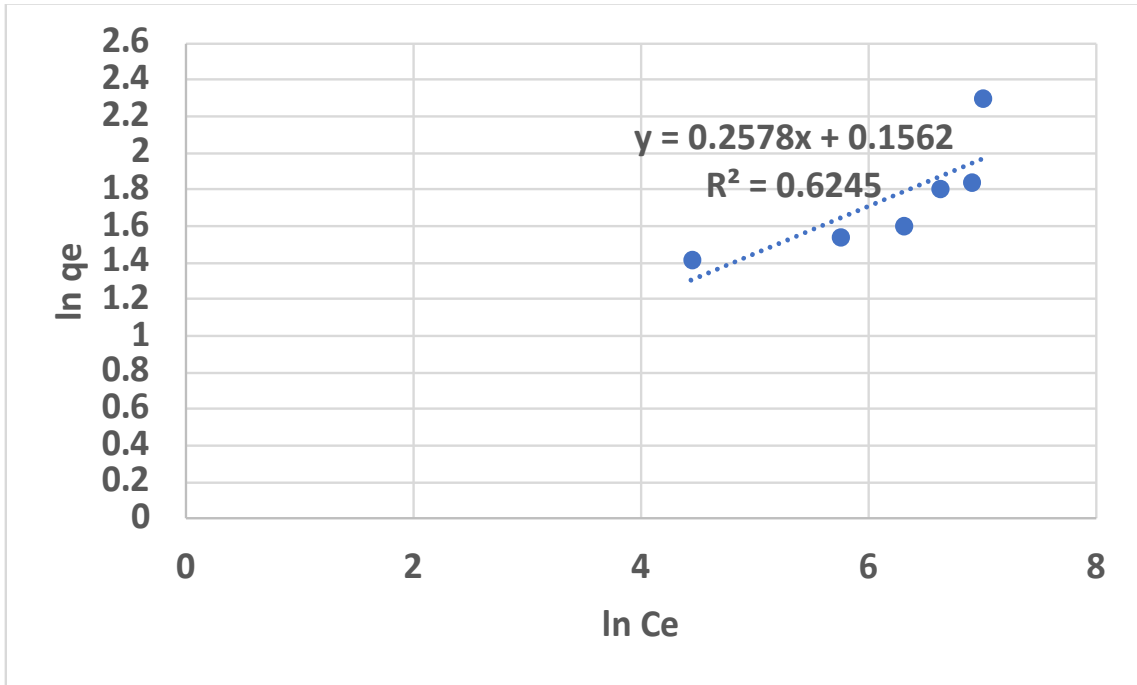
Figure D. 3: Freundlich model of alkaline MES surfactant + CaCl2 + nano-silica (Grey Berea)
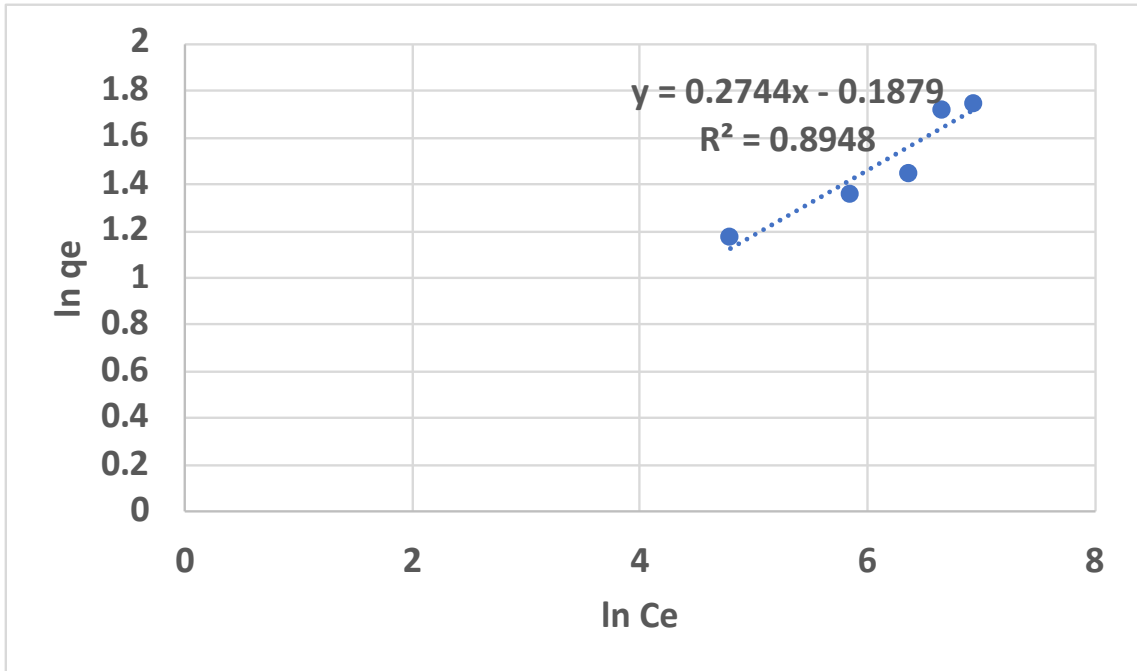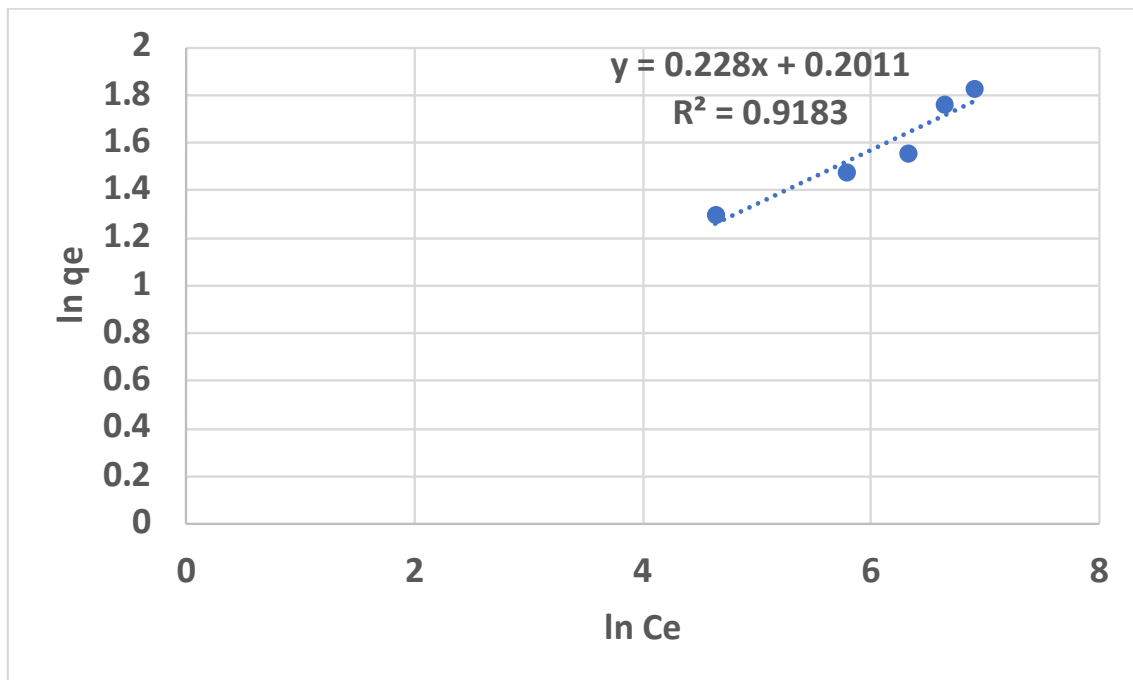

Figure D. 4: Freundlich model of alkaline MES surfactant + CaCl2 + nano-polystyrene (Grey Berea)

Figure D. 5: Freundlich model of alkaline MES surfactant + MgCl2 (Grey Berea)

Figure D. 6: Freundlich model of alkaline MES surfactant + MgCl2 + nano-silica (Grey
Berea)

Figure D. 7: Freundlich model of alkali*n*e MES surfactant + $MgCl_2$ + nano-polystyrene (Grey Berea)

Figure D. 8: Freundlich model of alkaline MES surfactant (Buff Berea)

Figure D. 9: Freundlich model of alkaline MES surfactant + CaCl2 (Buff Berea)

Figure D. 10: Freundlich model of alkaline MES surfactant + CaCl2 + nano-silica (Buff Berea)

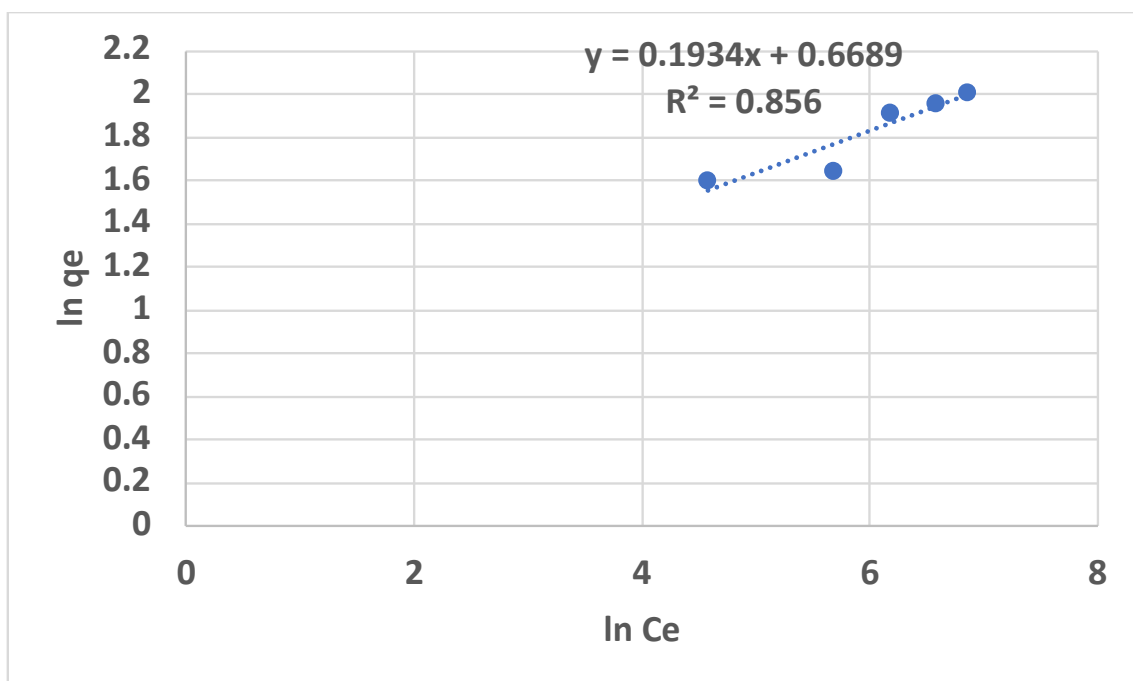Figure D. 11: Freundlich model of alkaline MES surfactant + CaCl2 + nano-polystyrene (Buff Berea)

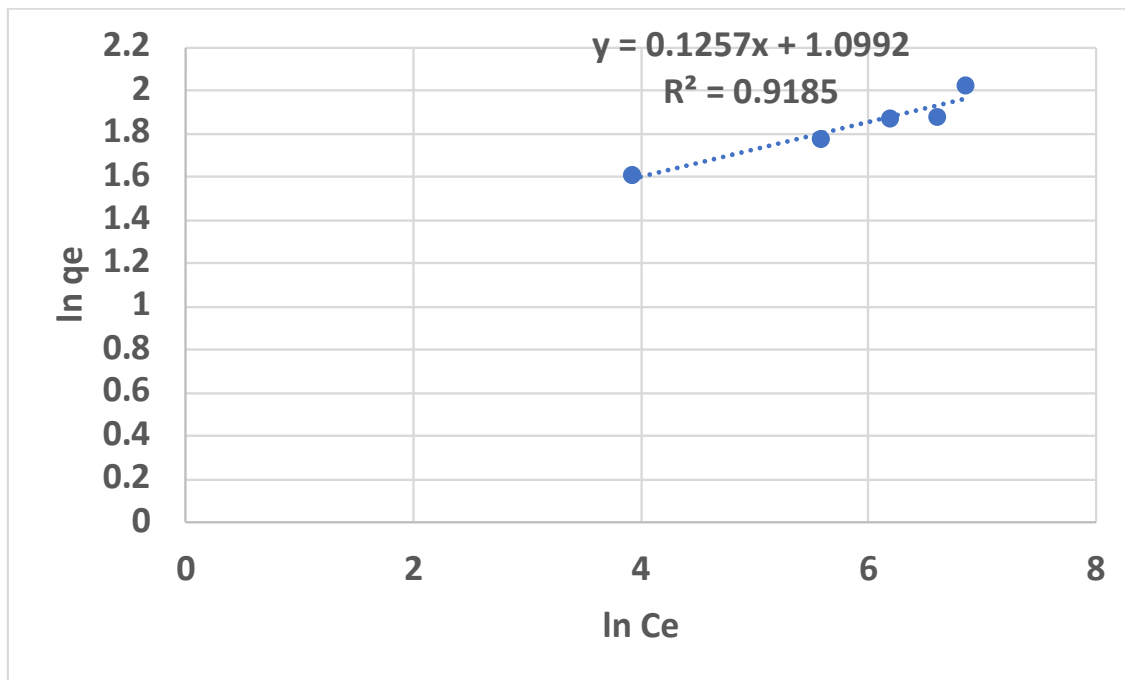Figure D. 12: Freundlich model of alkaline MES surfactant + MgCl2 (Buff Berea)

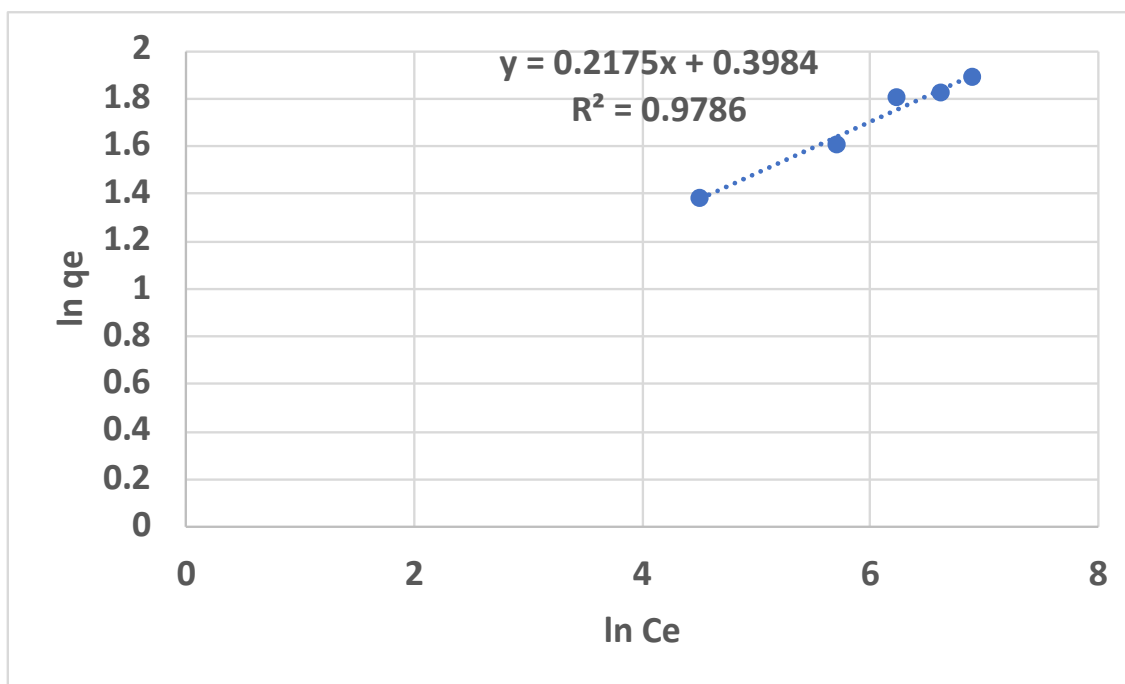Figure D. 13: Freundlich model of alkaline MES surfactant + MgCl2 + nano-silica (Buff Berea)

Figure D. 14: Freundlich model of alkaline MES surfactant + MgCl2 + nano-polystyrene (Buff)

Appendix E: Figures Of Experimental Works

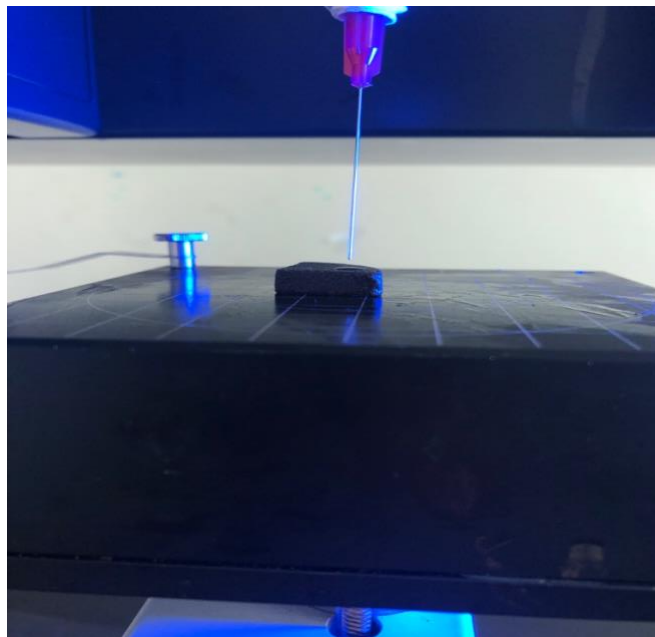Figure E. 1: Preparation of rock samples (sliced and grinded)

Figure E. 2: Contact angle measurement by using Drop Shape Analyzer

Figure E. 3: Shaking the synthesized solutions with Grey Berea fines (equilibrium process)

Figure E. 4: Confining and Back Pressure control and valves control

Figure E. 5: Pump used for core-flooding test and adjust the flow rates

Figure E. 6: Oil recovered during core-flooding test

Figure E. 7: Lowest contact angle obtained with the synthesized solution of 750ppm MES + 250ppm CaCl2 + alkaline condition (Grey Berea)

Figure E. 8: Lowest contact angle obtained with the synthesized solution of 750ppm MES + 250ppm CaCl2 + alkaline condition (Buff Berea)